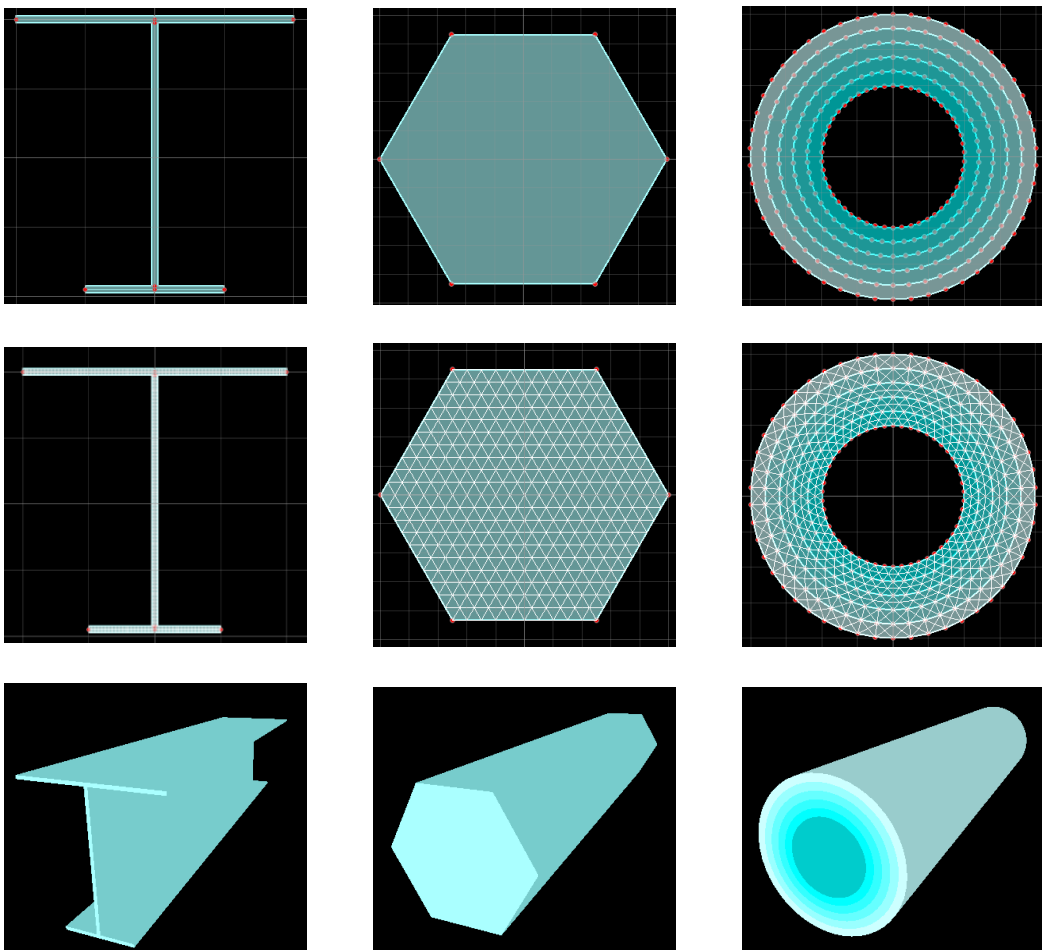


---

# MSASECT2 USER MANUAL

---



User Manual for

## MSASECT2-Matrix Structural Analysis for Arbitrary Cross-sections

Document Version: 1.0  
Tuesday, March 07, 2023



# **MSASECT2**

**Matrix Structural Analysis  
for Arbitrary Cross-sections**

---

Copyright © 2023 Siwei Liu and Ronald D. Ziemian, All Right Reserved.



# **MSASECT2**

## **Matrix Structural Analysis for Arbitrary Cross-sections**

---

### **Important Disclaimer**

Considerable care has been taken to ensure the accuracy of this software. However, the user assumes full responsibility for its use, and the developers or distributors will not be liable for any damage caused by the use or misuse of this software.

The user should have a thorough understanding of the software's modeling, analysis, and design algorithms, and should compensate for any aspects that are not addressed. We recommend that a qualified and experienced engineer be appointed to check the input and verify the results produced by the software. The engineer should take professional responsibility for the information that is used.

By using this software, you agree to these terms and conditions.

# Contents

Title	Page
<b>1. INTRODUCTION .....</b>	<b>3</b>
1.1 GENERAL .....	3
1.2 COPYRIGHT AND DISCLAIMER .....	4
1.3 SYSTEM REQUIREMENTS .....	6
<b>2. USER INTERFACE.....</b>	<b>7</b>
2.1 OVERVIEW.....	7
2.2 RIBBON MENU .....	8
2.2.1 <i>Home tab</i> .....	8
2.2.2 <i>Template tab</i> .....	14
2.2.3 <i>Export tab</i> .....	39
2.3 MAIN WINDOW .....	39
2.3.1 <i>Design information</i> .....	39
2.3.2 <i>Input menu (Centerline module)</i> .....	40
2.3.3 <i>Input menu (Outline module)</i> .....	41
2.3.4 <i>Drawing Canvas</i> .....	42
2.3.5 <i>Massage window</i> .....	43
2.3.6 <i>Output window (for section properties)</i> .....	44
<b>3. THEORETICAL BACKGROUND .....</b>	<b>47</b>
3.1 COORDINATE METHOD.....	47
3.1.1 <i>Section modelling</i> .....	47
3.1.2 <i>Warping ordinate</i> .....	49
3.1.3 <i>Wagner coefficients</i> .....	51
3.2 FINITE-ELEMENT-BASED METHOD .....	52
3.2.1 <i>Section modelling</i> .....	52
3.2.2 <i>Shape functions and Jacobian matrix of the CST element</i> .....	55
3.2.3 <i>Basic geometric properties</i> .....	55
3.2.4 <i>Torsion and warping properties</i> .....	56
3.2.5 <i>Shear coefficients</i> .....	61
<b>4. VERIFICATION EXAMPLES.....</b>	<b>67</b>
4.1 SECTION PROPERTIES FOR THIN-WALLED SECTIONS .....	67
4.2 GEOMETRIC AND TORSIONAL PROPERTIES .....	71
4.3 SHEAR COEFFICIENTS .....	75
4.3 YIELD SURFACE .....	77
4.3.1 <i>Symmetric sections</i> .....	77
4.3.2 <i>Nonsymmetric sections</i> .....	79
<b>REFERENCES .....</b>	<b>94</b>

## List of Figures

Title	Page
<b>Figure 1</b> Modeling an open section via points and segments .....	49
<b>Figure 2</b> The coordinates and the warping ordinate at a point.....	51
<b>Figure 3</b> Example of section modeling.....	53
<b>Figure 4</b> Constant strain triangle (CST) element.....	54
<b>Figure 5</b> Dimensions of the mono-symmetric-I section .....	68
<b>Figure 6</b> Four sections for the verification of CM method.....	69
<b>Figure 7</b> Verification examples of geometric and torsional properties.....	72
<b>Figure 8</b> Comparation results. ....	75
<b>Figure 9</b> Verification examples of shear deformation coefficients. (Unit: m) .....	76
<b>Figure 10</b> Doubly symmetric sections (Unit: mm).....	77
<b>Figure 11</b> Comparison results for the doubly symmetric sections.....	79
<b>Figure 12</b> Nonsymmetric sections (Unit: mm) .....	80
<b>Figure 13</b> Comparison results for section A .....	83
<b>Figure 14</b> Comparison results for section B .....	86
<b>Figure 15</b> Comparison results for section C .....	89
<b>Figure 16</b> Comparison results for section D.....	92

## 1. Introduction

### 1.1 General

MSASECT2 (Matrix Structural Analysis for Arbitrary Cross-sections) is a comprehensive module for generating accurate section properties in frame analysis, hosted on the Mastan platform. The module is based on the coordinate and finite-element-based methods developed by the Mastan team for analyzing thin-walled and general cross-sections.

**Some characteristics of MASTAN2 include:**

- 1) Section can be molded using centerline or outline.
- 2) Section can be meshed into fibers.
- 3) Section 3D view is provided.
- 4) Section properties, including the geometric properties, torsion properties, warping properties, Wagner coefficients, and shear coefficients, for arbitrary cross-sections can be generated.
- 5) Full yield surfaces for arbitrary cross-sections can be calculated.
- 6) Standard libraries of material and sections are included.

This software is stand-alone module and integrated with MASTAN2, which means a smooth working flow can be achieved by using them. And it is also possible to directly output and export results Text and Adobe PDF TM for additional use. We wish you much success using MSASECT2 and MASTAN2, and welcome for your valuable comments and suggestions. Thank you.

## 1.2 Copyright and Disclaimer

The MASECT2 software is developed by Siwei Liu (Assistant Professor, The Hong Kong Polytechnic University) and Ronald D. Ziemian (Professor, Bucknell University) for educational and research use only. The copyright of the MASECT2 belongs to Siwei Liu and Ronald D. Ziemian, all right reserved.

### **Disclaimer:**

Considerable care has been taken to ensure the accuracy of this software. Nevertheless, responsibility for the use of this software rests with the user and the developers or the distributors will not be responsible for any kind of damage caused by the use or misuse of this software.

The user must explicitly understand the basic assumptions of the software modeling, analysis and design algorithms and compensate for the aspects that are not addressed. A qualified and experienced engineer must be appointed to check the input and verify the results produced by the software. The engineer should take professional responsibility for the information that is used.

### **Third-party Libraries:**

This software includes open source and third-party software components, including the following:

- argparse: A Python module for parsing command-line arguments, licensed under the Python Software Foundation license.
- gmsh: A 3D finite element grid generator with a built-in CAD engine and post-processor, licensed under the GPL license.
- matplotlib: A library for creating static, animated, and interactive visualizations in Python, licensed under the Matplotlib license.
- meshio: A package for reading and writing mesh data in various formats in Python, licensed under the MIT license.
- numpy: The fundamental package for scientific computing with Python, licensed under the BSD license.
- openpyxl: A library for reading and writing Excel files, licensed under the MIT license.
- PyOpenGL: A Python wrapper for OpenGL, licensed under the BSD license, licensed under the BSD license.

- PySide6: A Python binding for the Qt application framework, licensed under the LGPL version 3.
- pyqtgraph: A pure-Python graphics and GUI library built on PyQt4/PyQt5/PySide/PySide2 and numpy, licensed under the MIT license.
- scipy: A library for scientific computing and technical computing, licensed under the BSD license.
- Shapely: A package for manipulating and analyzing geometric objects in Python, licensed under the BSD license.
- tqdm: A package for adding progress bars to loops and iterables in Python, licensed under the MIT license.
- uuid: A Python module provides functionalities for generating and handling UUIDs (Universally Unique Identifiers), licensed under the Python Software Foundation license.
- vispy: A high-performance interactive 2D/3D visualization library, licensed under the BSD license.

We acknowledge the valuable contributions of the developers and communities behind these libraries. The terms of their respective licenses apply to the use of these components in this software.

For more information on the licenses used by these components, please refer to the documentation provided with the software or the websites of the respective projects.

### **1.3 System Requirements**

Before installing and using the software, make sure your computer meets the following requirements:

#### **Windows**

- Windows 7 (all editions)
- Windows 8 (all editions)
- Windows 10 (all editions)
- Windows 11 (all editions)

#### **macOS**

- macOS 10.13 High Sierra or later

#### **Linux**

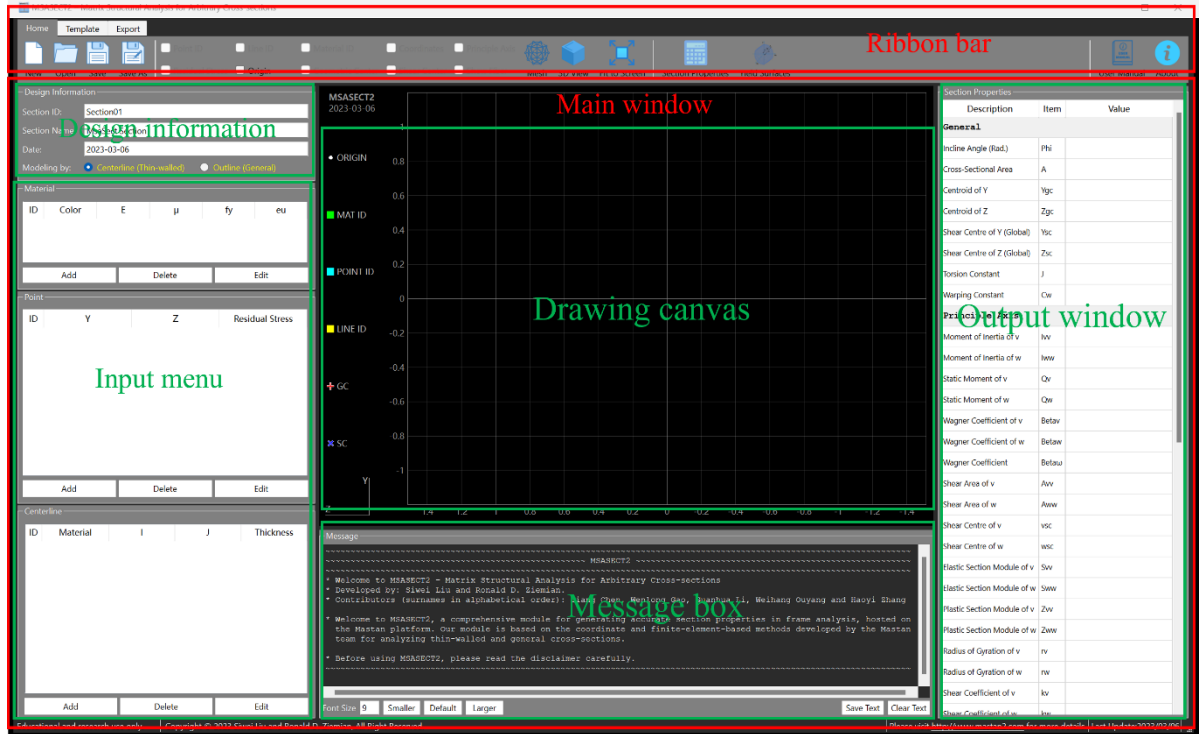
- Ubuntu 18.04 LTS or later
- Fedora 28 or later, or equivalent

Please note that the software may not work properly on operating systems other than those listed above. Additionally, some features may require additional system resources. If you are unsure whether your computer meets the requirements, please consult your system administrator or technical support.

## 2. User Interface

### 2.1 Overview

The overview of the Main Screen is demonstrated as below:



## 2.2 Ribbon Menu

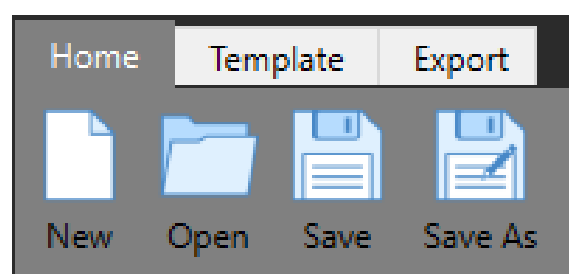
The ribbon menu is composed of three parts, which are Home tab, Template tab, and Export tab.

### 2.2.1 Home tab

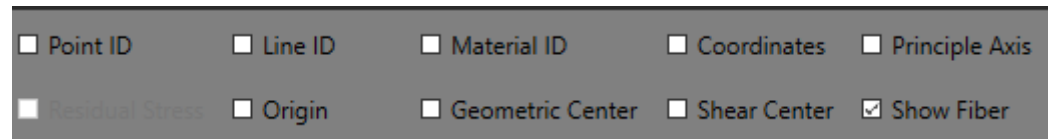
The Home tab in the ribbon menu is shown below:



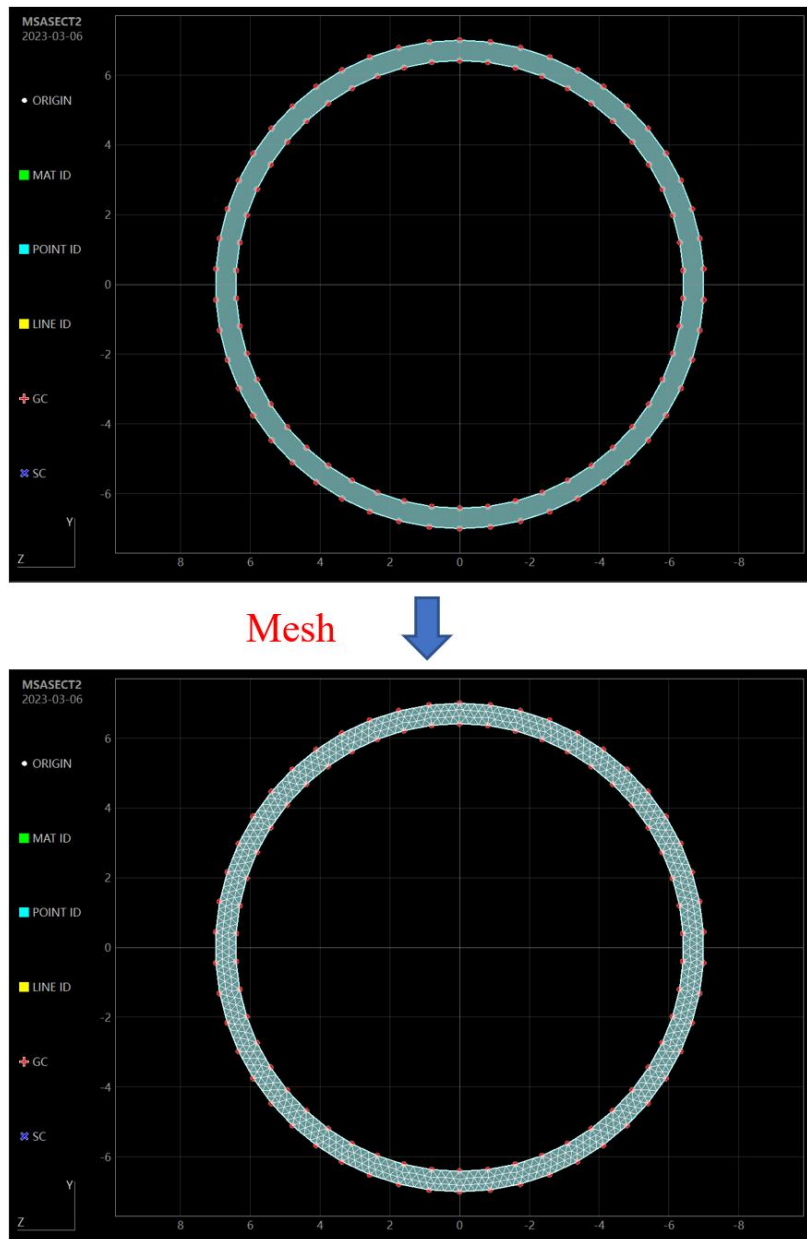
#### New, Open, Save, and Save As



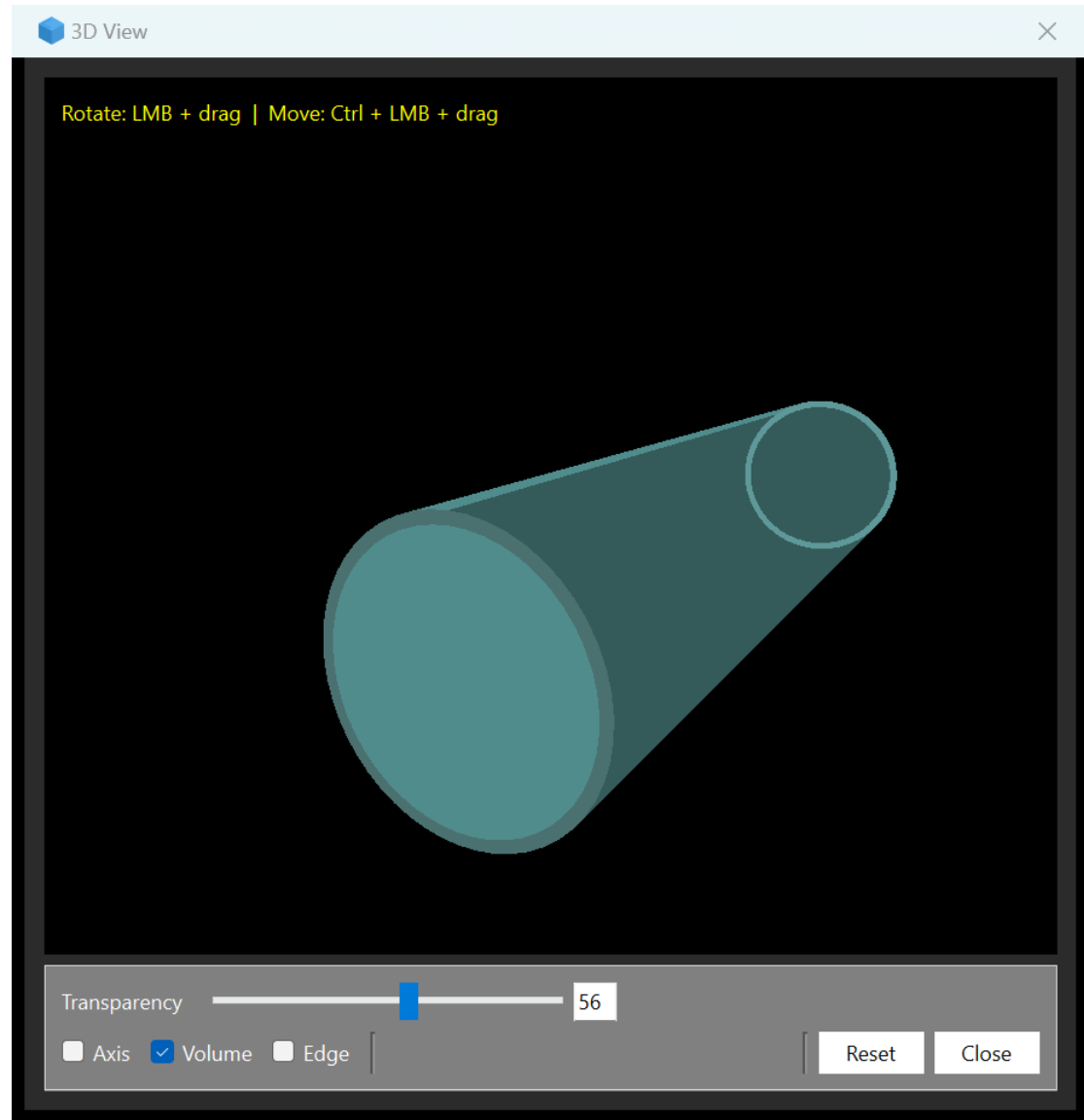
#### Visibility Setting



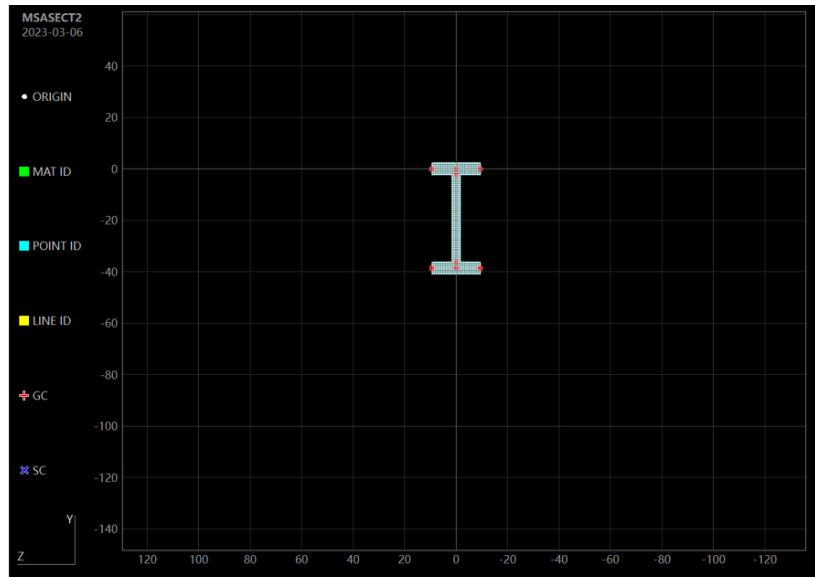
## Mesh



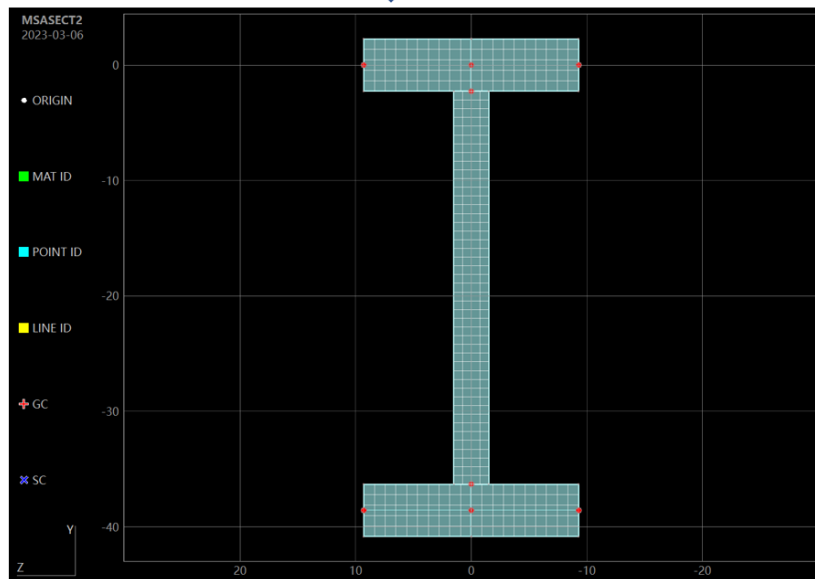
## **3D View**



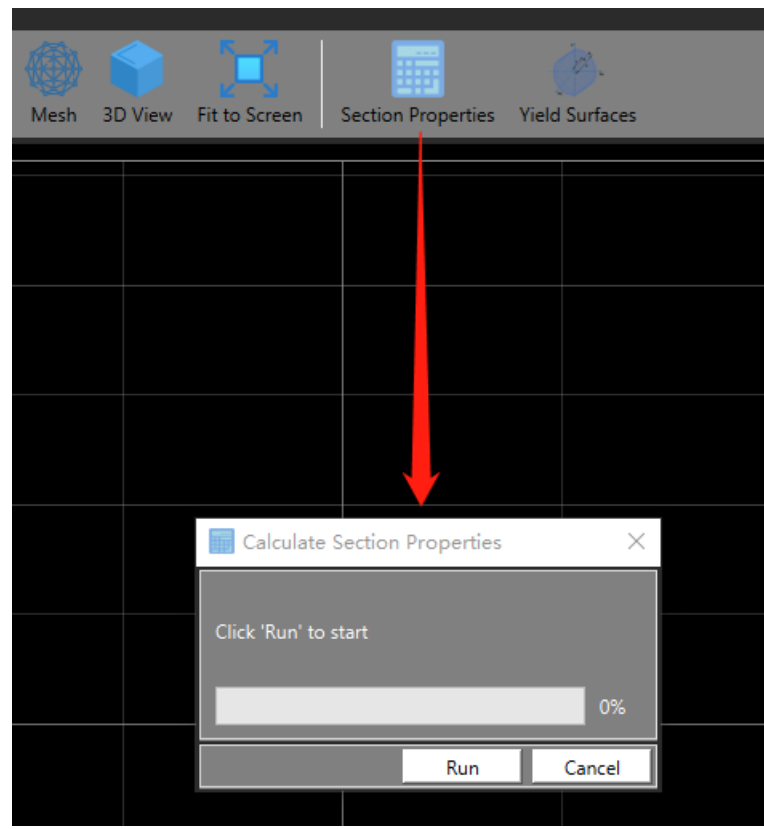
## Fit to Screen



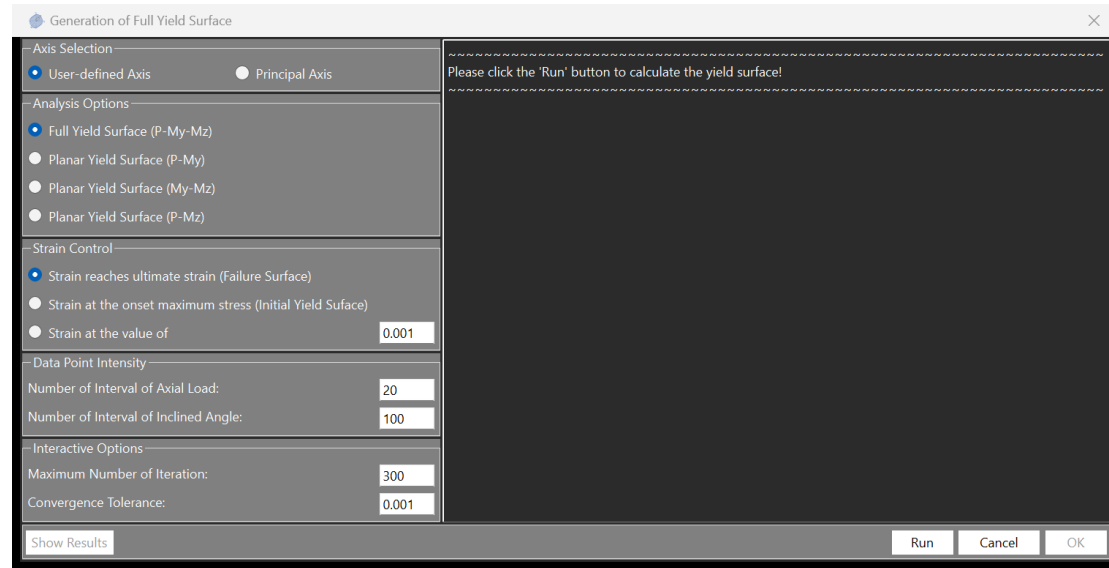
Fit to Screen

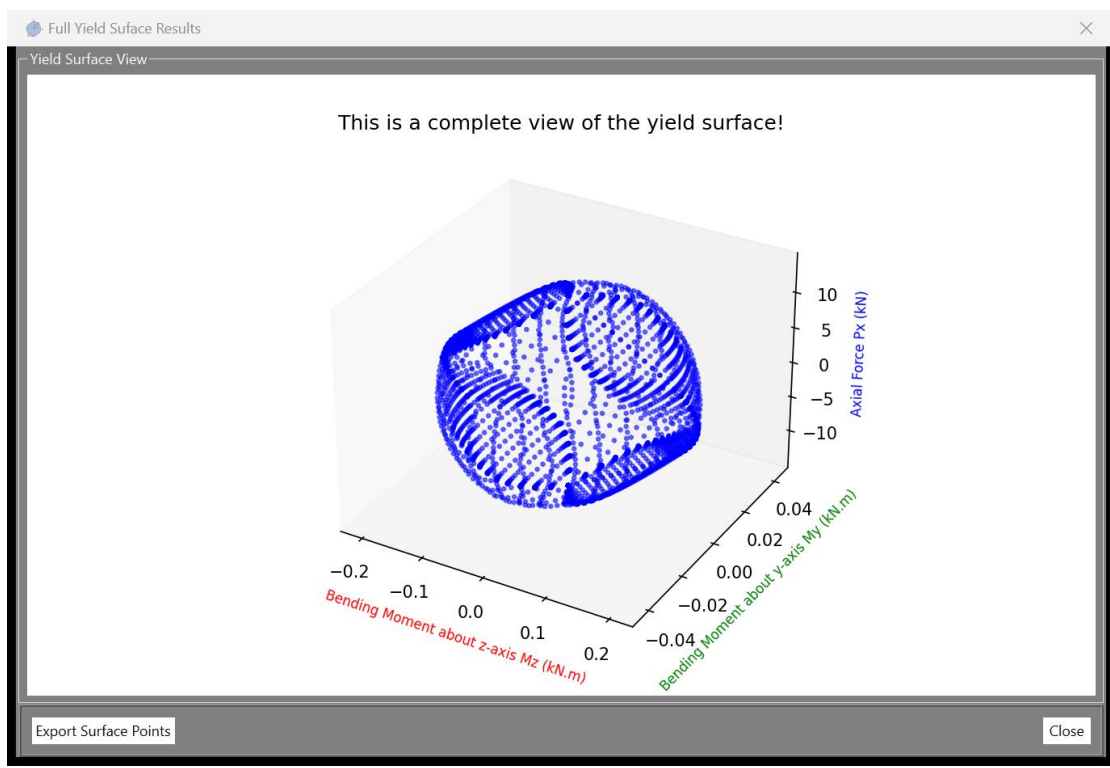


## Section properties



## Yield surface





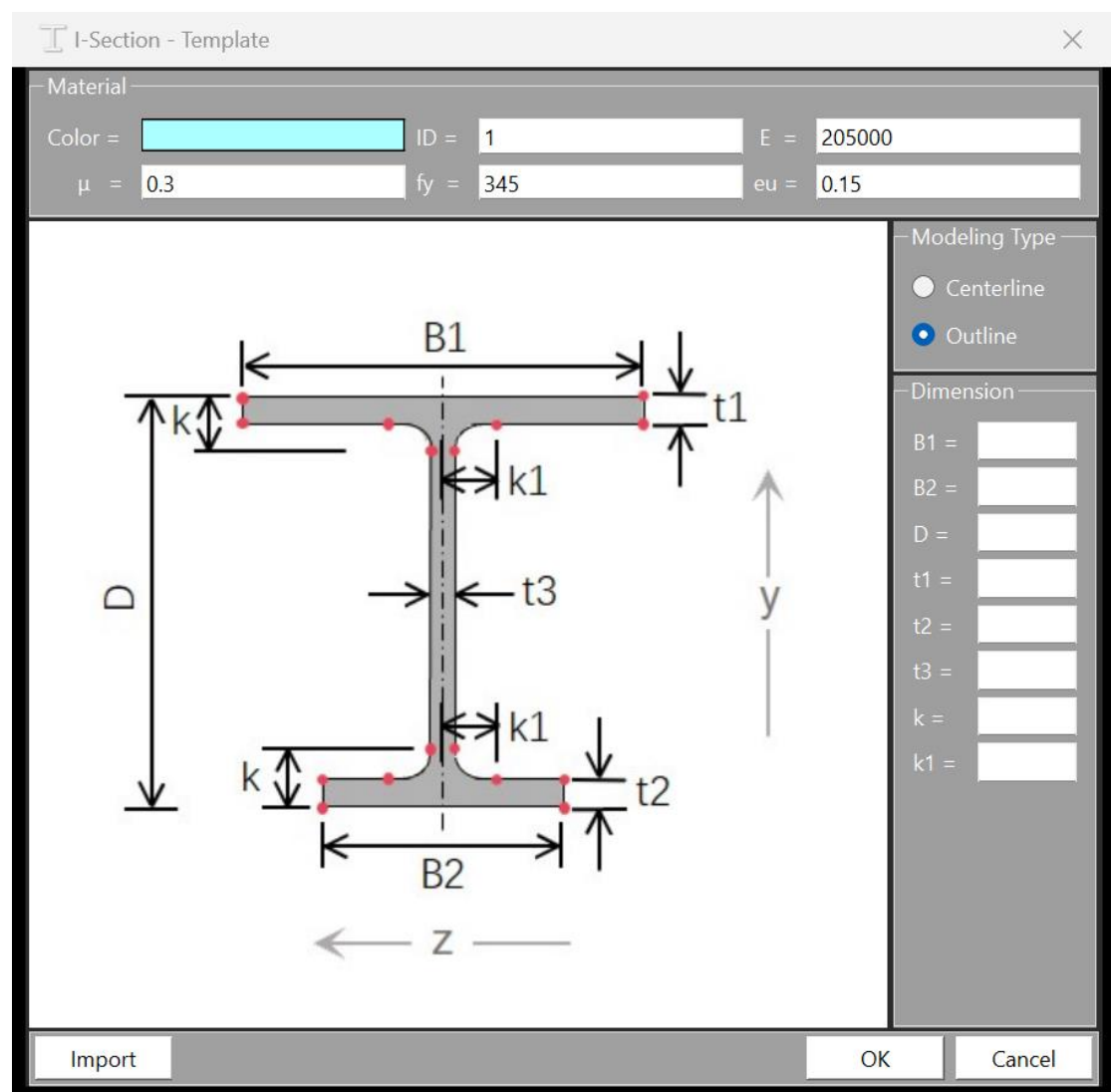
## 2.2.2 Template tab

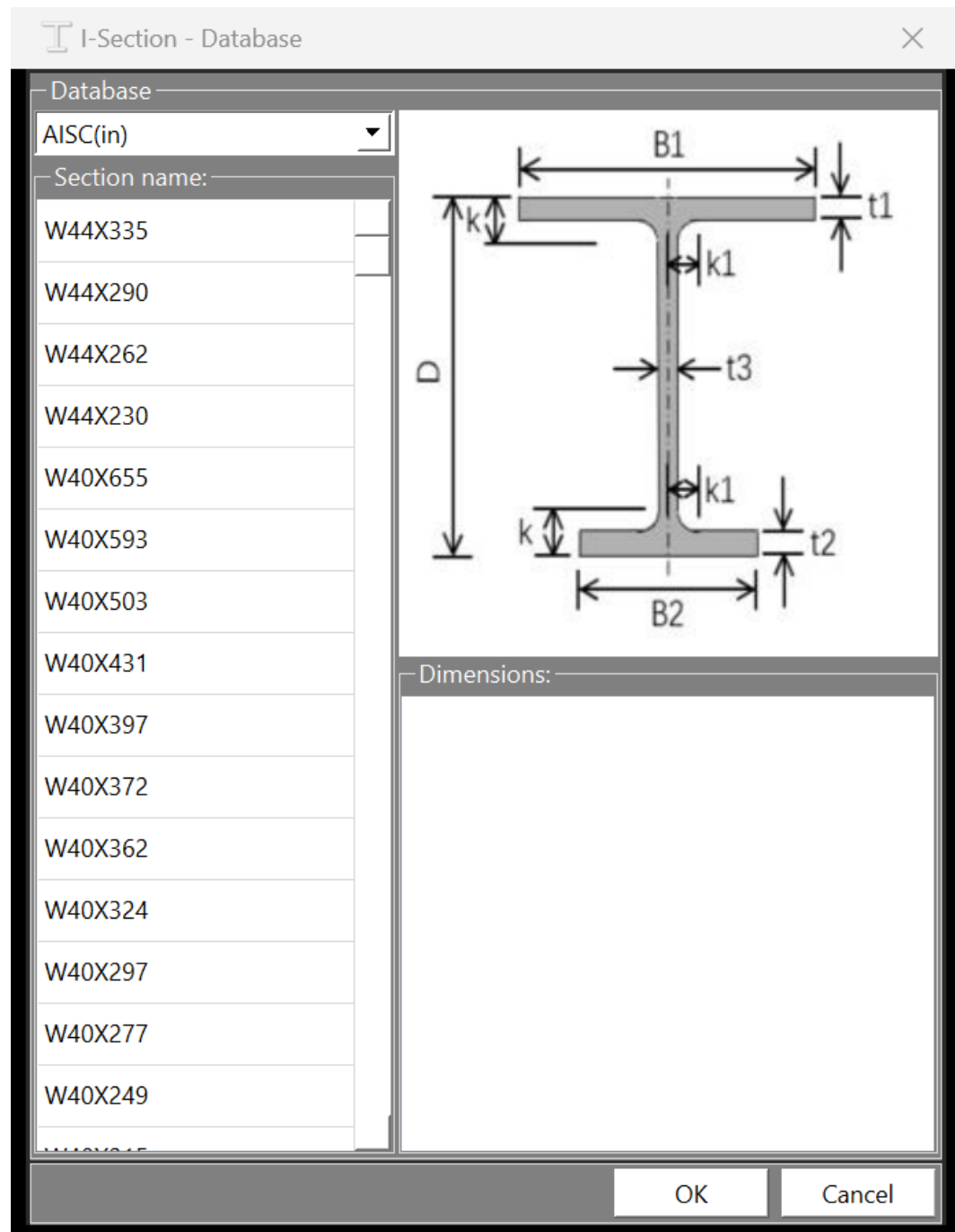
The Template tab in the ribbon menu is shown below:



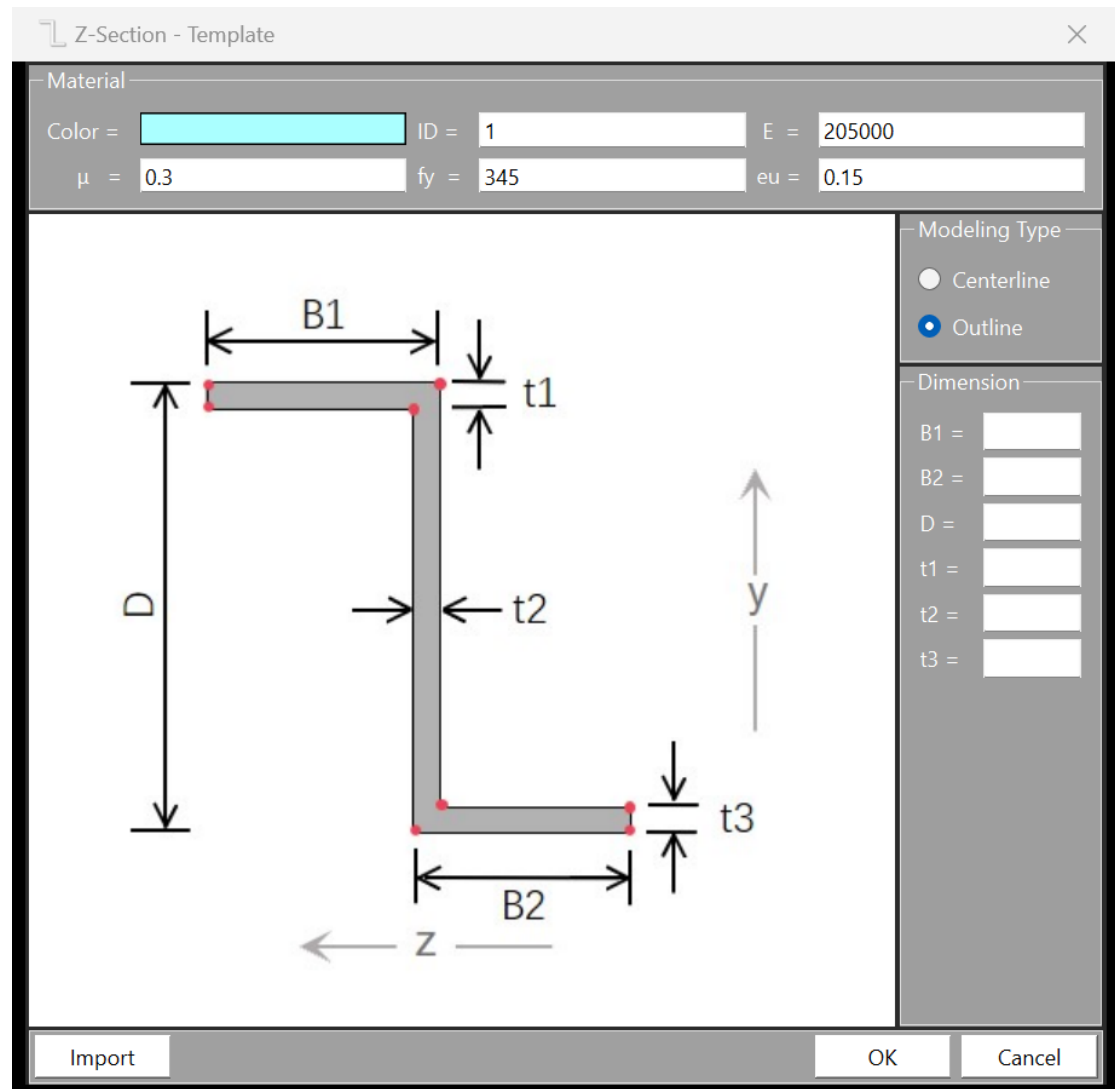
### Open Section

#### I-Section

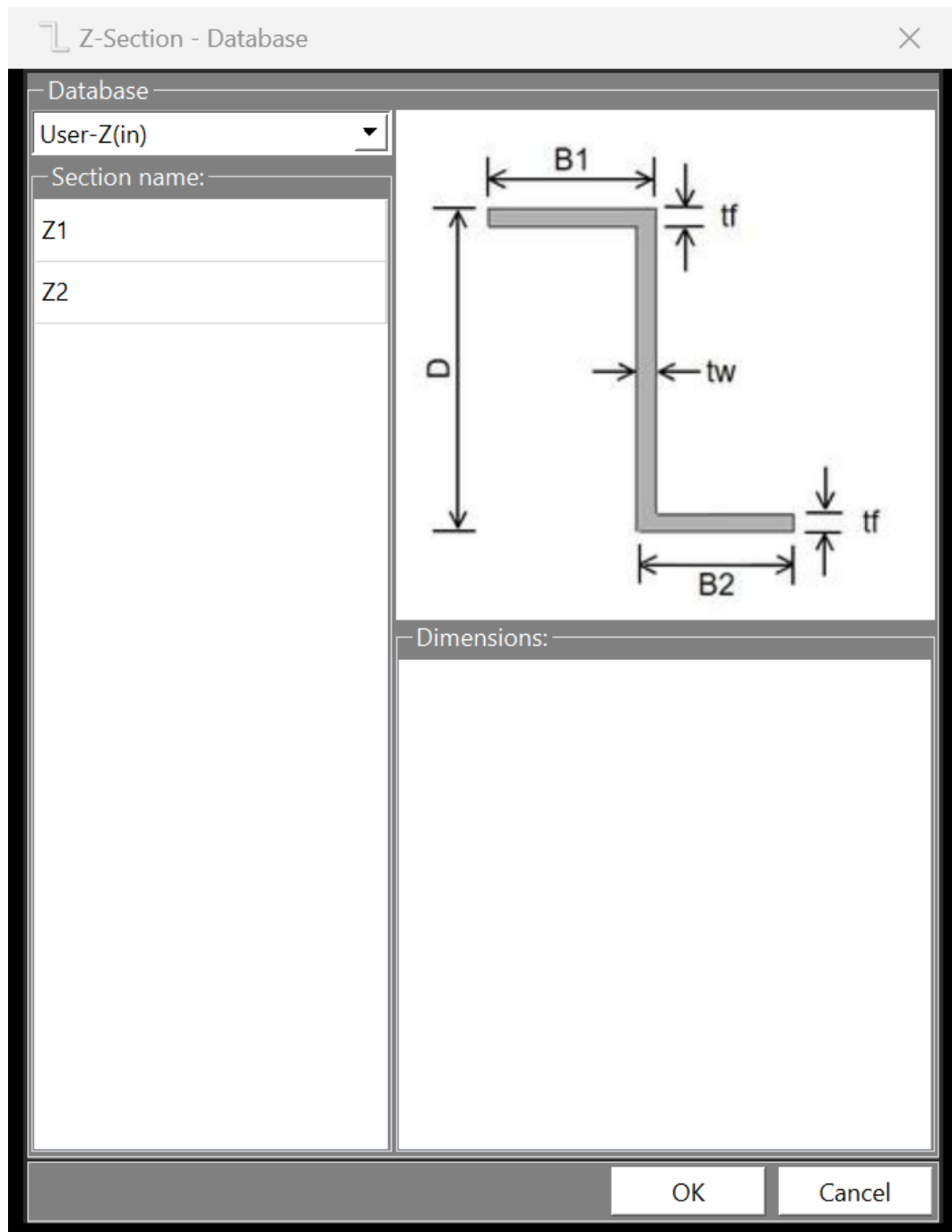


**I-Section -> Import**

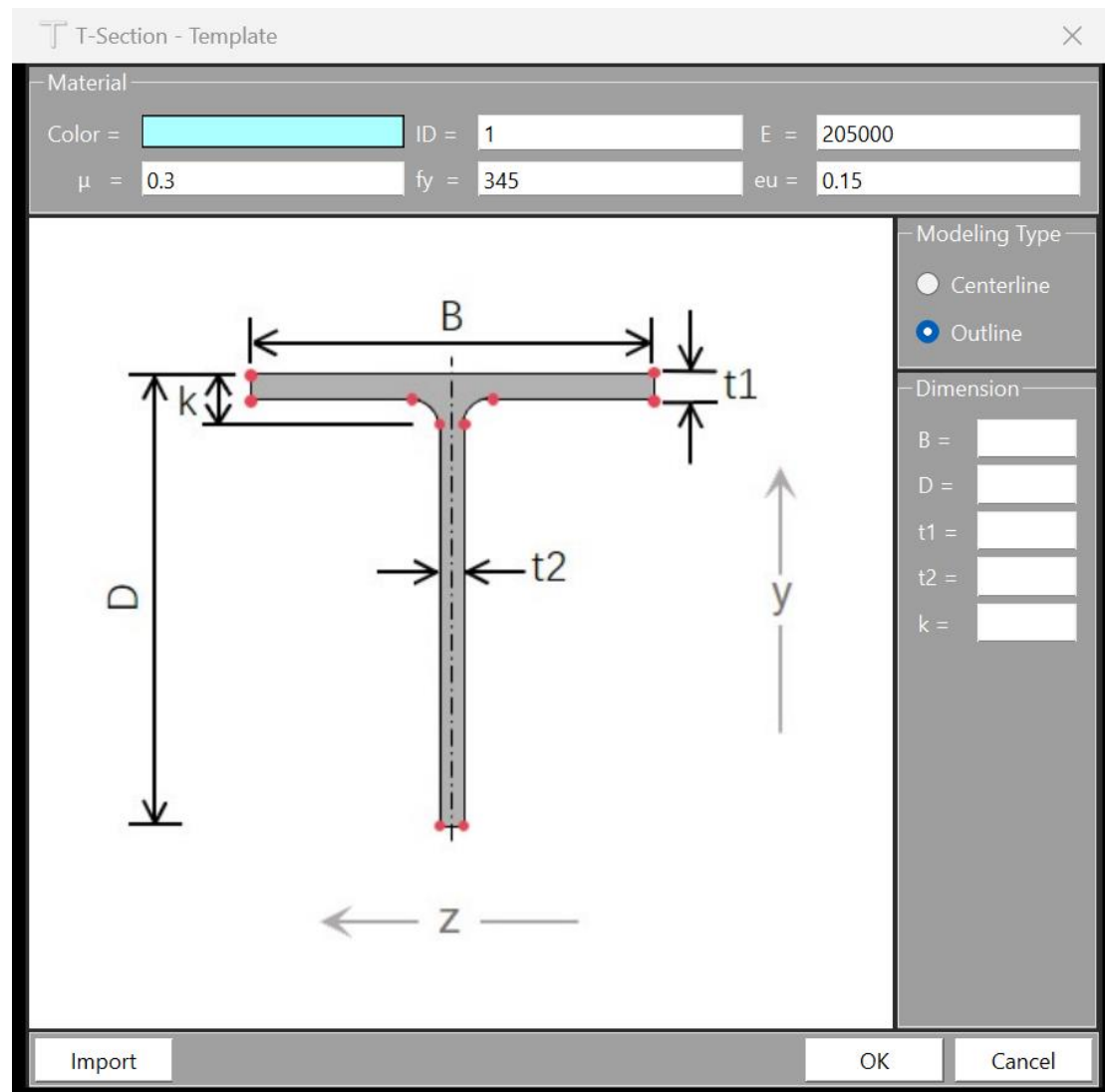
## Z-Section



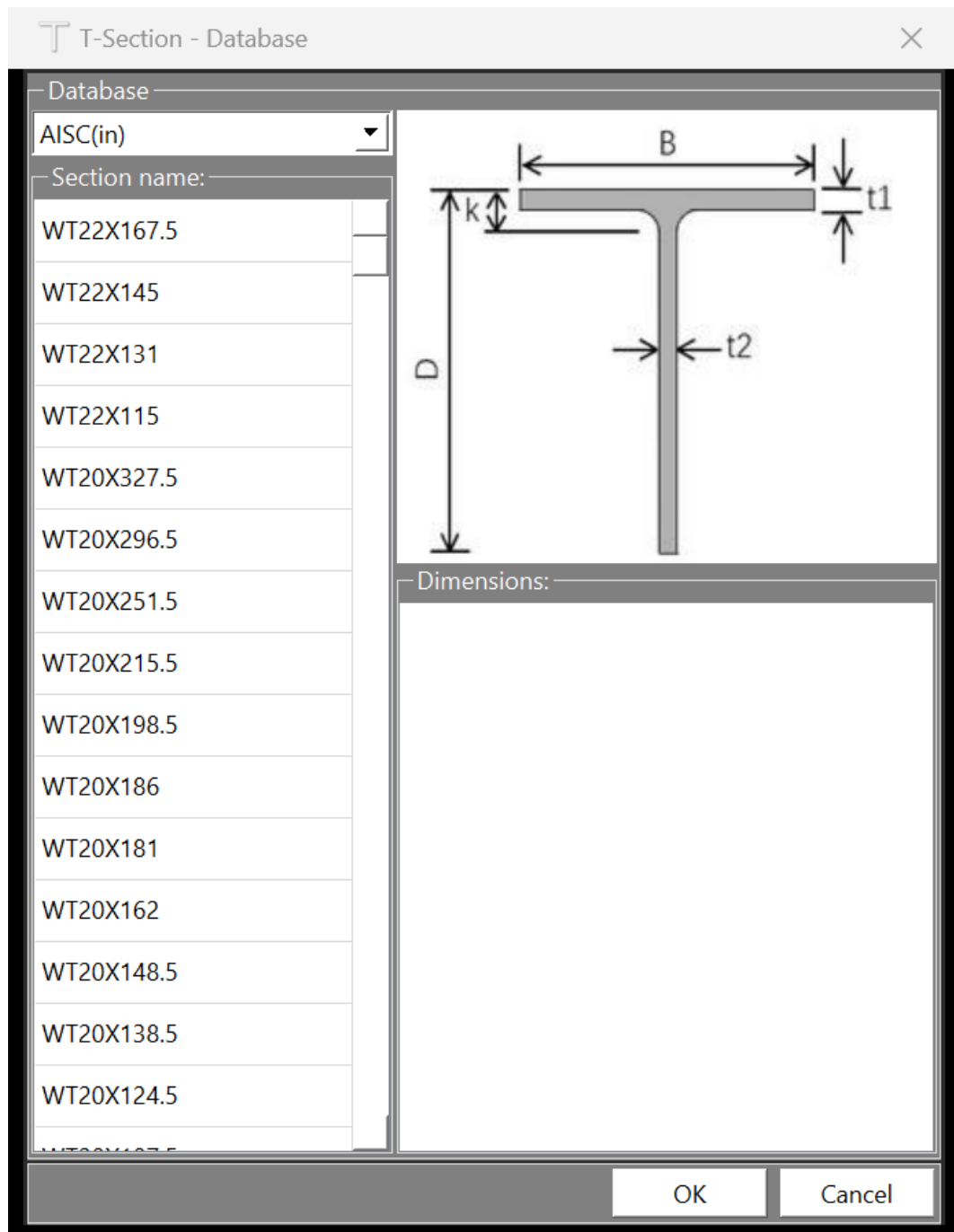
## Z-Section -> Import



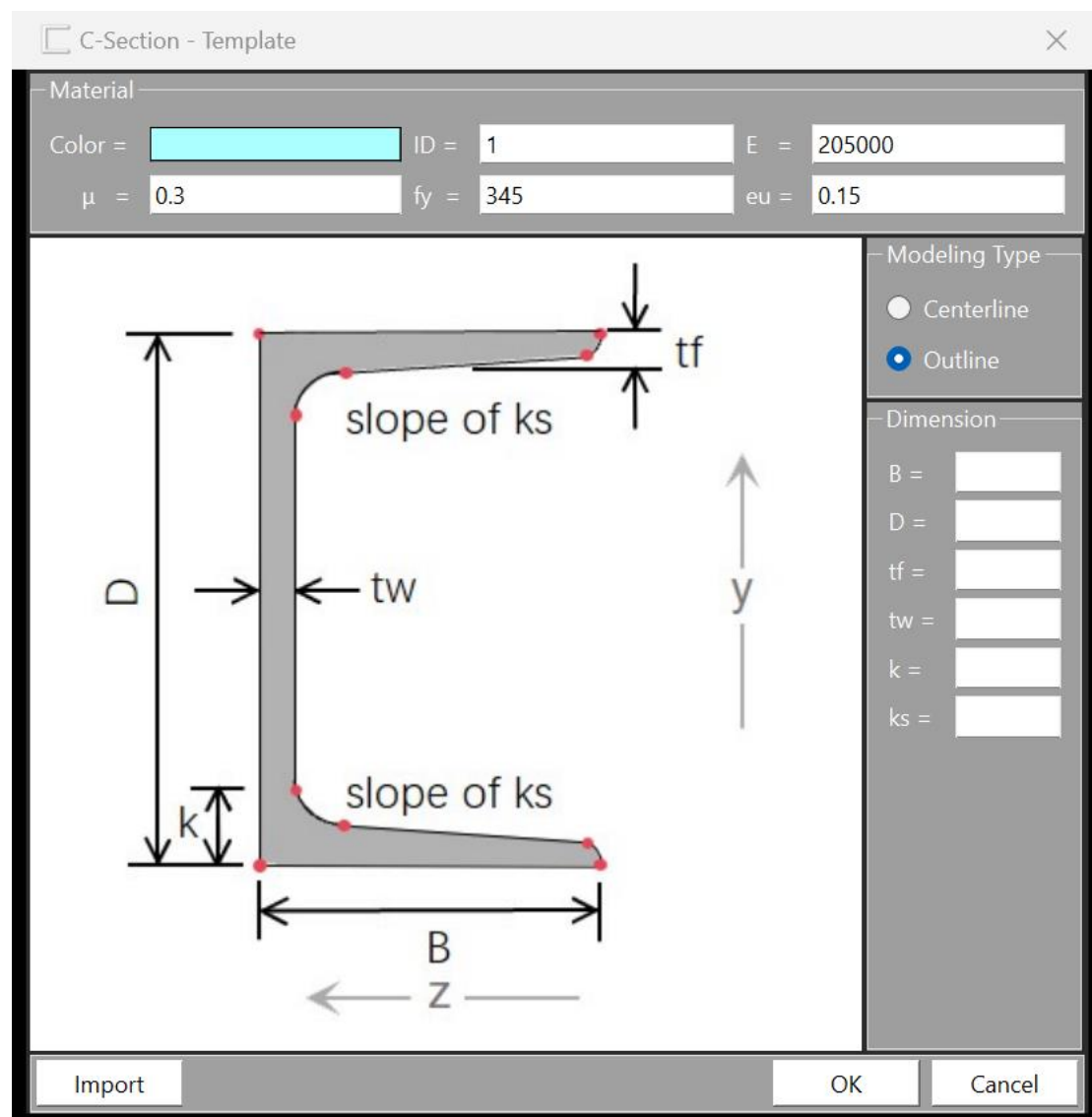
## T-Section



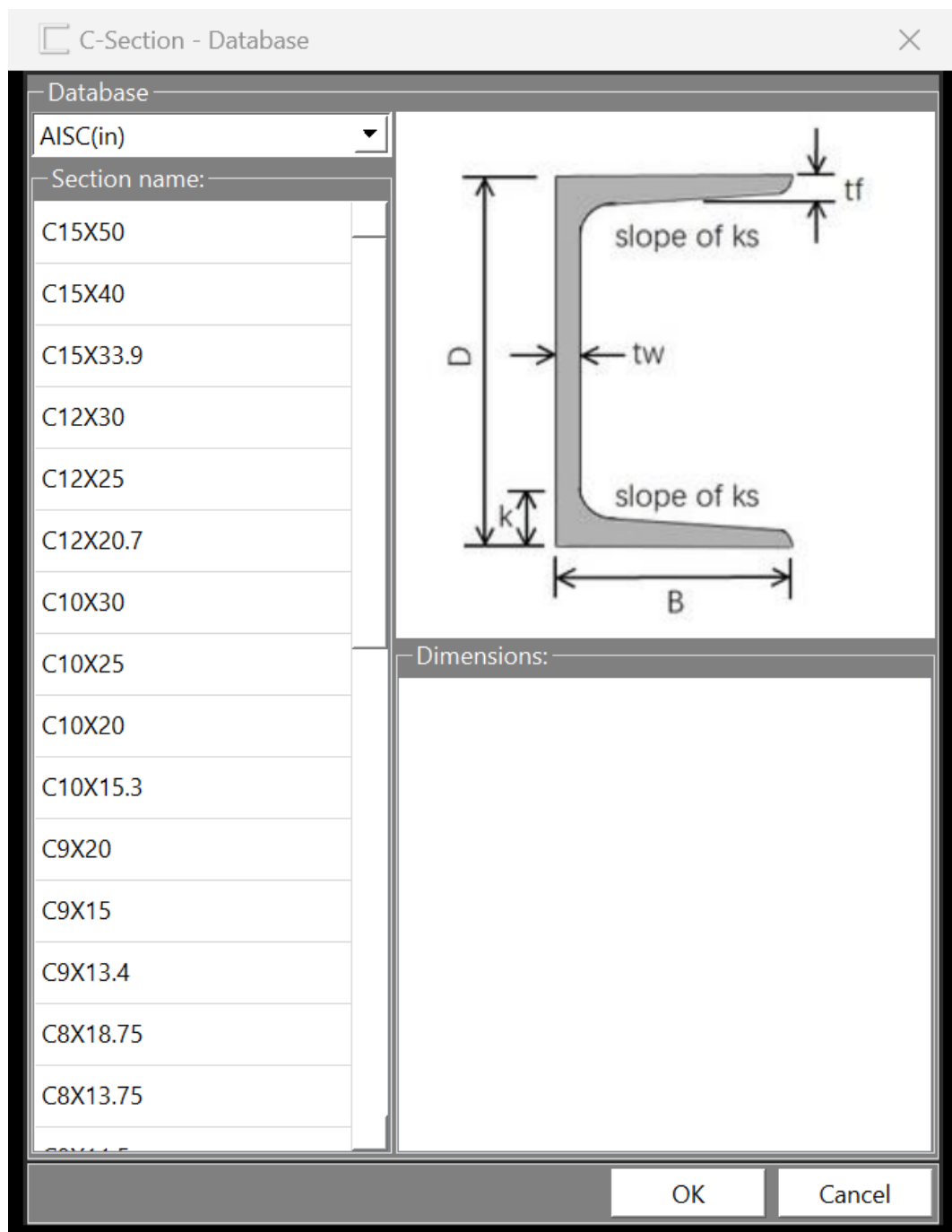
## T-Section -> Import



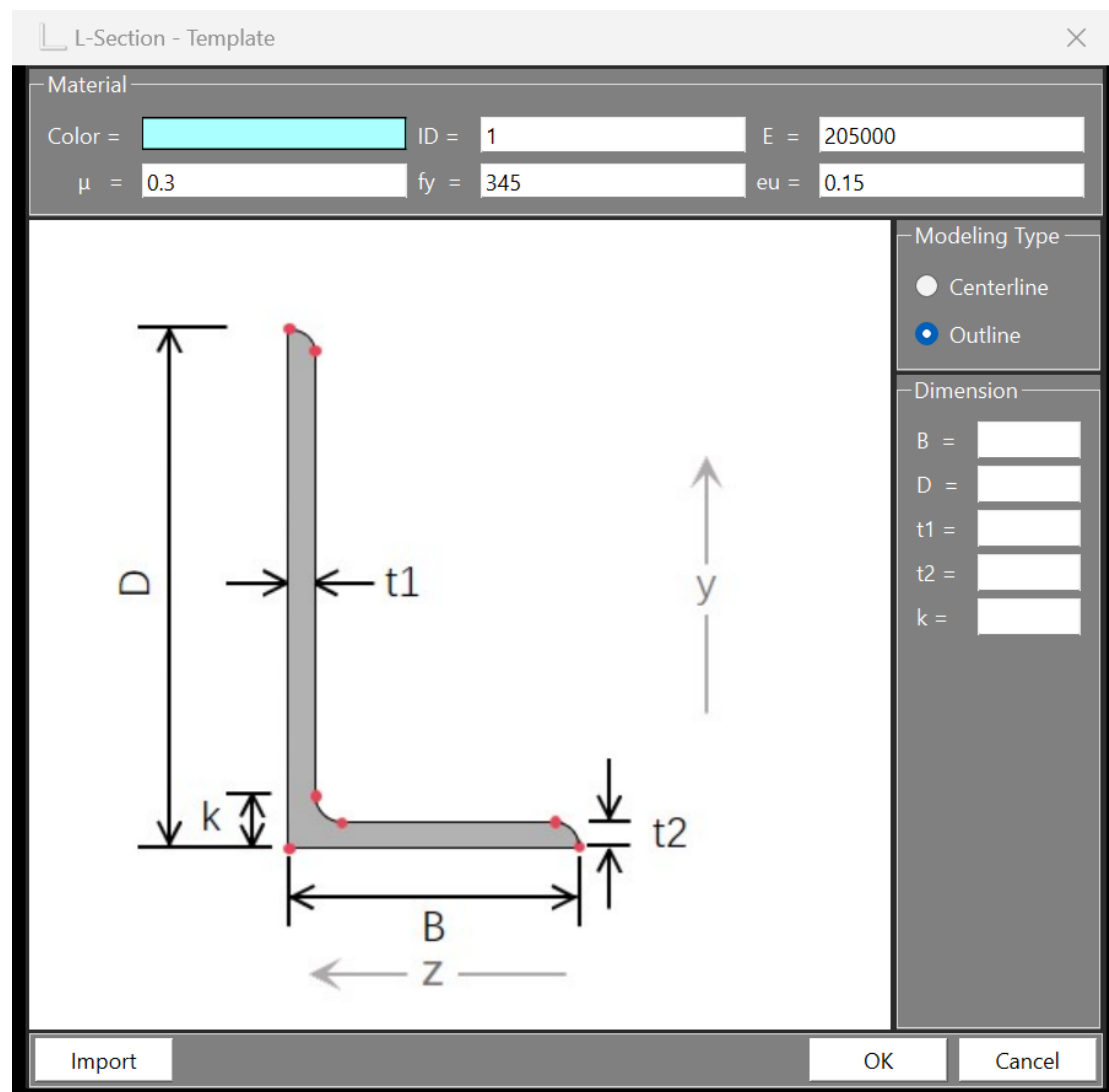
## C-Section



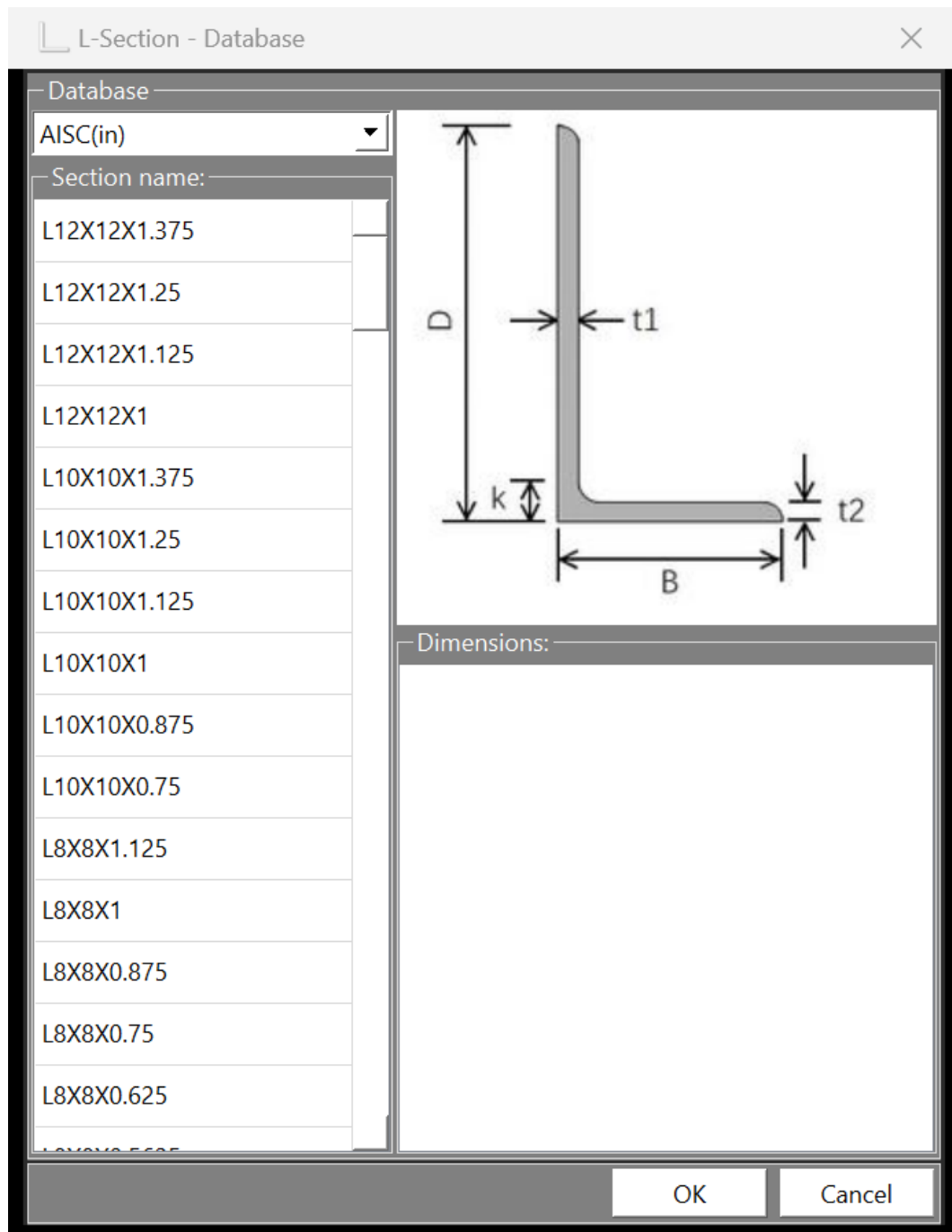
## C-Section -> Import



## L-Section -> Import

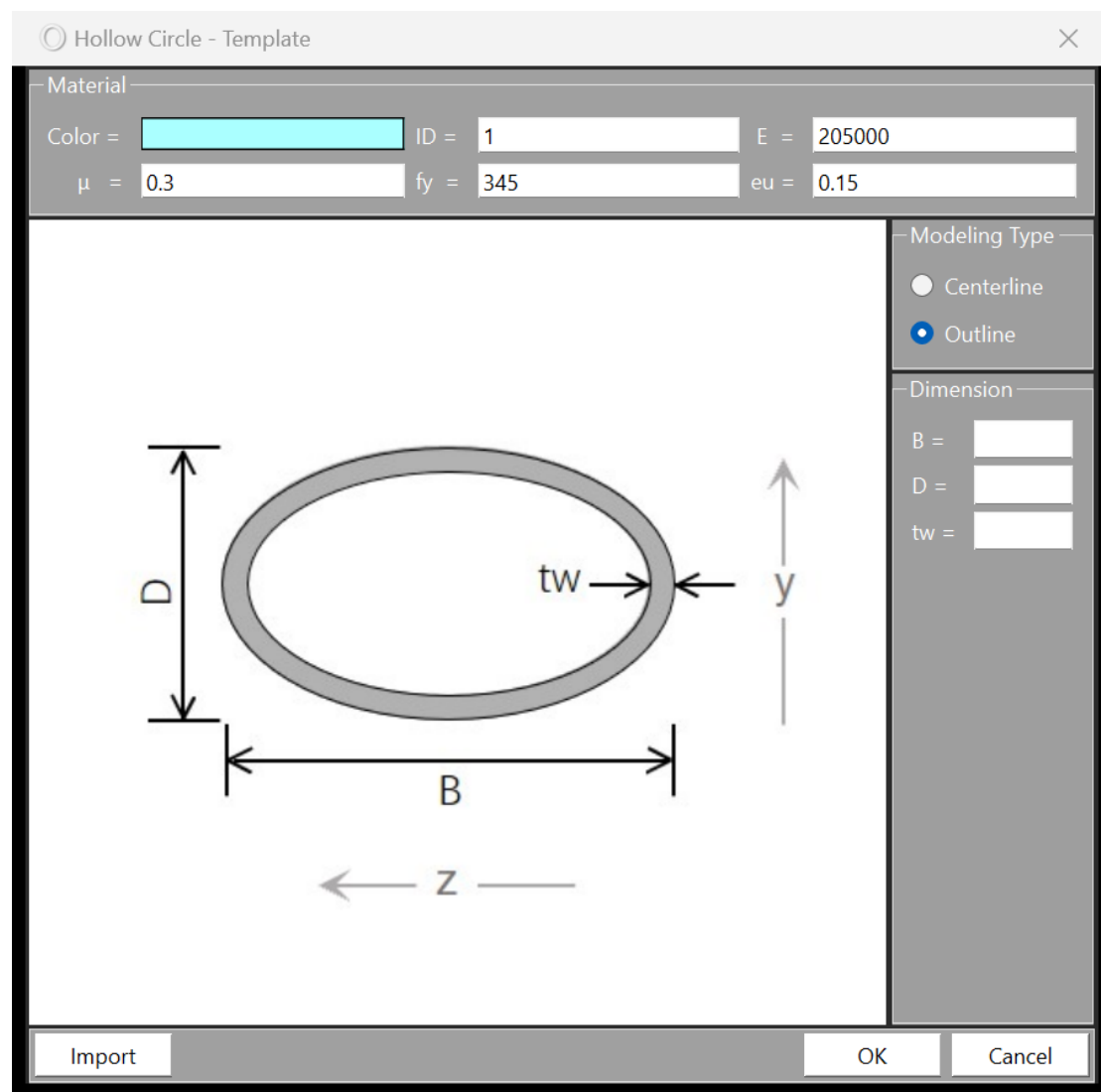


## L-Section -> Import

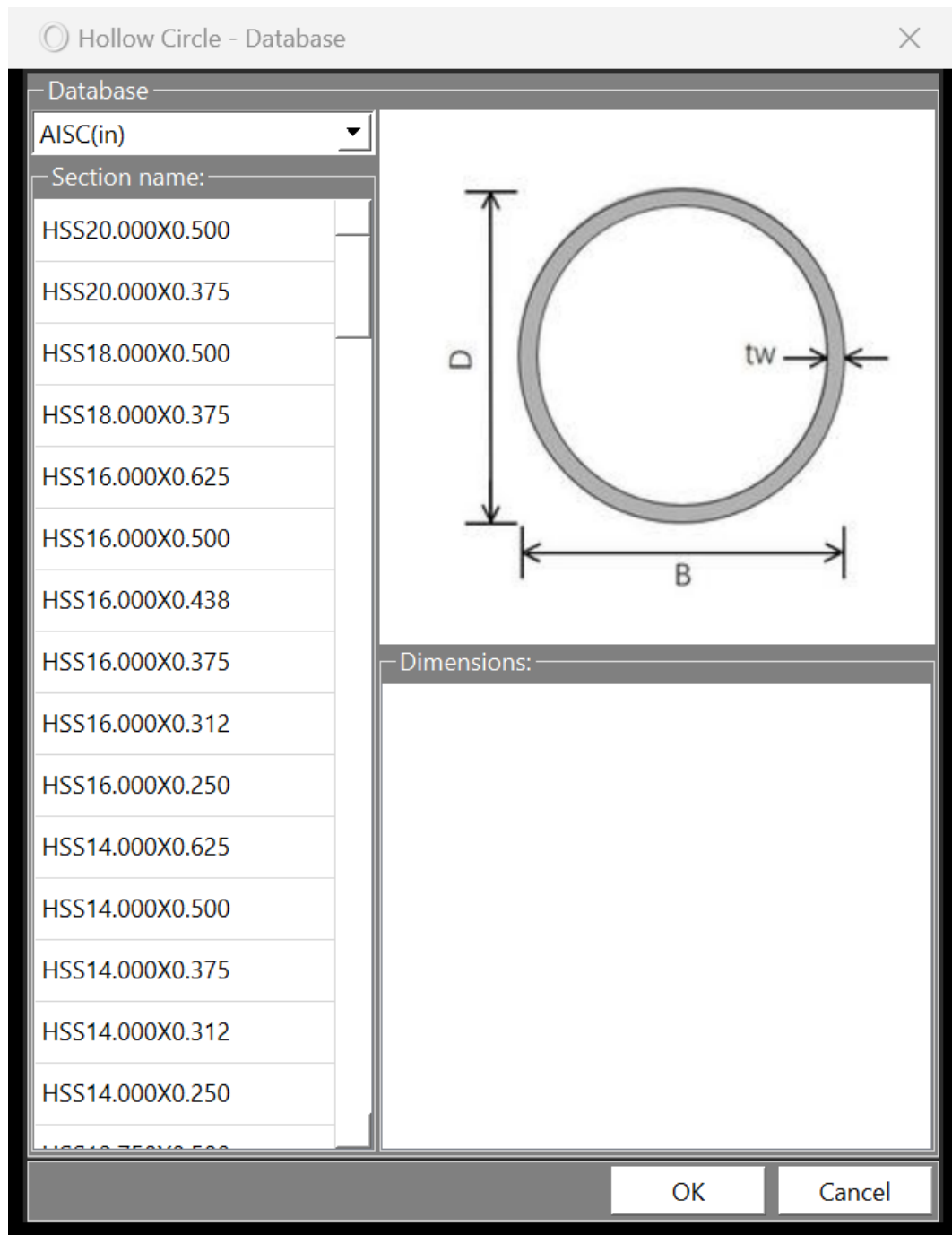


## Closed Section

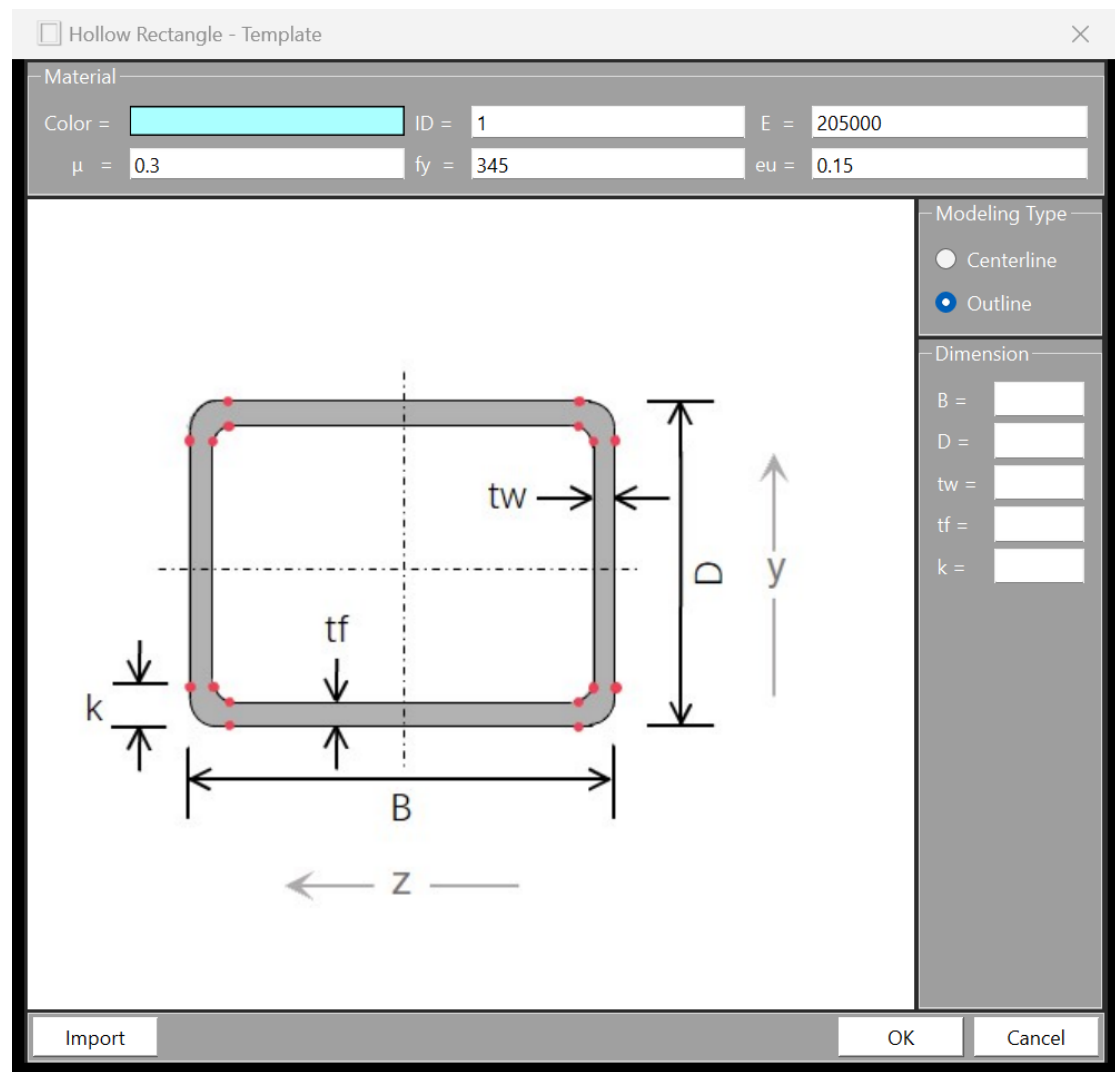
### Hollow Circle



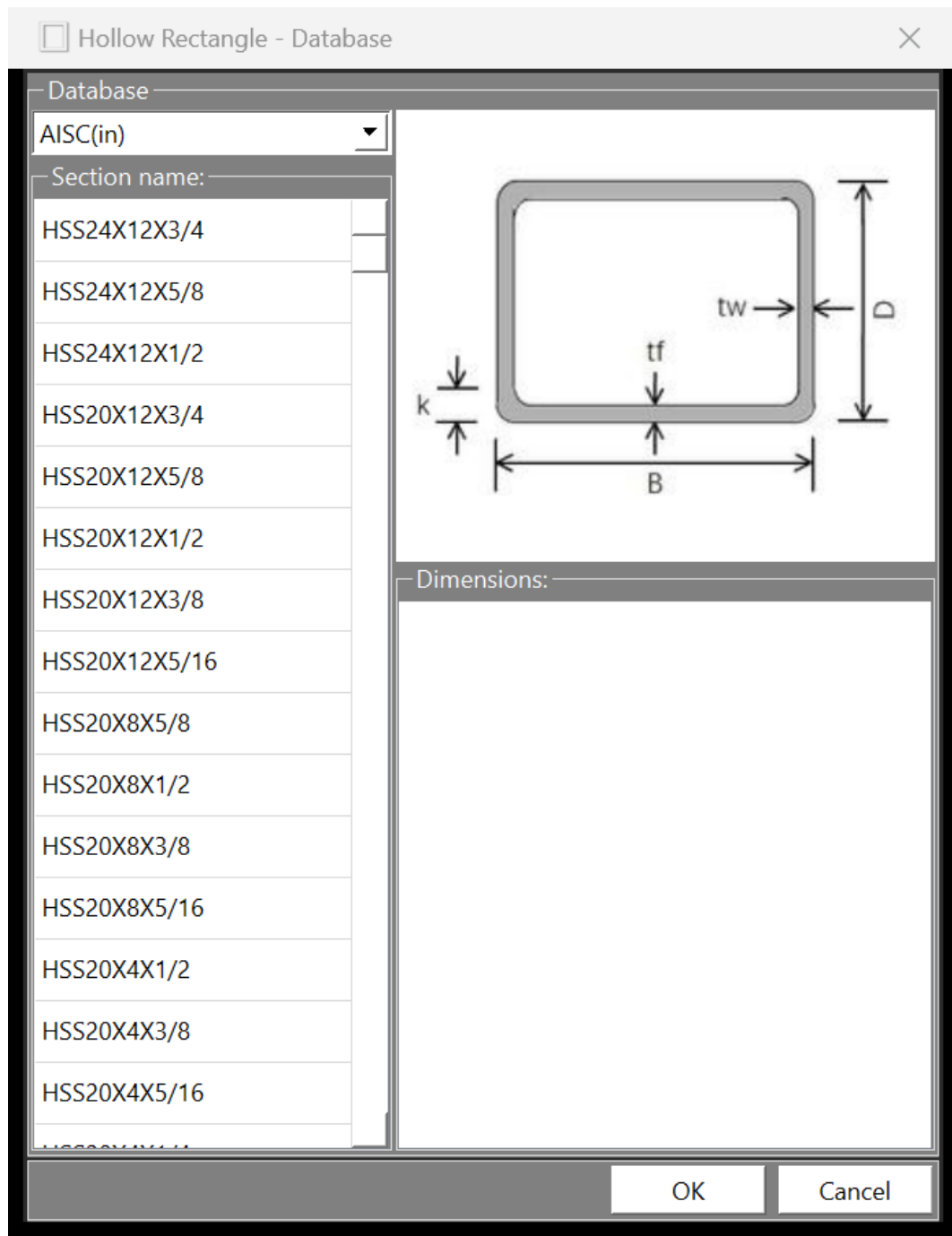
## Hollow Circle -> Import



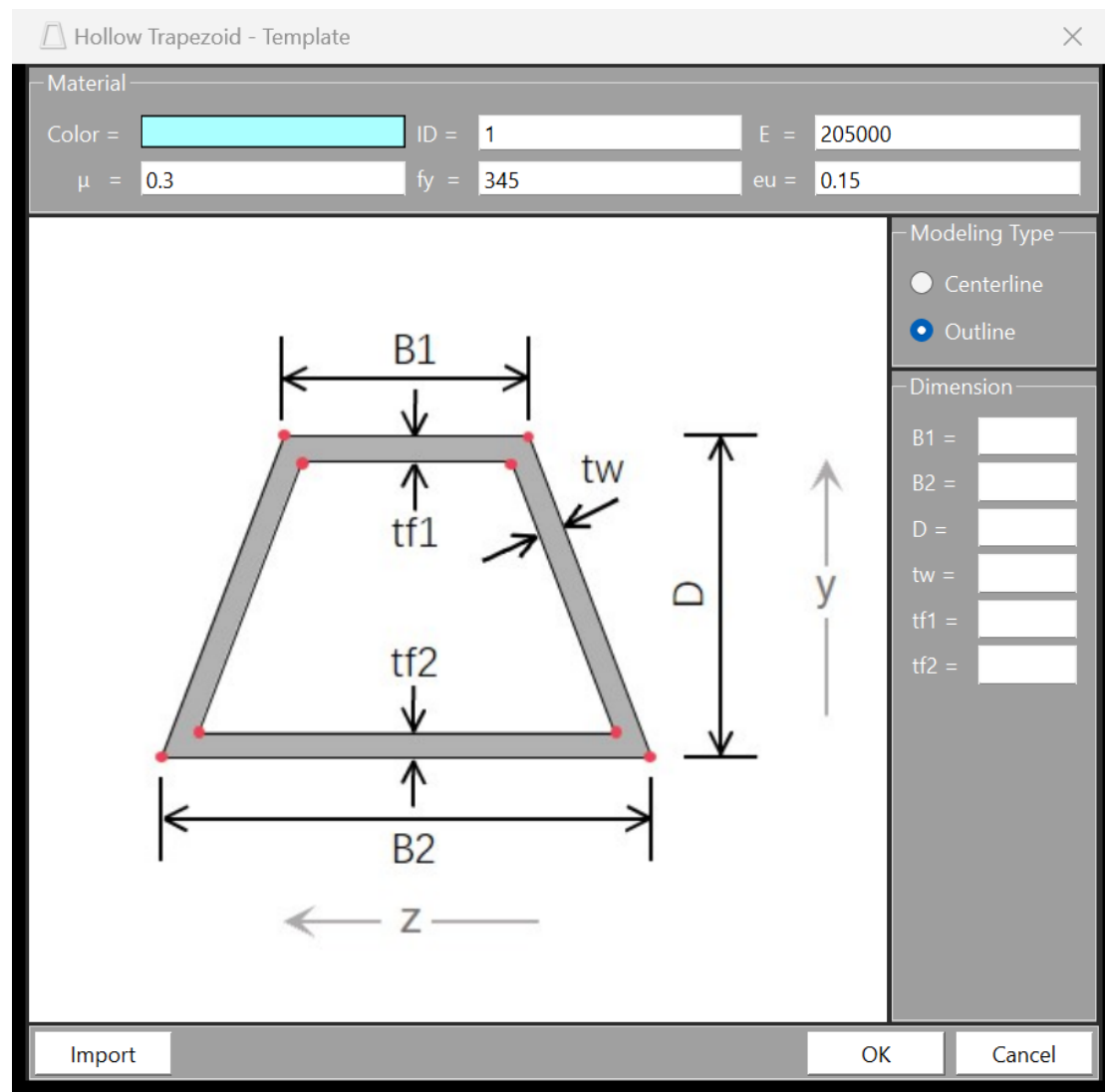
## Hollow Rectangle



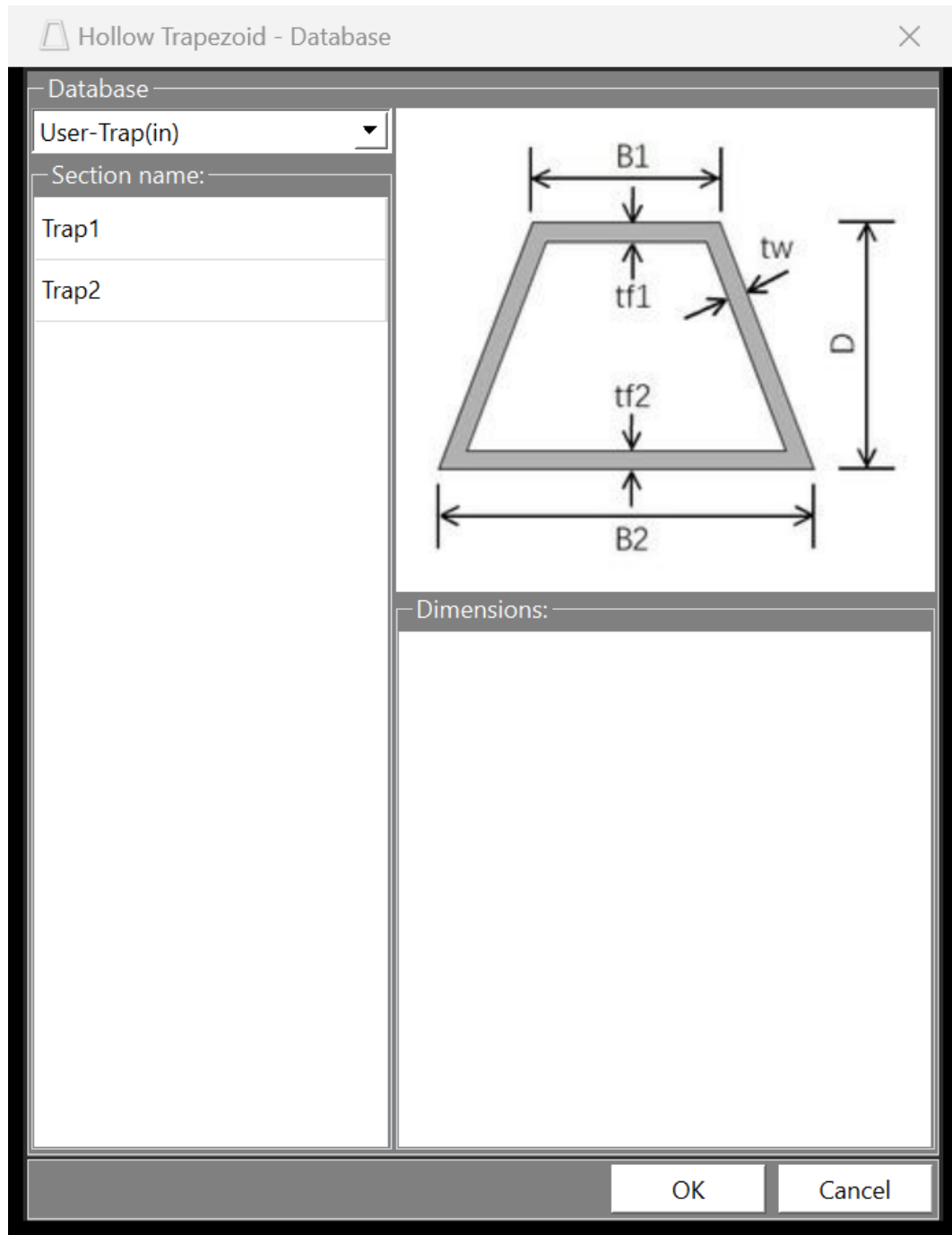
## Hollow Rectangle -> Import



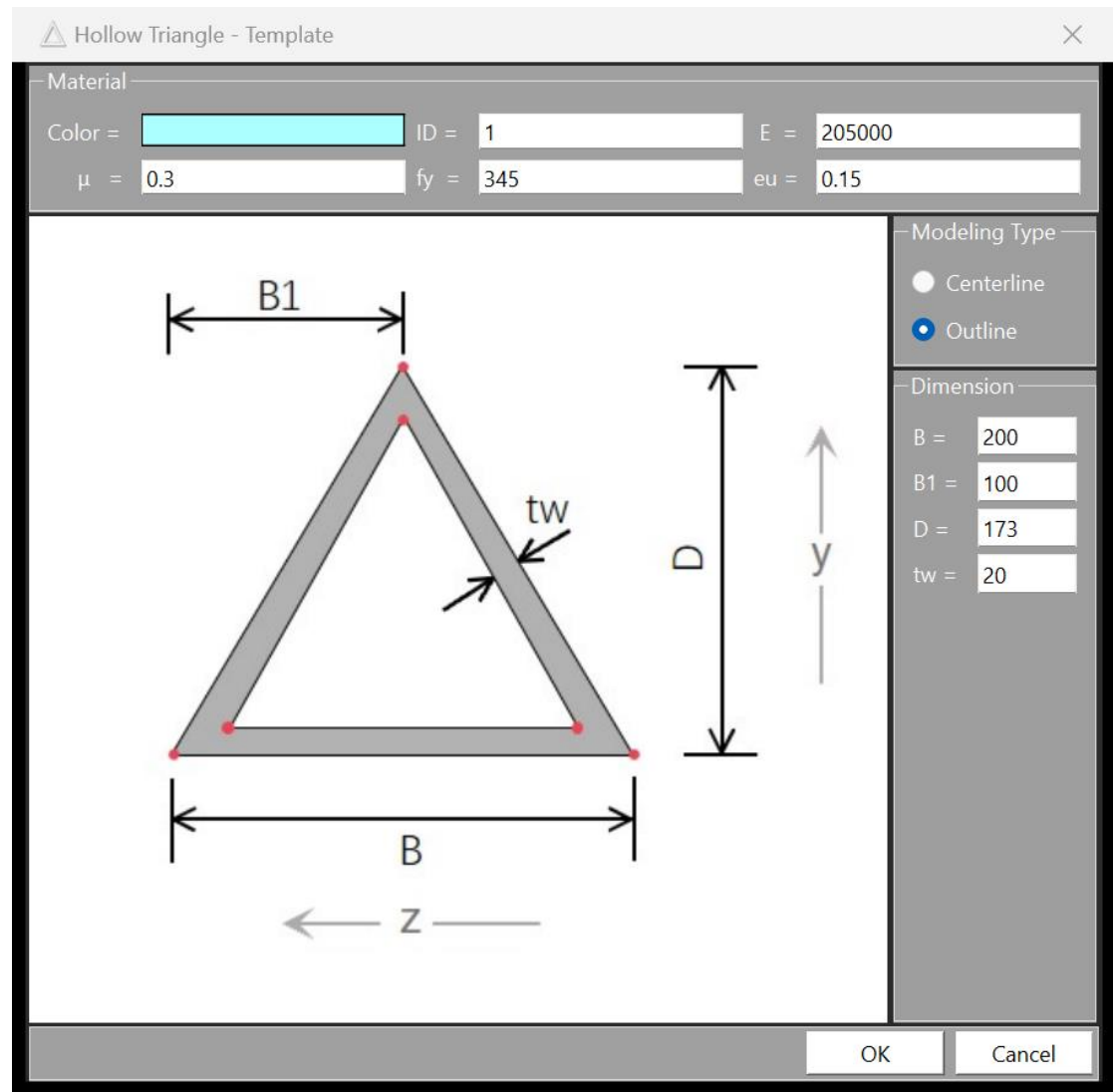
## Hollow Trapezoid -> Import



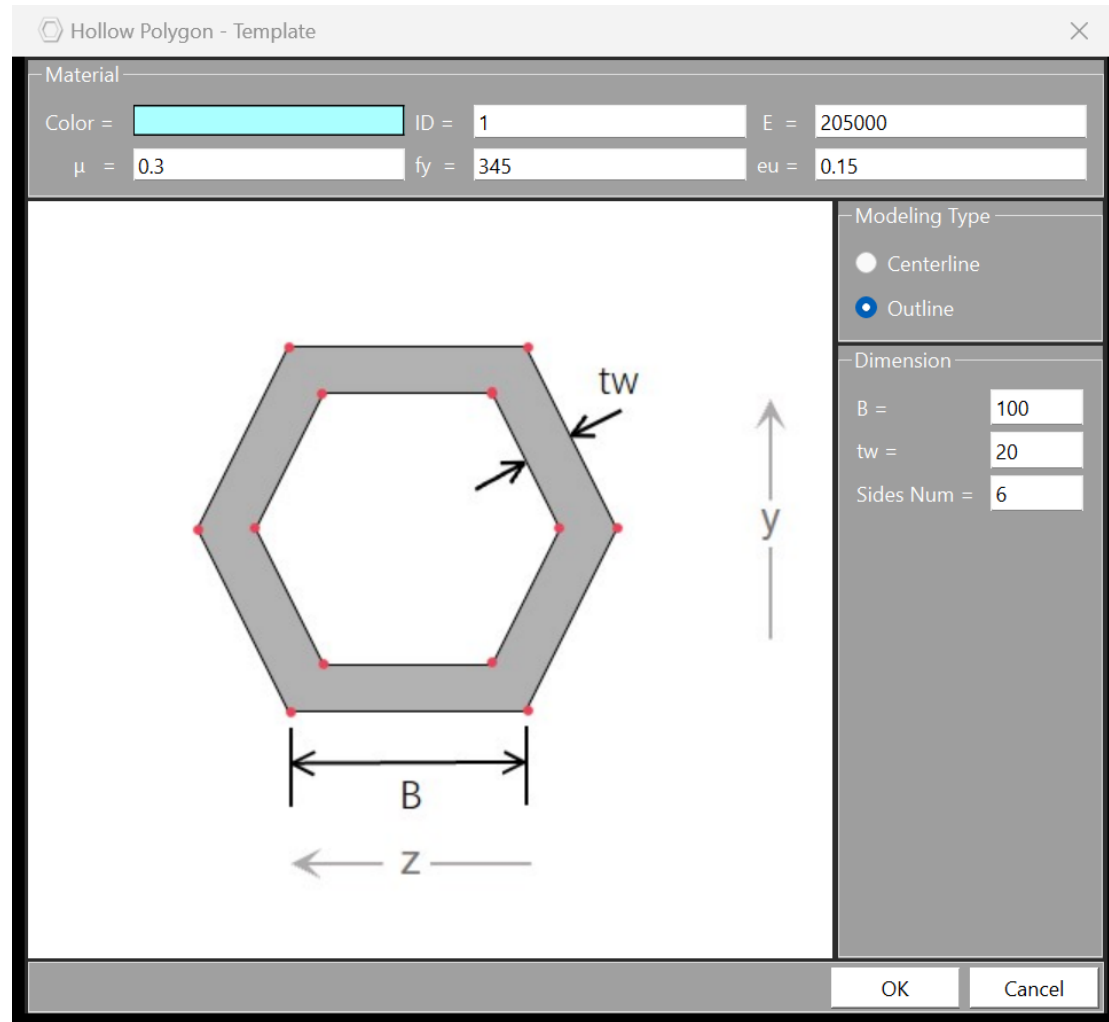
### Hollow Trapezoid -> Import



## Hollow Triangle

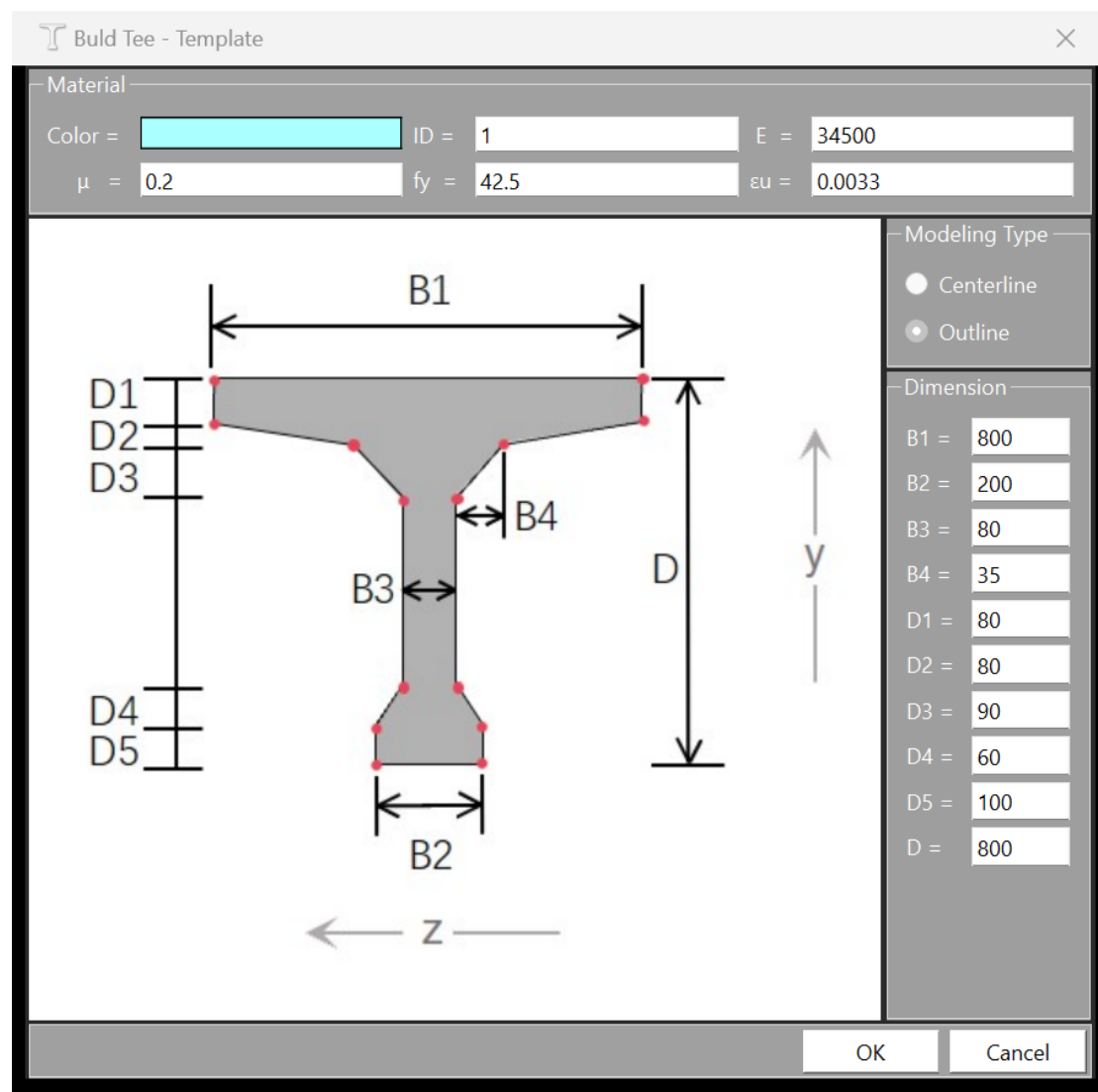


## Hollow Polygon

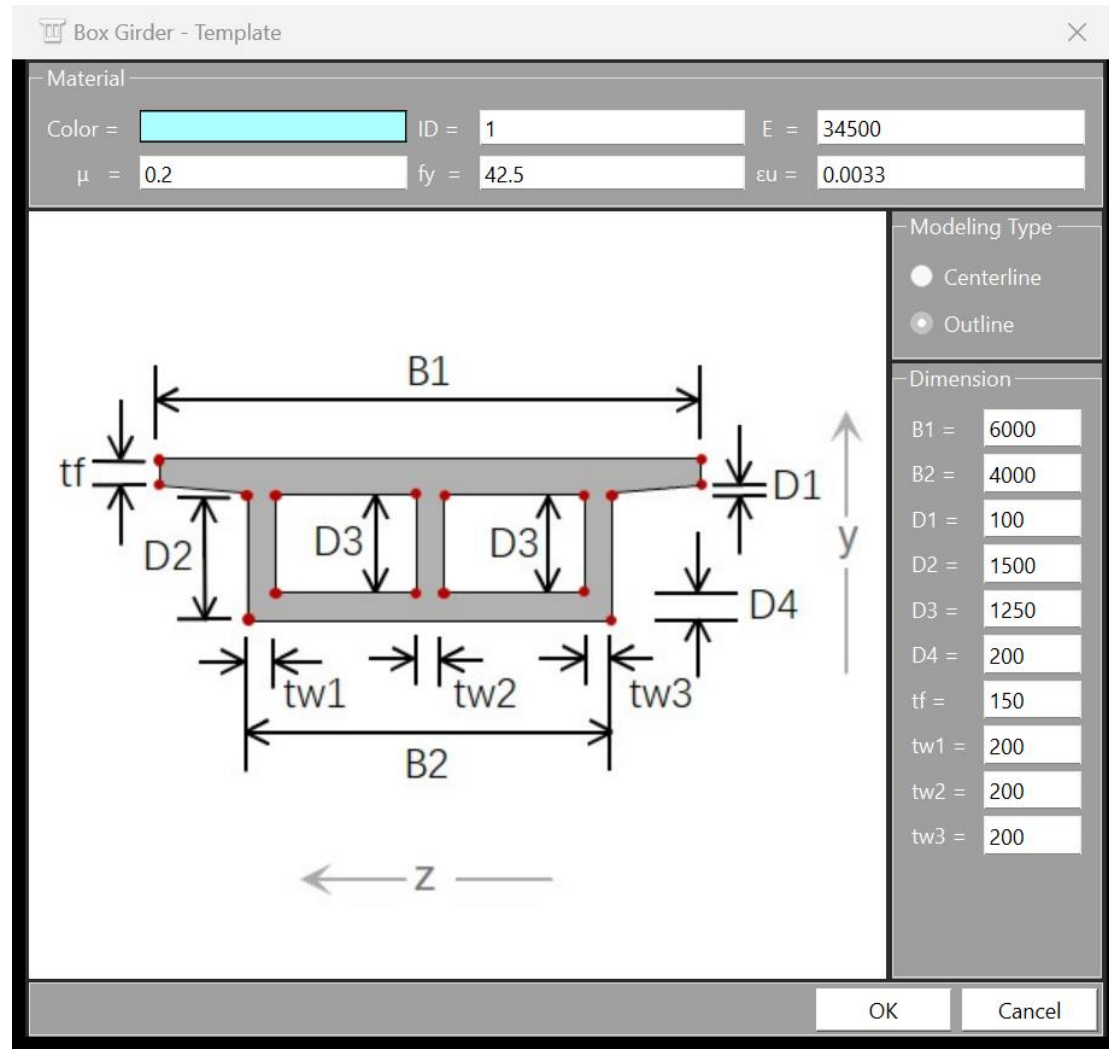


## Girder Section

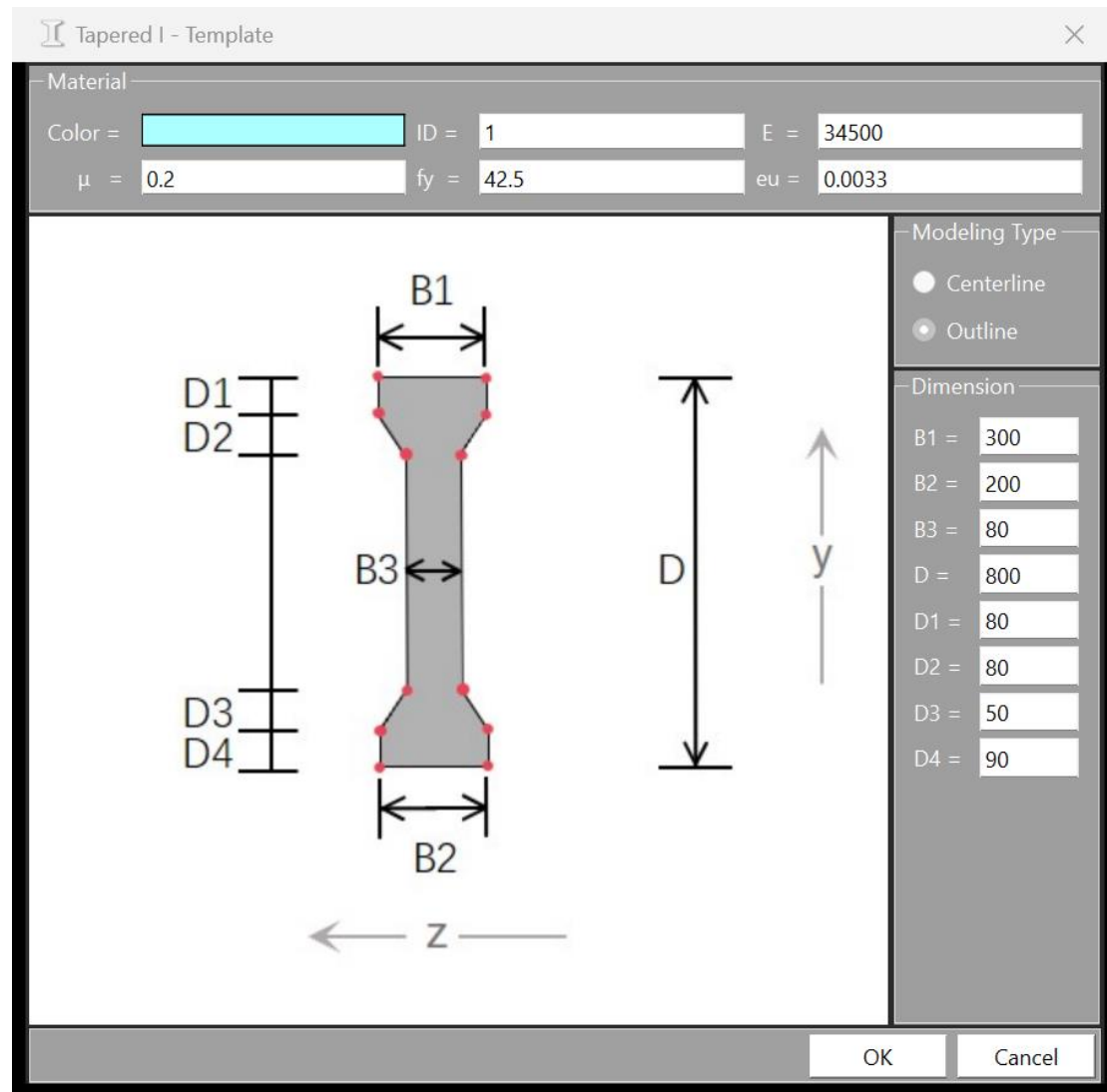
### Buld Tee



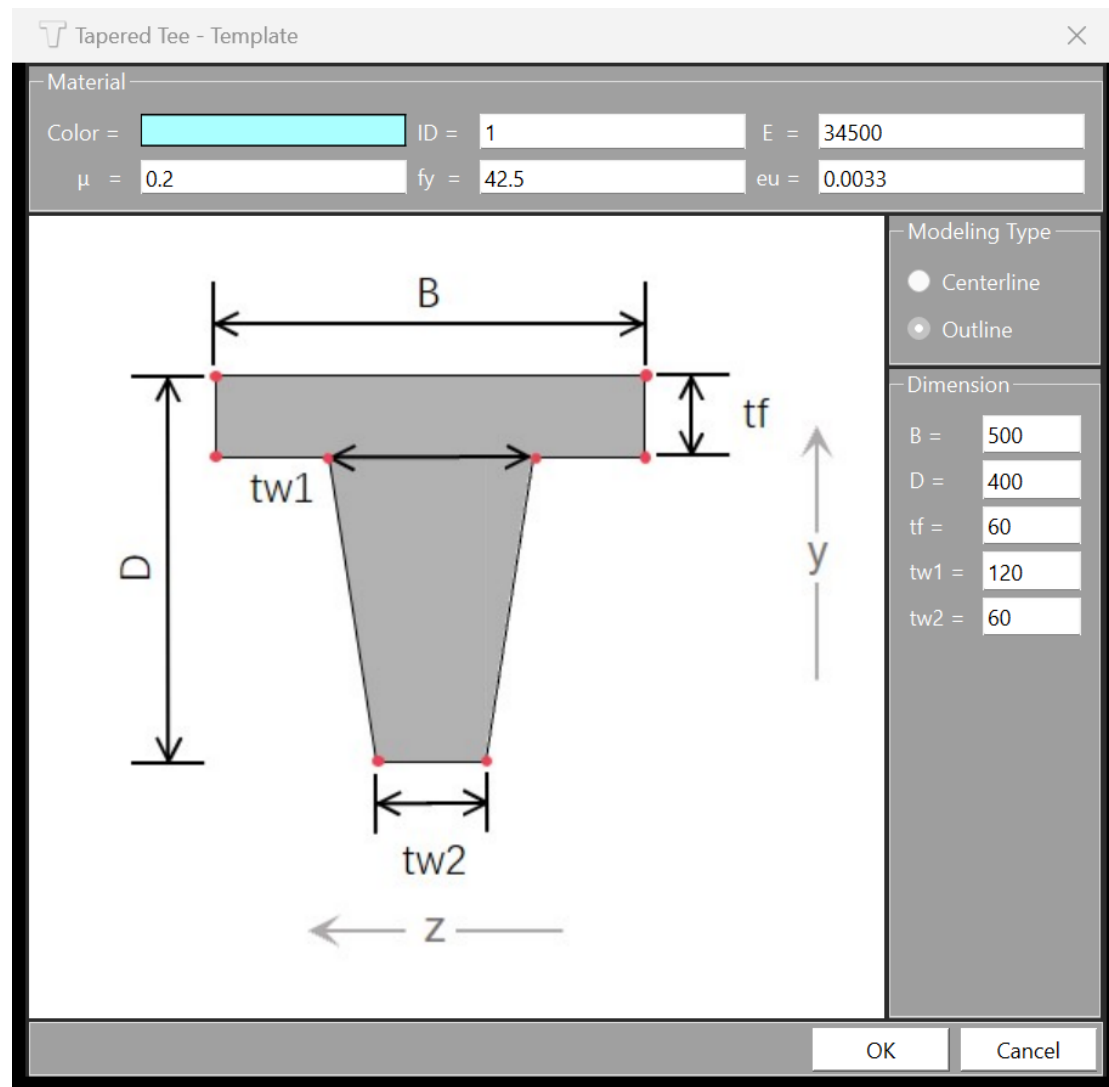
## Box Girder



## Tapered I

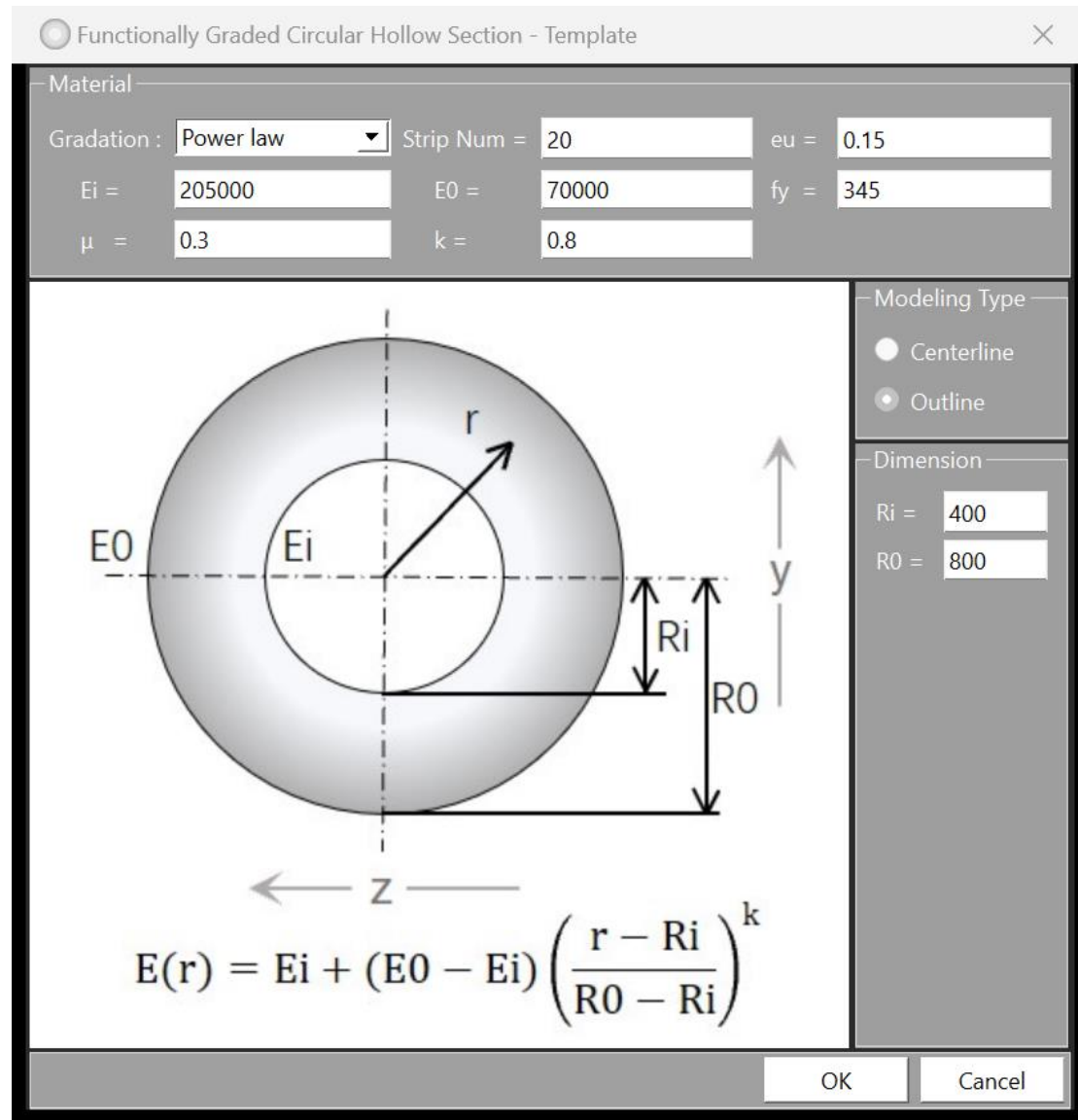


## Tapered Tee

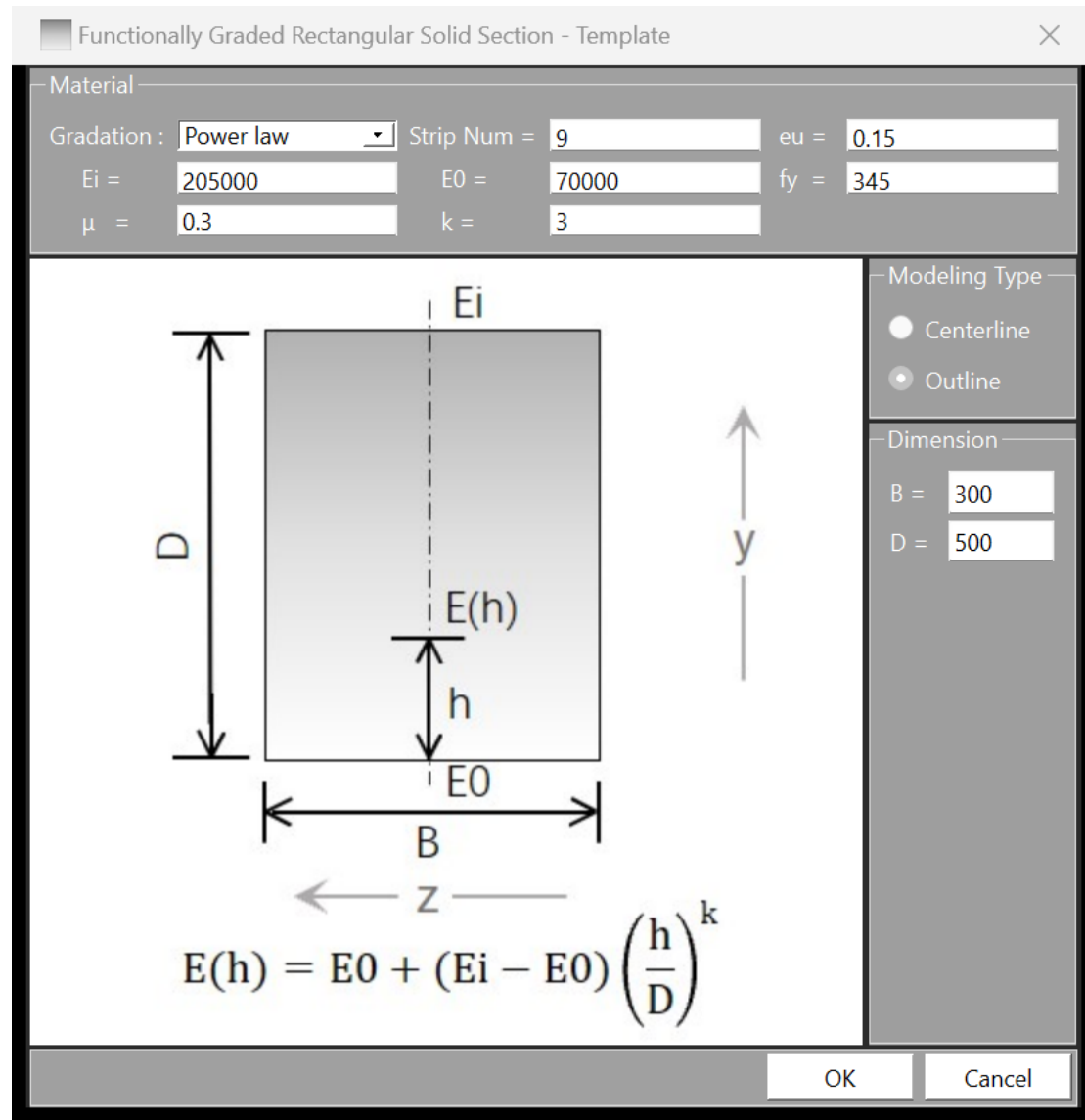


## Functionally Graded Section

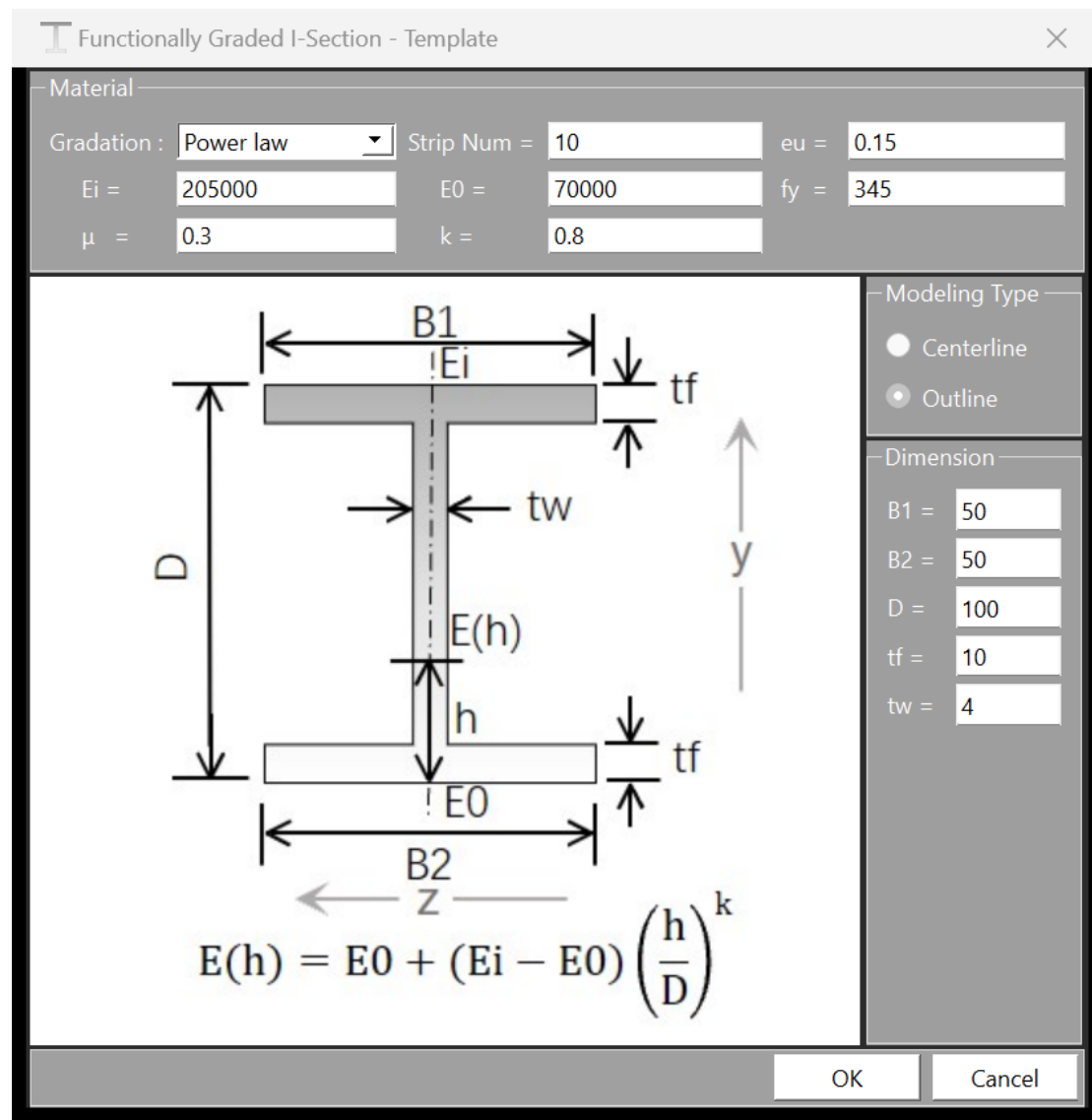
### Functionally Graded Circular Hollow Section



## Functionally Graded Rectangular Solid Section



## Functionally Graded I-Section



### 2.2.3 Export tab

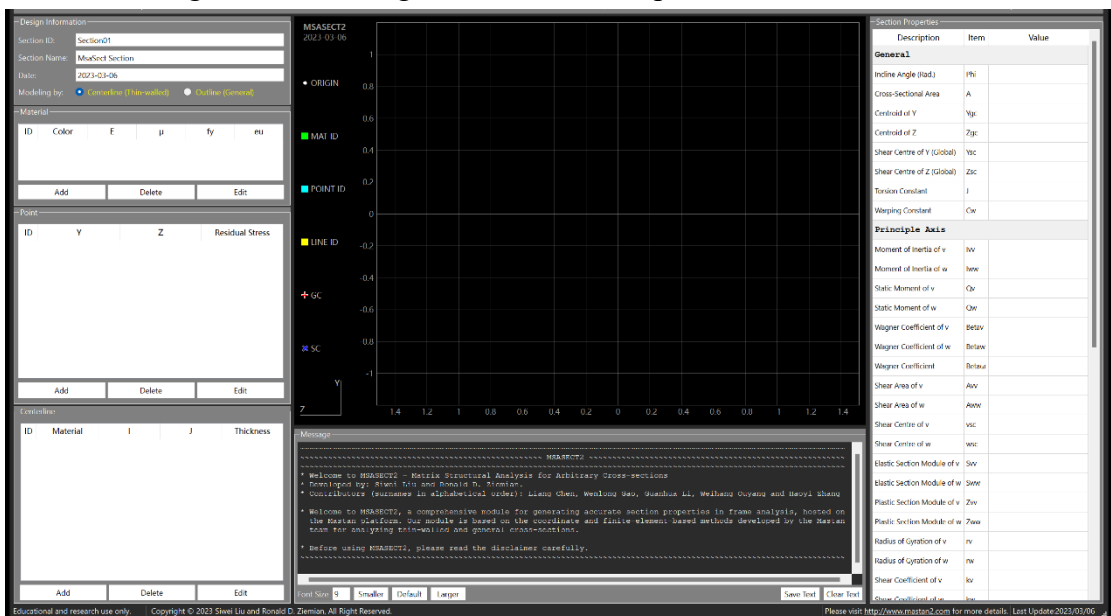
The Template tab in the ribbon menu is shown below:



It should be noted that the function “Export to Mastan 2” is still under development.

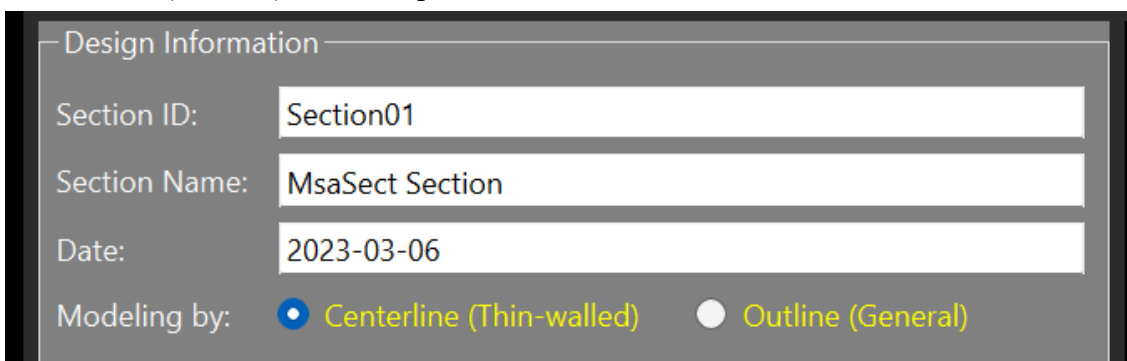
## 2.3 Main window

The Main window can be divided into five parts, including Design information, Input menu, Drawing canvas, Message window, and Output window, as shown below:



### 2.3.1 Design information

The design information and the modelling pattern, including Centerline (Thin-walled) and Outline (General), can be inputted and selected here:



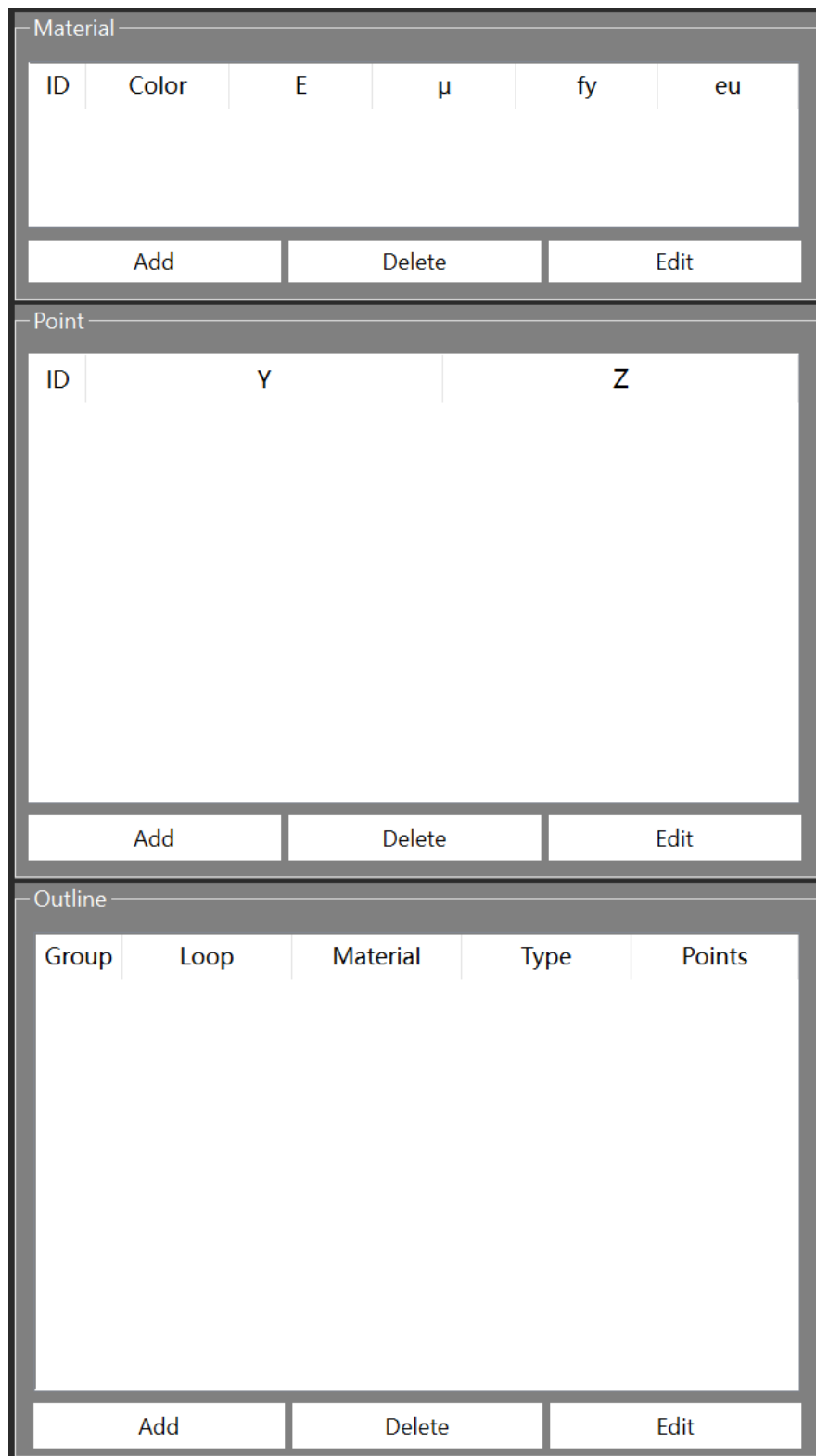
### 2.3.2 Input menu (*Centerline module*)

If the selected modelling pattern is Centerline (Thin-walled), the input menu is as shown below:

Material					
ID	Color	E	$\mu$	$f_y$	$\epsilon_u$
Add	Delete		Edit		
Point					
ID	Y	Z	Residual Stress		
Add	Delete		Edit		
Centerline					
ID	Material	I	J	Thickness	
Add	Delete		Edit		

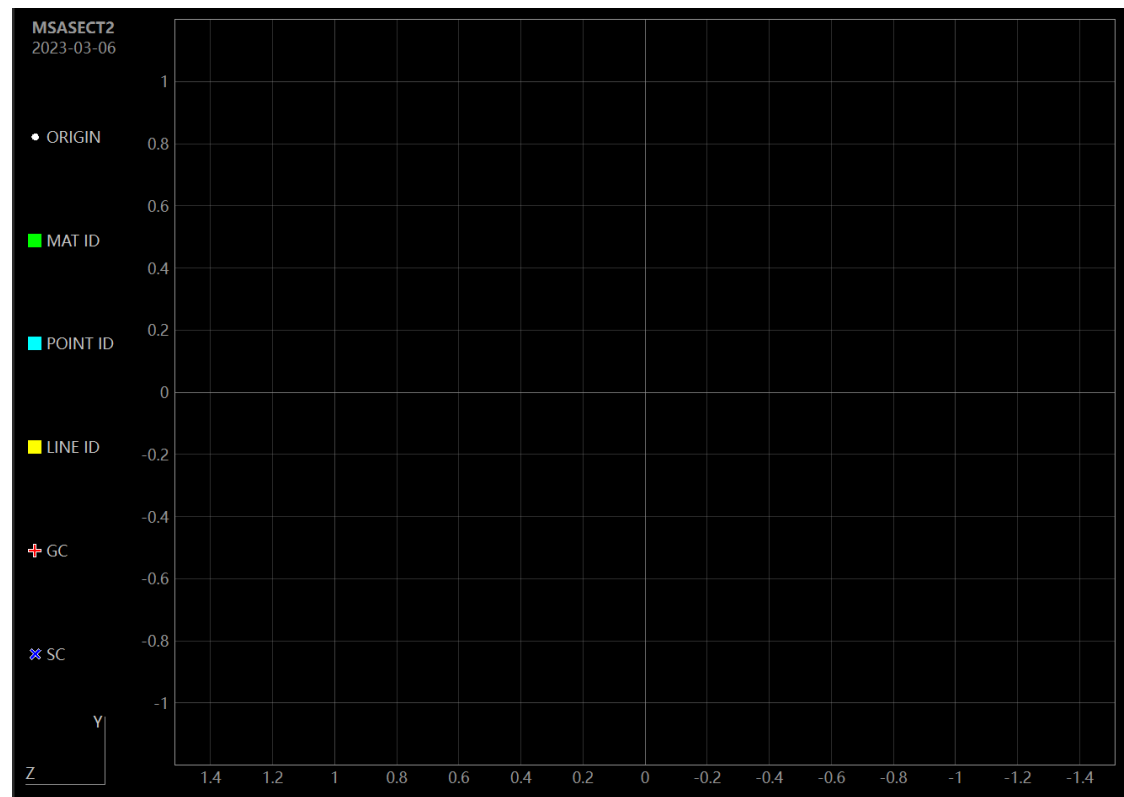
### 2.3.3 Input menu (*Outline module*)

If the selected modelling pattern is Outline (General), the input menu is as shown below:

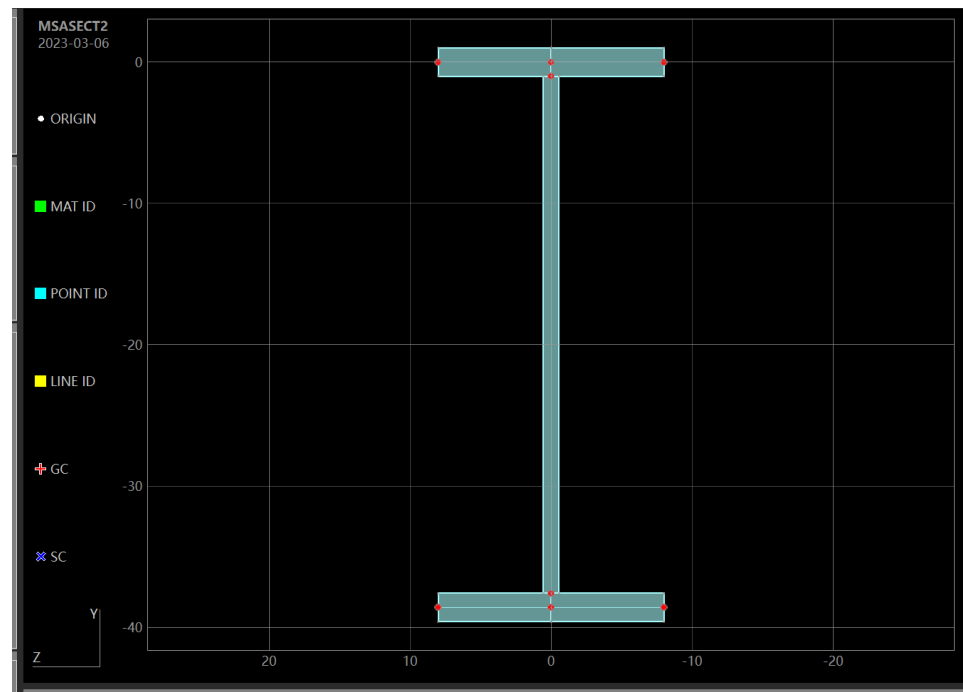


### 2.3.4 Drawing Canvas

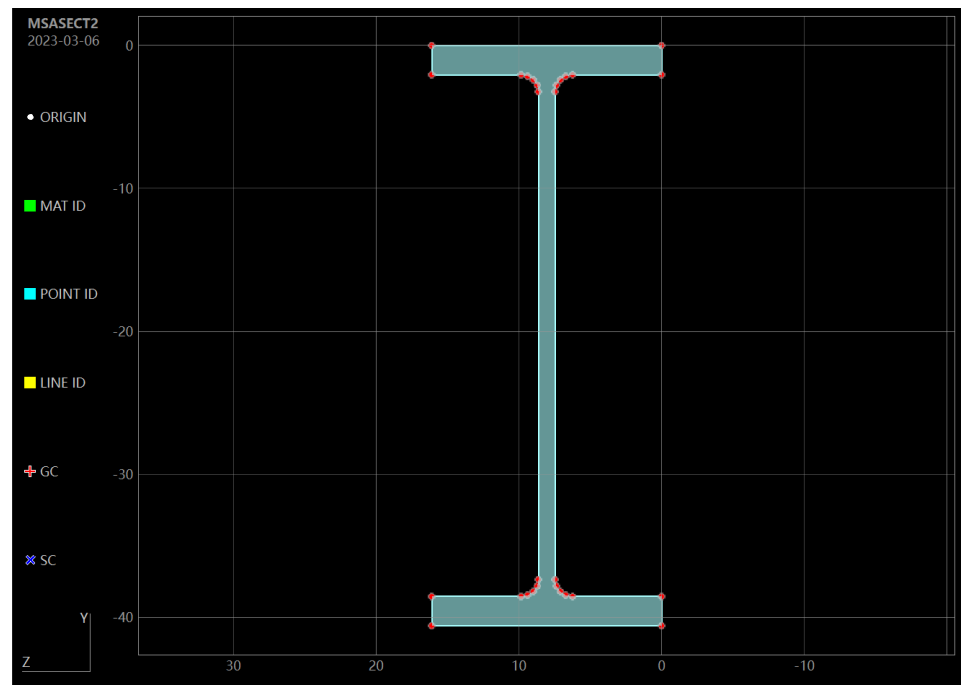
The drawing canvas is as shown below:



When the modelling pattern is Centerline (Thin-walled), the visualized model is as show below:

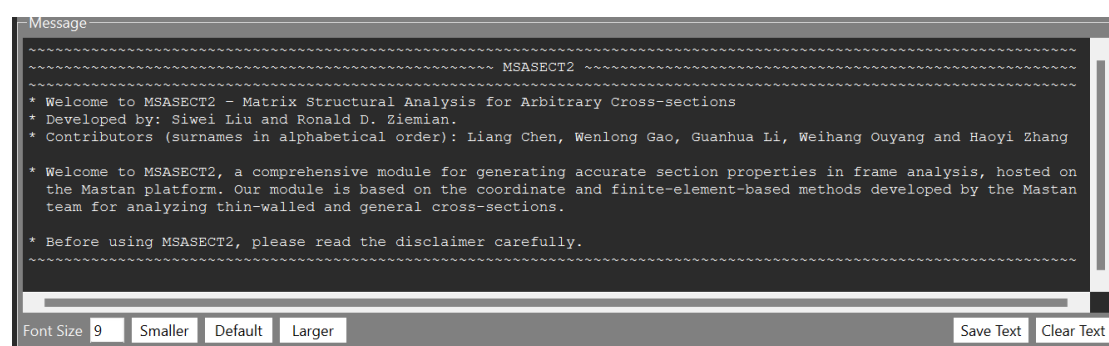


When the modelling pattern is Outline (General), the visualized model is as show below:



### 2.3.5 Message window

The Message window is as shown below:



### 2.3.6 Output window (for section properties)

The calculated section properties will be summarized in the output window as:

Section Properties		
Description	Item	Value
<b>General</b>		
Incline Angle (Rad.)	Phi	
Cross-Sectional Area	A	
Centroid of Y	Ygc	
Centroid of Z	Zgc	
Shear Centre of Y (Global)	Ysc	
Shear Centre of Z (Global)	Zsc	
Torsion Constant	J	
Warping Constant	Cw	

<b>Principle Axis</b>		
Moment of Inertia of v	Iv	
Moment of Inertia of w	Iww	
Static Moment of v	Qv	
Static Moment of w	Qw	
Wagner Coefficient of v	Betav	
Wagner Coefficient of w	Betaw	
Wagner Coefficient	Betaw	
Shear Area of v	Avv	
Shear Area of w	Aww	
Shear Centre of v	vsc	
Shear Centre of w	wsc	
Elastic Section Module of v	Svv	
Elastic Section Module of w	Sww	
Plastic Section Module of v	Zvv	
Plastic Section Module of w	Zww	
Radius of Gyration of v	rv	
Radius of Gyration of w	rw	
Shear Coefficient of v	kv	
Shear Coefficient of w	kw	

<b>User-Defined Axis</b>		
Moment of Inertia of y	Iyy	
Moment of Inertia of z	Izz	
Product of Inertia	Iyz	
Static Moment of y	Qy	
Static Moment of z	Qz	
Wagner Coefficient of y	Betay	
Wagner Coefficient of z	Betaz	
Wagner Coefficient	Betaw	
Shear Area of y	Ayy	
Shear Area of z	Azz	
Shear Centre of y	ysc	
Shear Centre of z	zsc	
Plastic Section Module of y	Syy	
Plastic Section Module of z	Szz	
Elastic Section Module of y	Zyy	
Elastic Section Module of z	Zzz	
Radius of Gyration of y	ry	
Radius of Gyration of z	rz	
Shear Coefficient of y	ky	
Shear Coefficient of z	kz	

### 3. Theoretical Background

The MSASECT2 is based on the coordinate method and finite-element-based method developed by the Mastan team for the cross-section analyze of thin-walled and general sections.

#### 3.1 Coordinate method

In a conventional beam-column element that includes warping, there are five cross-section properties that are required for a three-dimensional analysis, including the cross-sectional area  $A$ , second moments of area  $I_y$  and  $I_z$  about the y- and z- axes, torsional constant  $J$ , and warping constant  $I_\omega$ . For most common sections, these properties can be easily calculated using closed-form equations that are readily available. To consider the effects of non-symmetric sections, five additional section properties are needed, including the coordinates of the shear center ( $z_s$  and  $y_s$ ) and the Wagner coefficients ( $\beta_y$ ,  $\beta_z$  and  $\beta_\omega$ ) (Chen and Atsuta 2007). For thin-walled sections of relatively simple shapes, such as mono-symmetric-I, T-, and L-shapes, the mathematical expressions of the Wagner coefficients can be generated (Ziemian 2010), but such expressions are complicated and perhaps difficult to use in routine practice. For the more complex shapes, the use of Wagner coefficients is often avoided due to the complexity of calculating their values, which could thereby result in significant errors when computing structural behaviour. To resolve such difficulties, a generalized computational approach for providing these properties for arbitrary thin-walled sections was developed.

##### 3.1.1 Section modelling

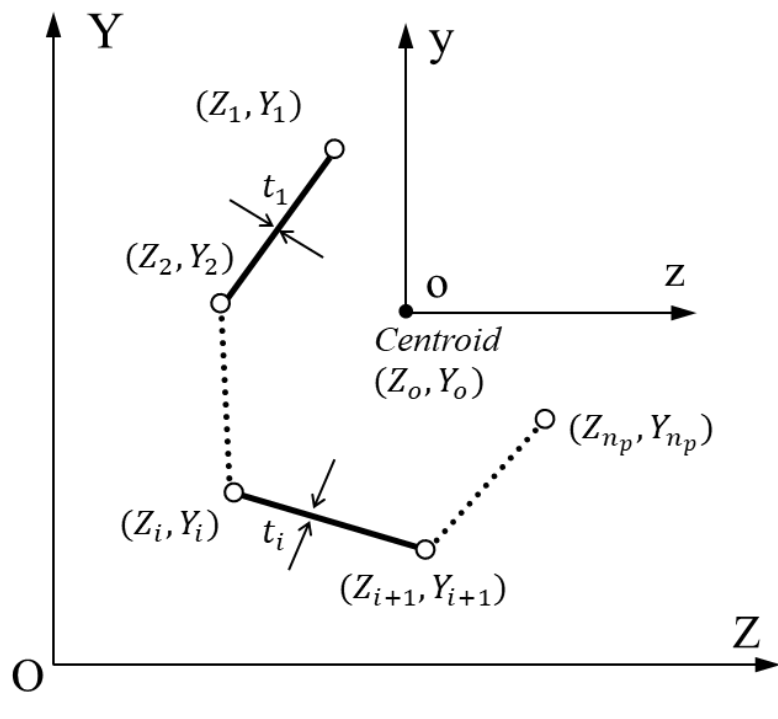
An open-section can be modelled via a series of points and segments as indicated in **Figure 1**, which will be classified as either Chain-Type or Tree-Type. Each segment is a line element constructed by two points with the plate thickness  $t$ . A global coordinate system, namely the Z-O-Y axis, is initially established for describing the positions of points; and a local axis with the origin as the centroid (i.e., z-o-y axis) is determined for computing the related section parameters. The coordinates of the centroid of the section can then be computed by,

$$Z_o = \frac{\sum_{i=1}^{n_s} L_i t_i (Z_{Li} + Z_{Ri}) / 2}{A} \quad (1)$$

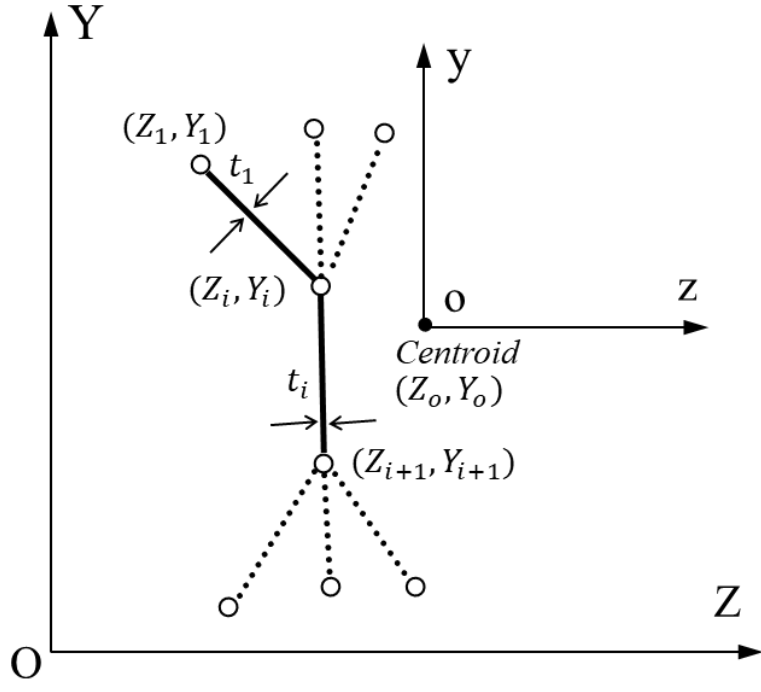
$$Y_o = \frac{\sum_{i=1}^{n_s} L_i t_i (Y_{Li} + Y_{Ri}) / 2}{A} \quad (2)$$

where  $n_s$  is the total number of segments; the subscripts  $L$  and  $R$  denote the start and end points of the  $i^{\text{th}}$  segment, respectively;  $L_i$  is the length of the  $i^{\text{th}}$  segment; and  $A$  is the total cross-section area, which is given by,

$$A = \sum_{i=1}^{n_s} L_i t_i \quad (3)$$



(a) Chain-Type



(b) Tree-Type

**Figure 1** Modeling an open section via points and segments

The coordinates  $(z_i, y_i)$  of the  $i^{\text{th}}$  point in the z-o-y axis are given by,

$$z_i = Z_i - Z_o \quad (4)$$

$$y_i = Y_i - Y_o \quad (5)$$

### 3.1.2 Warping ordinate

The warping ordinate  $\omega_{oi}$  and  $\omega_{si}$  of the  $i^{\text{th}}$  point can be calculated by referring to the centroid and the shear center, respectively, and are thereby given as,

$$\omega_{oi} = \omega_{oj} + [y_j(z_i - z_j) - z_j(y_i - y_j)] \quad (6)$$

$$\omega_{si} = \omega_{sj} + [(z_s - z_j)(y_i - y_j) - (y_s - y_j)(z_i - z_j)] \quad (7)$$

where the subscript  $j$  represents the previous point in the Chain-Type section and also represents the upper level point in a Tree-Type section; and  $z_s$  and  $y_s$  are the coordinates of the shear center and can be calculated by,

$$y_s = (I_z I_{\omega z} - I_{yz} I_{\omega y}) / (I_y I_z - I_{yz}^2) \quad (8)$$

$$z_s = (I_y I_{\omega y} - I_{yz} I_{\omega z}) / (I_y I_z - I_{yz}^2) \quad (9)$$

where,

$$I_z = \int_A y^2 dA = \sum_{i=1}^{n_s} \left( \frac{y_{Li} + y_{Ri}}{2} \right)^2 A_i + \frac{1}{12} (y_{Li} - y_{Ri})^2 A_i \quad (10)$$

$$I_y = \int_A z^2 dA = \sum_{i=1}^{n_s} \left( \frac{z_{Li} + z_{Ri}}{2} \right)^2 A_i + \frac{1}{12} (z_{Li} - z_{Ri})^2 A_i \quad (11)$$

$$I_{yz} = \int_A yz dA = \sum_{i=1}^{n_s} \left( \frac{z_{Li} + z_{Ri}}{2} \right) \left( \frac{y_{Li} + y_{Ri}}{2} \right) A_i \quad (12)$$

$$+ \sum_{i=1}^{n_s} \left( \frac{z_{Li} + z_{Ri}}{2} \right) \left( \frac{y_{Li} + y_{Ri}}{2} \right) A_i$$

$$I_{\omega z} = \int_A z \omega_o dA = \sum_{i=1}^{n_s} \frac{A_i}{6} [\omega_{oLi}(2z_{Li} + z_{Ri}) + \omega_{oRi}(z_{Li} + 2z_{Ri})] \quad (13)$$

$$I_{\omega y} = \int_A y \omega_o dA = \sum_{i=1}^{n_s} \frac{A_i}{6} [\omega_{oLi}(2y_{Li} + y_{Ri}) + \omega_{oRi}(y_{Li} + 2y_{Ri})] \quad (14)$$

in which  $\omega_o$  is the warping ordinate that is illustrated in **Figure 2**; and  $y, z$  are point coordinates with reference to the centroid.

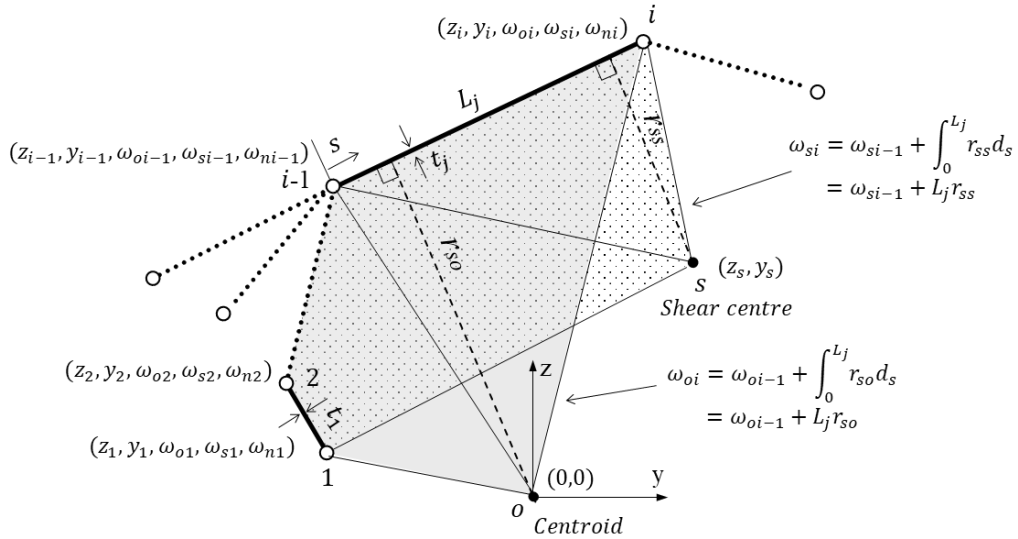


**Figure 2** The coordinates and the warping ordinate at a point

The normalized warping ordinate  $\omega_n$  is determined as following,

$$\omega_n = \frac{1}{A} \int \omega_s dA - \omega_s = \frac{1}{2A} \sum_{i=1}^{n_s} (\omega_{Lsi} + \omega_{Rsi}) A_i - \omega_s \quad (15)$$

With these equations, the coordinate and the warping ordinate of an arbitrary point on the cross section are obtained (as illustrated in **Figure 2**) and will now be used for calculating the Wagner coefficients.

### 3.1.3 Wagner coefficients

With the availability of the coordinates and warping ordinate for the segment end points, the three Wagner coefficients can be calculated from the following equations.

$$\rho = \frac{1}{2} \int (\tau^3 + \tau v^2) dA - 2\tau \quad (16)$$

$$\begin{aligned}
& + \frac{1}{12I_y} \sum_{i=1}^{n_s} A_i [y_{Ri}^2(z_{Li} + 3z_{Ri}) + 3(z_{Li} + z_{Ri})(z_{Li}^2 + z_{Ri}^2)] - 2z_s \\
\beta_z = & \frac{1}{I_z} \int_A (y^3 + yz^2) dA - 2y_s \tag{17}
\end{aligned}$$

$$\begin{aligned}
& = \frac{1}{12I_z} \sum_{i=1}^{n_s} A_i [2z_{Li}z_{Ri}(y_{Li} + y_{Ri}) + z_{Li}^2(3y_{Li} + y_{Ri})] \\
& \quad + \frac{1}{12I_z} \sum_{i=1}^{n_s} A_i [z_{Ri}^2(y_{Li} + 3y_{Ri}) + 3(y_{Li} + y_{Ri})(y_{Li}^2 + y_{Ri}^2)] - 2y_s \\
\beta_\omega = & \frac{1}{I_\omega} \int_A \omega_n (y^2 + z^2) dA \\
= & \frac{1}{12I_\omega} \sum_{i=1}^{n_s} A_i [\omega_{Li}(3y_{Li}^2 + 2y_{Li}y_{Ri} + y_{Ri}^2 + 3z_{Li}^2 + 2z_{Li}z_{Ri} + z_{Ri}^2)] \tag{18} \\
& + \frac{1}{12I_\omega} \sum_{i=1}^{n_s} A_i [\omega_{Ri}(y_{Li}^2 + 2y_{Li}y_{Ri} + 3y_{Ri}^2 + z_{Li}^2 + 2z_{Li}z_{Ri} + 3z_{Ri}^2)]
\end{aligned}$$

Finally, the warping constant  $I_\omega$  can be computed from,

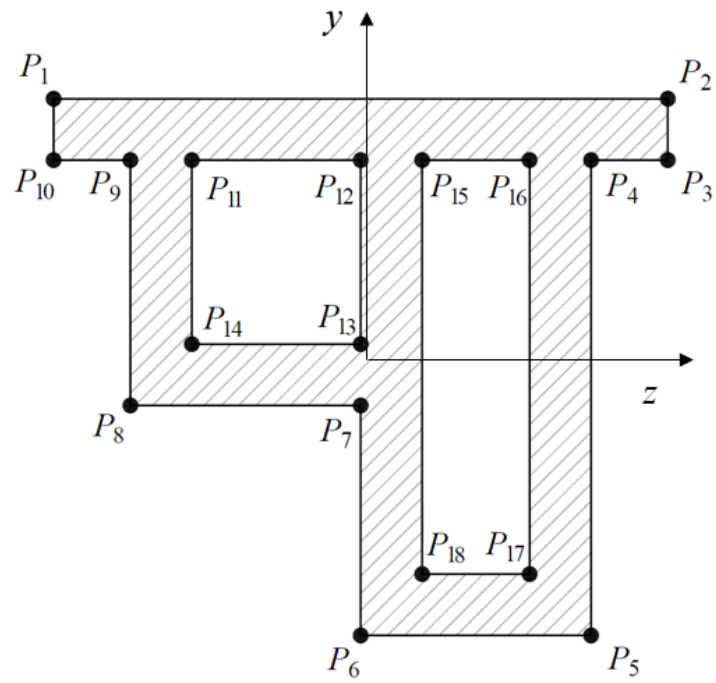
$$I_\omega = \int_A \omega_n^2 dA = \sum_{i=1}^{n_s} A_i \left[ \omega_{Lni}\omega_{Rni} + \frac{(\omega_{Rni} - \omega_{Lni})^2}{3} \right] \tag{19}$$

## 3.2 Finite-element-based method

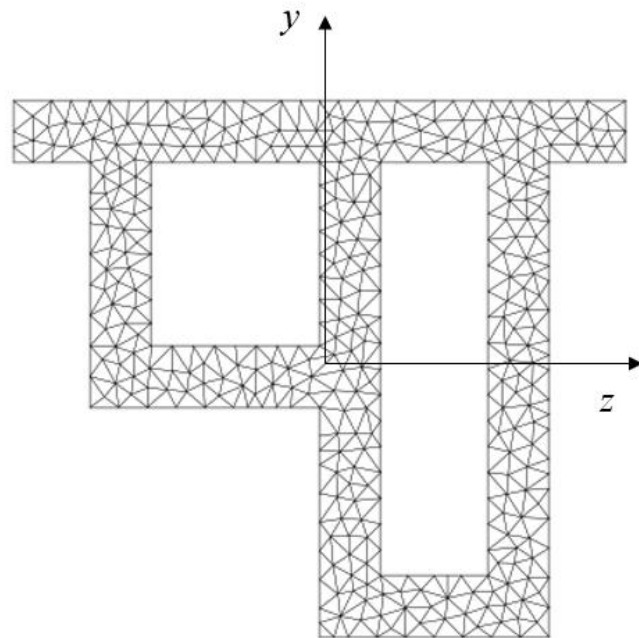
### 3.2.1 Section modelling

An 2D FE-based cross-section analysis algorithm is employed to calculate section properties for nonsymmetric thick-walled sections. Instead of modelling the cross-section with the centerline as in the CM method, this research adopted a new cross-section modelling method using the outline. This method not only is applicable to arbitrary sections but also can take the wall thickness into considerations. A modelling example of a complex section is provided in **Figure 3** (a), where the vertices of the

cross-section  $P_i$  are firstly described with coordinates and then connected by outlines  $L_i$ .



(a) Section modelling



(b) Generated FE mesh

**Figure 3** Example of section modeling

As shown in **Figure 3 (a)**, the outlines are defined as:

$$L_1 = P_1 \rightarrow P_2 \rightarrow P_3 \rightarrow P_4 \dots P_8 \rightarrow P_9 \rightarrow P_{10} \rightarrow P_1$$

$$L_2 = P_{11} \rightarrow P_{12} \rightarrow P_{13} \rightarrow P_{14} \rightarrow P_{11}$$

$$L_3 = P_{15} \rightarrow P_{16} \rightarrow P_{17} \rightarrow P_{18} \rightarrow P_{15}$$

Note that the outlines can be classified as the ones for solids and holes. In this example,  $L_1$  describes a continuous solid outline where FE mesh will be generated within the enclosed region;  $L_2$  and  $L_3$  describe continuous hole outlines where FE mesh will be deleted within the enclosed region, as shown in **Figure 3 (b)**.

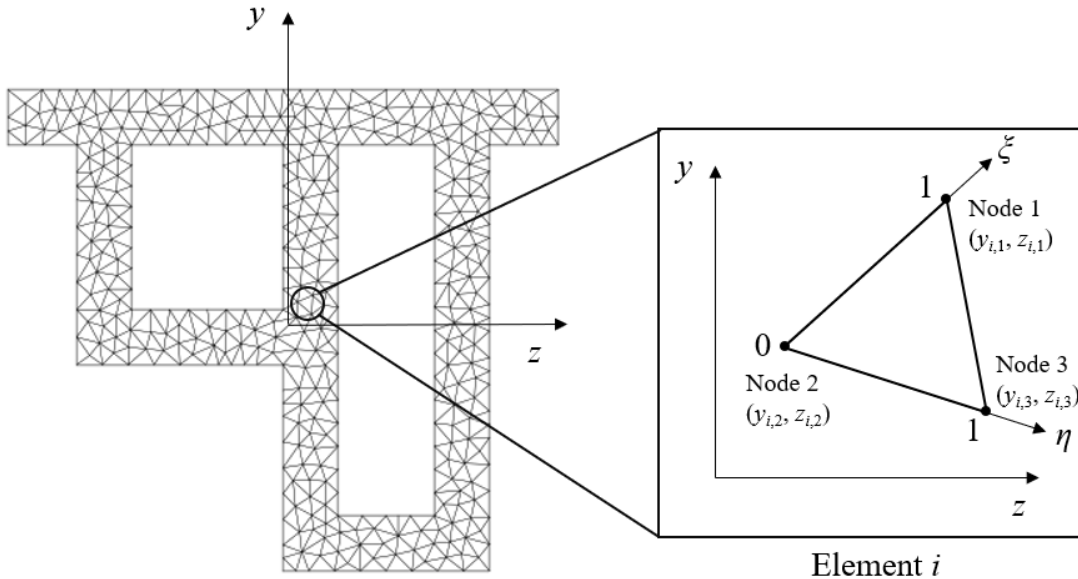


**Figure 4** Constant strain triangle (CST) element

An iso-parametric constant strain triangle (CST) element is employed to generate 2D-meshes of cross-sections. The CST element is a simple and efficient triangular finite element for the cross-section analysis. Besides, the element has a high adaptability to mesh sections with arbitrary shapes. As shown in **Figure 4**, besides the global coordinate system  $y$ -o- $z$ , a local coordinate system  $\eta$ -o- $\xi$  will be established to derive the element formulations. Note that the nodes for each element will be listed following anticlockwise sequences.

### 3.2.2 Shape functions and Jacobian matrix of the CST element

The CST element is a simple first-order element. The shape function  $N$  and Jacobian matrix  $J$  of this element are defined as:

$$N(\eta, \xi) = [\eta \quad \xi \quad 1 - \eta - \xi] \quad (20)$$

$$J = \begin{bmatrix} \frac{\partial z}{\partial \eta} & \frac{\partial y}{\partial \eta} \\ \frac{\partial z}{\partial \xi} & \frac{\partial y}{\partial \xi} \end{bmatrix} = \begin{bmatrix} \frac{\partial N}{\partial \eta} \\ \frac{\partial N}{\partial \xi} \end{bmatrix} [z^e \quad y^e] = \begin{bmatrix} z_1 - z_3 & y_1 - y_3 \\ z_2 - z_3 & y_2 - y_3 \end{bmatrix} \quad (21)$$

where the superscript  $e$  denotes column vectors containing element nodal global coordinates, for example,  $y^e = (y_1, y_2, y_3)$ .

### 3.2.3 Basic geometric properties

The calculation of area  $A$ , global coordinate of centroid  $y_c$  and  $z_c$ , and moment of inertia  $I_y$ ,  $I_z$  and  $I_{yz}$  in this study is based on geometric approaches. Since the cross-section will be meshed into a series of CST elements, those basic geometric properties can be calculated by,

$$A = \sum A^e = \frac{1}{2} \sum_{i=1}^{NE} \sum_{j=1}^n (y_{i,j+1} z_{i,j} - y_{i,j} z_{i,j+1}) \quad (22)$$

$$y_c = \frac{\sum A^e y_c^e}{A} = \frac{1}{6A} \sum_{i=1}^{NE} \sum_{j=1}^n (y_{i,j} + y_{i,j+1})(y_{i,j+1} z_{i,j} - y_{i,j} z_{i,j+1}) \quad (23)$$

$$z_c = \frac{\sum A^e z_c^e}{A} = \frac{1}{6A} \sum_{i=1}^{NE} \sum_{j=1}^n (z_{i,j} + z_{i,j+1})(y_{i,j+1} z_{i,j} - y_{i,j} z_{i,j+1}) \quad (24)$$

$$I_y = \sum I_y^e = \frac{1}{12} \sum_{i=1}^{NE} \sum_{j=1}^n (y_{i,j+1} z_{i,j} - y_{i,j} z_{i,j+1})(z_{i,j}^2 + z_{i,j} z_{i,j+1} + z_{i,j+1}^2) \quad (25)$$

$$I_z = \sum I_z^e = \frac{1}{12} \sum_{i=1}^{NE} \sum_{j=1}^n (y_{i,j+1} z_{i,j} - y_{i,j} z_{i,j+1}) (y_{i,j}^2 + y_{i,j} y_{i,j+1} + y_{i,j+1}^2) \quad (26)$$

$$I_{yz} = \sum I_{yz}^e = \frac{1}{24} \sum_{i=1}^{NE} \sum_{j=1}^n (y_{i,j+1} z_{i,j} - y_{i,j} z_{i,j+1}) \\ \times [y_{i,j+1} z_{i,j} + y_{i,j} z_{i,j+1} + 2(y_{i,j} z_{i,j} + y_{i,j+1} z_{i,j+1})] \quad (27)$$

where  $n = 3$  is the number of nodes in each element. Note that in the triangular element,  $y_{n+1} = y_1$  and  $z_{n+1} = z_1$ .

### 3.2.4 Torsion and warping properties

To get the torsion and warping properties of a cross-section, a classic Saint-Venant torsion problem should be considered, in which the principle of virtual work gives:

$$\delta W = \delta W_{int} - \delta W_{ext} = \int_V \boldsymbol{\sigma} \delta \boldsymbol{\epsilon} dV - \int_L m_x \delta \theta dx = 0 \quad (28)$$

where  $m_x$  is the torque per length uniformly distributed along the entire member length  $L$ ,  $\theta$  is the twist angle of the member. This can be expressed in a strain from as:

$$\int_V G \left[ \left( \left( \frac{\partial \boldsymbol{\omega}}{\partial z} - y \right) \frac{\partial}{\partial x} \delta \theta + \frac{\partial \theta}{\partial x} \frac{\partial}{\partial z} \delta \boldsymbol{\omega} \right) \frac{\partial \theta}{\partial x} \left( \frac{\partial \boldsymbol{\omega}}{\partial z} - y \right) \right] \\ + \left[ \left( \frac{\partial \boldsymbol{\omega}}{\partial y} - z \right) \frac{\partial}{\partial x} \delta \theta + \frac{\partial \theta}{\partial x} \frac{\partial}{\partial y} \delta \boldsymbol{\omega} \right] \frac{\partial \theta}{\partial x} \left( \frac{\partial \boldsymbol{\omega}}{\partial y} + z \right) dV - \int_L m_x \delta \theta dx = 0 \quad (29)$$

where  $\boldsymbol{\omega}$  is the warping ordinate function and the  $\delta \theta$  term can be separated as:

$$\int_L G \frac{\partial}{\partial x} \delta \theta \frac{\partial \theta}{\partial x} dx \int_A \left[ \left( \left( \frac{\partial \boldsymbol{\omega}}{\partial y} \right)^2 + \left( \frac{\partial \boldsymbol{\omega}}{\partial z} \right)^2 + z \frac{\partial \boldsymbol{\omega}}{\partial y} - y \frac{\partial \boldsymbol{\omega}}{\partial z} \right) \right. \\ \left. + \left( z \frac{\partial \boldsymbol{\omega}}{\partial y} - y \frac{\partial \boldsymbol{\omega}}{\partial z} + y^2 + z^2 \right) \right] dA - \int_L m_x \delta \theta dx \quad (30)$$

in which, the first part of the  $\delta\theta$  term can be simplified with the Green's theorem and harmonic function:

$$\begin{aligned} & \int_A \left[ \left( \frac{\partial \omega}{\partial y} \right)^2 + \left( \frac{\partial \omega}{\partial z} \right)^2 + z \frac{\partial \omega}{\partial y} - y \frac{\partial \omega}{\partial z} \right] dA \\ &= \oint \omega \left[ \left( \frac{\partial \omega}{\partial y} + z \right) n_y + \left( \frac{\partial \omega}{\partial z} - y \right) n_z \right] ds \end{aligned} \quad (31)$$

Where  $n_y$  and  $n_z$  are the module of vector components along  $y$  and  $z$ -axis. The vector is outward normal to the outline  $s$  of the cross section. Based on the surface condition, this part equals to zero. The following part of  $\delta\theta$  term can be simplified to  $J$ , it leads to:

$$\begin{aligned} & \int_L G \frac{\partial}{\partial x} \delta\theta \frac{\partial\theta}{\partial x} dx \int_A \left[ \left( z \frac{\partial \omega}{\partial y} - y \frac{\partial \omega}{\partial z} + y^2 + z^2 \right) \right] dA - \int_L m_x \delta\theta dx \\ &= \int_L \frac{d}{dx} \delta\theta GJ \frac{d\theta}{dx} dx - \int_L m_x \delta\theta dx = \int_L \delta\theta \left( \frac{d}{dx} GJ \frac{d\theta}{dx} - m_x \right) dx \end{aligned} \quad (32)$$

This part also equals to zero based on the governing equation for torsional motion along the longitudinal  $x$ -axis. Hence the rest  $\delta\omega$  term would be:

$$\begin{aligned} & \int_V G \left( \frac{\partial \theta}{\partial x} \right)^2 \left( \frac{\partial}{\partial y} \delta\omega \frac{\partial \omega}{\partial y} + \frac{\partial}{\partial z} \delta\omega \frac{\partial \omega}{\partial z} + \frac{\partial}{\partial y} \delta\omega z - \frac{\partial}{\partial z} \delta\omega y \right) dV \\ &= G \int_L \left( \frac{\partial \theta}{\partial x} \right)^2 dx \int_A \left[ \left( \frac{\partial}{\partial y} \delta\omega \frac{\partial \omega}{\partial y} + \frac{\partial}{\partial z} \delta\omega \frac{\partial \omega}{\partial z} \right) - \left( \frac{\partial}{\partial z} \delta\omega y - \frac{\partial}{\partial y} \delta\omega z \right) \right] dA = 0 \end{aligned} \quad (33)$$

This gives that:

$$\int_A \left[ \left( \frac{\partial}{\partial y} \delta\omega \frac{\partial \omega}{\partial y} + \frac{\partial}{\partial z} \delta\omega \frac{\partial \omega}{\partial z} \right) - \left( \frac{\partial}{\partial z} \delta\omega y - \frac{\partial}{\partial y} \delta\omega z \right) \right] dA = 0 \quad (34)$$

By solving this equation, the warping ordinate function  $\omega(y, z)$  can be solved. The above equation can be written in the FE formulation. For each CST element it can be approximated written as:

$$\int_0^1 \int_0^{1-\xi} \delta \boldsymbol{\omega}^{eT} \left[ \left( \frac{\partial \mathbf{N}^T}{\partial y} \frac{\partial \mathbf{N}}{\partial y} + \frac{\partial \mathbf{N}^T}{\partial z} \frac{\partial \mathbf{N}}{\partial z} \right) \boldsymbol{\omega}^e - \left( \mathbf{N} \mathbf{y}^e \frac{\partial \mathbf{N}^T}{\partial z} - \mathbf{N} \mathbf{z}^e \frac{\partial \mathbf{N}^T}{\partial y} \right) \right] \frac{1}{2} \det|\mathbf{J}| d\eta d\xi = 0 \quad (35)$$

It gives that:

$$\int_0^1 \int_0^{1-\xi} \left[ \left( \frac{\partial \mathbf{N}^T}{\partial y} \frac{\partial \mathbf{N}}{\partial y} + \frac{\partial \mathbf{N}^T}{\partial z} \frac{\partial \mathbf{N}}{\partial z} \right) \boldsymbol{\omega}^e - \left( \mathbf{N} \mathbf{y}^e \frac{\partial \mathbf{N}^T}{\partial z} - \mathbf{N} \mathbf{z}^e \frac{\partial \mathbf{N}^T}{\partial y} \right) \right] \frac{1}{2} \det|\mathbf{J}| d\eta d\xi = 0 \quad (36)$$

The element stiffness matrix  $\mathbf{K}^e$  and load vector  $\mathbf{P}_w^e$  are formulated as:

$$\mathbf{K}^e = \int_0^1 \int_0^{1-\xi} \left( \frac{\partial \mathbf{N}^T}{\partial y} \frac{\partial \mathbf{N}}{\partial y} + \frac{\partial \mathbf{N}^T}{\partial z} \frac{\partial \mathbf{N}}{\partial z} \right) \frac{1}{2} \det|\mathbf{J}| d\eta d\xi \quad (37)$$

$$\mathbf{P}_w^e = \int_0^1 \int_0^{1-\xi} \left( \mathbf{N} \mathbf{y}^e \frac{\partial \mathbf{N}^T}{\partial z} - \mathbf{N} \mathbf{z}^e \frac{\partial \mathbf{N}^T}{\partial y} \right) \frac{1}{2} \det|\mathbf{J}| d\eta d\xi \quad (38)$$

The Gaussian quadrature method is adopted to solve the numerical integrations above and improve computational efficiency. Seven Gauss points are introduced on the CST element as per introduced by Bathe (Bathe 2006), and the above equations can be written as:

$$\mathbf{K}^e = \frac{1}{2} \sum_{i=1}^n \left[ \frac{\partial \mathbf{N}(\eta_i, \xi_i)^T}{\partial y} \frac{\partial \mathbf{N}(\eta_i, \xi_i)}{\partial y} + \frac{\partial \mathbf{N}(\eta_i, \xi_i)^T}{\partial z} \frac{\partial \mathbf{N}(\eta_i, \xi_i)}{\partial z} \right] \det|\mathbf{J}| \quad (39)$$

$$\mathbf{P}_w^e = \frac{1}{2} \sum_{i=1}^n \left[ \mathbf{N}(\eta_i, \xi_i) \mathbf{y}^e \frac{\partial \mathbf{N}(\eta_i, \xi_i)^T}{\partial z} - \mathbf{N}(\eta_i, \xi_i) \mathbf{z}^e \frac{\partial \mathbf{N}(\eta_i, \xi_i)^T}{\partial y} \right] \det|\mathbf{J}| \quad (40)$$

Where  $n = 7$  is the number of Gauss points and  $W_i$  is the weight of each Gauss points. The total stiffness matrix  $\mathbf{K}$  and load vector  $\mathbf{P}_w$  for warping ordinate function can therefore be formed with elemental matrices:

$$\mathbf{K} = \sum^{NE} \mathbf{K}^e \quad (41)$$

$$\mathbf{P}_w = \sum^{NE} \mathbf{P}_w^e \quad (42)$$

$$\mathbf{K}\boldsymbol{\omega} = \mathbf{P}_w \quad (43)$$

where  $NE$  is the number of CST elements. Nodal values of warping ordinate function as a column vector can be obtained by solving this equation. Note that a boundary condition shall be applied first by fixing the warping DOF of an arbitrary node. The location of shear center,  $y_s$  and  $z_s$ , is then calculated:

$$y_s = \frac{1}{I_y} \int_A z \omega dA = \frac{1}{I_y} \sum^{NE} \int_0^1 \int_0^{1-\xi} \mathbf{N} \mathbf{z}^e \mathbf{N} \boldsymbol{\omega}^e \frac{1}{2} \det|\mathbf{J}| d\eta d\xi \quad (44)$$

$$= \frac{1}{2I_y} \sum^{NE} \sum_{i=1}^n W_i \mathbf{N}(\eta_i, \xi_i) \mathbf{z}^e \mathbf{N}(\eta_i, \xi_i) \boldsymbol{\omega}^e \det|\mathbf{J}|$$

$$z_s = \frac{1}{I_z} \int_A y \omega dA = \frac{1}{I_z} \sum^{NE} \int_0^1 \int_0^{1-\xi} \mathbf{N} \mathbf{y}^e \mathbf{N} \boldsymbol{\omega}^e \frac{1}{2} \det|\mathbf{J}| d\eta d\xi \quad (45)$$

$$= \frac{1}{2I_z} \sum^{NE} \sum_{i=1}^n W_i \mathbf{N}(\eta_i, \xi_i) \mathbf{y}^e \mathbf{N}(\eta_i, \xi_i) \boldsymbol{\omega}^e \det|\mathbf{J}|$$

where  $I_y$  and  $I_z$  are moments of inertia. The warping ordinate function  $\boldsymbol{\omega}$  can be standardized to  $\boldsymbol{\omega}_s$ :

$$\begin{aligned} \boldsymbol{\omega}_s &= \boldsymbol{\omega} - \frac{1}{A} \int_A \boldsymbol{\omega} dA + z_s \mathbf{y} - y_s \mathbf{z} \\ &= \boldsymbol{\omega} - \frac{1}{A} \sum^{NE} \int_0^1 \int_0^{1-\xi} \mathbf{N} \boldsymbol{\omega}^e \frac{1}{2} \det|\mathbf{J}| d\eta d\xi + z_s \mathbf{y} - y_s \mathbf{z} \end{aligned} \quad (46)$$

$$= \boldsymbol{\omega} - \frac{1}{2A} \sum_{i=1}^{NE} \sum_{i=1}^n W_i \mathbf{N}(\eta_i, \xi_i) \boldsymbol{\omega}^e \det|\mathbf{J}| + z_s \mathbf{y} - y_s \mathbf{z}$$

The calculation of torsional constant  $J$ , warping constant  $I_w$  and Wagner coefficients  $\beta_y$ ,  $\beta_z$ ,  $\beta_\omega$  are given as:

$$\begin{aligned} J &= \int_A \left[ \frac{\partial \boldsymbol{\omega}_s}{\partial y} (z - z_s) + (z - z_s)^2 \right] - \left[ \frac{\partial \boldsymbol{\omega}_s}{\partial z} (y - y_s) - (y - y_s)^2 \right] dA \\ &= \sum_{i=1}^{NE} \int_0^1 \int_0^{1-\xi} \left[ \left[ \frac{\partial \mathbf{N}}{\partial y} \boldsymbol{\omega}_s^e (\mathbf{N} \mathbf{z}^e - z_s) + (\mathbf{N} \mathbf{z}^e - z_s)^2 \right] \right. \\ &\quad \left. - \left[ \frac{\partial \mathbf{N}}{\partial z} \boldsymbol{\omega}_s^e (\mathbf{N} \mathbf{y}^e - y_s) - (\mathbf{N} \mathbf{y}^e - y_s)^2 \right] \right] \frac{1}{2} \det|\mathbf{J}| d\eta d\xi \end{aligned} \quad (47)$$

$$\begin{aligned} &= \frac{1}{2} \sum_{i=1}^{NE} \sum_{i=1}^n W_i \left[ \left[ \frac{\partial \mathbf{N}(\eta_i, \xi_i)}{\partial y} \boldsymbol{\omega}_s^e [\mathbf{N}(\eta_i, \xi_i) \mathbf{z}^e - z_s] + [\mathbf{N}(\eta_i, \xi_i) \mathbf{z}^e - z_s]^2 \right] \right. \\ &\quad \left. - \left[ \frac{\partial \mathbf{N}(\eta_i, \xi_i)}{\partial z} \boldsymbol{\omega}_s^e [\mathbf{N}(\eta_i, \xi_i) \mathbf{y}^e - y_s] + [\mathbf{N}(\eta_i, \xi_i) \mathbf{y}^e - y_s]^2 \right] \right] \det|\mathbf{J}| \end{aligned}$$

$$I_\omega = \int_A \boldsymbol{\omega}_s^2 dA = \sum_{i=1}^{NE} \int_0^1 \int_0^{1-\xi} (\mathbf{N} \boldsymbol{\omega}^e)^2 \frac{1}{2} \det|\mathbf{J}| d\eta d\xi \quad (48)$$

$$= \frac{1}{2} \sum_{i=1}^{NE} \sum_{i=1}^n W_i [\mathbf{N}(\eta_i, \xi_i) \boldsymbol{\omega}^e]^2 \det|\mathbf{J}|$$

$$\beta_y = \frac{1}{I_y} \int_A \bar{z}^3 + \bar{z} \bar{y}^2 dA - 2z_s \quad (49)$$

$$= \frac{1}{I_y} \sum_{i=1}^{NE} \int_0^1 \int_0^{1-\xi} [(\mathbf{N} \bar{\mathbf{z}}^e)^3 + \mathbf{N} \bar{\mathbf{z}}^e (\mathbf{N} \bar{\mathbf{y}}^e)^2] \frac{1}{2} \det|\mathbf{J}| d\eta d\xi - 2z_s$$

$$\begin{aligned}
&= \frac{1}{2I_y} \sum_{i=1}^{NE} \sum_{i=1}^n W_i [[N(\eta_i, \xi_i) \bar{z}^e]^3 + N(\eta_i, \xi_i) \bar{z}^e [N(\eta_i, \xi_i) \bar{y}^e]^2] \det|J| - 2z_s \\
&\beta_z = \frac{1}{I_z} \int_A \bar{y}^3 + \bar{y} \bar{z}^2 dA - 2y_s \\
&= \frac{1}{I_z} \sum_{i=1}^{NE} \int_0^1 \int_0^{1-\xi} [(N\bar{y}^e)^3 + N\bar{y}^e (N\bar{z}^e)^2] \frac{1}{2} \det|J| d\eta d\xi - 2y_s
\end{aligned} \tag{50}$$

$$\begin{aligned}
&\beta_\omega = \frac{1}{I_\omega} \int_A \omega (\bar{y}^2 + \bar{z}^2) dA \\
&= \frac{1}{I_\omega} \sum_{i=1}^{NE} \int_0^1 \int_0^{1-\xi} N\omega^e [(N\bar{y}^e)^2 + (N\bar{z}^e)^2] \frac{1}{2} \det|J| d\eta d\xi \\
&= \frac{1}{2I_\omega} \sum_{i=1}^{NE} \sum_{i=1}^n W_i N(\eta_i, \xi_i) \omega^e [[N(\eta_i, \xi_i) \bar{y}^e]^2 + [N(\eta_i, \xi_i) \bar{z}^e]^2] \det|J|
\end{aligned} \tag{51}$$

### 3.2.5 Shear coefficients

Assuming a beam subjected to a non-uniform bending moment  $M_z$  and a shear force  $V_y$ . The longitudinal normal stress can be calculated by:

$$\sigma_x = \frac{I_y M_z y - I_{yz} M_z z}{I_y I_z - I_{yz}^2} \tag{52}$$

With zero body force, the equation of equilibrium gives:

$$\frac{\partial \sigma_x}{\partial x} + \frac{\partial \tau_{xy}}{\partial y} + \frac{\partial \tau_{xz}}{\partial z} = 0 \tag{53}$$

Submitting equation(53) into equation (52) leads to:

$$\frac{\partial \tau_{xy}}{\partial y} + \frac{\partial \tau_{xz}}{\partial z} = \frac{V_y(I_{yz}z - I_yy)}{I_yI_z - I_{yz}^2} \quad (54)$$

For uniform isotropic materials, the kinetical strain-displacement equations can be expressed in Hooke's stress-strain relationship as:

$$\frac{\partial^2 \sigma_x}{\partial x \partial y} = \frac{1+\nu}{\nu} \frac{\partial}{\partial z} \left( \frac{\partial \tau_{xy}}{\partial z} - \frac{\partial \tau_{xz}}{\partial y} - \frac{\partial \tau_{yz}}{\partial x} \right) \quad (55)$$

$$\frac{\partial^2 \sigma_x}{\partial x \partial z} = \frac{1+\nu}{\nu} \frac{\partial}{\partial y} \left( \frac{\partial \tau_{xz}}{\partial y} - \frac{\partial \tau_{xy}}{\partial z} - \frac{\partial \tau_{yz}}{\partial x} \right) \quad (56)$$

Assuming no torsion,  $\tau_{yz}$  equals zero. Submitting equation (52)into equations (55) and (56) leads to:

$$\frac{\partial}{\partial y} \left( \frac{\partial \tau_{xy}}{\partial z} - \frac{\partial \tau_{xz}}{\partial y} \right) = \frac{\nu V_y I_{yz}}{(1+\nu)(I_y I_z - I_{yz}^2)} \quad (57)$$

$$\frac{\partial}{\partial z} \left( \frac{\partial \tau_{xz}}{\partial y} - \frac{\partial \tau_{xy}}{\partial z} \right) = \frac{\nu V_y I_y}{(1+\nu)(I_y I_z - I_{yz}^2)} \quad (58)$$

The shear function  $\Phi(y, z)$  can be employed to describe  $\tau_{xy}$  and  $\tau_{xz}$ :

$$\tau_{xy} = \frac{I_y I_z - I_{yz}^2}{2V_y(1+\nu)} \left[ \frac{\partial \Phi}{\partial y} + \nu \left( I_{yz}yz + I_y \frac{z^2 - y^2}{2} \right) \right] \quad (59)$$

$$\tau_{xz} = \frac{I_y I_z - I_{yz}^2}{2V_y(1+\nu)} \left[ \frac{\partial \Phi}{\partial z} + \nu \left( I_{yz} \frac{z^2 - y^2}{2} - I_y yz \right) \right] \quad (60)$$

Submitting equations (59) and (60) into equation (54), the partial derivative gives the governing equation:

$$\frac{\partial^2 \Phi}{\partial y^2} + \frac{\partial^2 \Phi}{\partial z^2} = 2(I_{yz}z - I_yy) \quad (61)$$

Since the beam is free of surface forces, the stress normal to the boundary curve shall be zero:

$$\tau_{xy}n_y + \tau_{xz}n_z = 0 \quad (62)$$

Where  $n_y$  and  $n_z$  are components of outward unit vector normal to the surface along  $y$  and  $z$  directions. Submitting equations (59) and (60) into equation (62) leads to:

$$\left[ \frac{\partial \Phi}{\partial y} + \nu \left( I_{yz}yz + I_y \frac{z^2 - y^2}{2} \right) \right] n_y + \left[ \frac{\partial \Phi}{\partial z} + \nu \left( I_{yz} \frac{z^2 - y^2}{2} - I_y yz \right) \right] n_z = 0$$

(63)

Utilizing the Galerkin's method, with an appropriate trial function  $f$ , a weak form can be established as:

$$\begin{aligned} & \int_A f \left[ \frac{\partial^2 \Phi}{\partial y^2} + \frac{\partial^2 \Phi}{\partial z^2} - 2(I_{yz}z - I_y y) \right] dA \\ & + \int_s f \left[ \nu \left( I_y yz - I_{yz} \frac{z^2 - y^2}{2} \right) n_z - \nu \left( I_{yz}yz + I_y \frac{z^2 - y^2}{2} \right) n_y \right. \\ & \left. - \left( \frac{\partial \Phi}{\partial y} n_y + \frac{\partial \Phi}{\partial z} n_z \right) \right] ds = 0 \end{aligned} \quad (64)$$

Using the Green's first identity for the first integral part and the divergence theorem for the second integral part, the equation can be transformed into:

$$\begin{aligned} & \int_A \left( \frac{\partial f}{\partial y} + \frac{\partial f}{\partial z} \right) \left( \frac{\partial \Phi}{\partial y} + \frac{\partial \Phi}{\partial z} \right) + 2f(1 + \nu)(I_{yz}z - I_y y) \\ & - \nu \left[ \frac{\partial f}{\partial y} \left( I_y yz - I_{yz} \frac{z^2 - y^2}{2} \right) + \frac{\partial f}{\partial z} \left( I_{yz}yz + I_y \frac{z^2 - y^2}{2} \right) \right] dA = 0 \end{aligned} \quad (65)$$

The above equation can be written in the elemental formulation:

$$\begin{aligned} & \int_0^1 \int_0^{1-\xi} f^{eT} \left[ \left( \frac{\partial \mathbf{N}^T}{\partial y} \frac{\partial \mathbf{N}}{\partial y} + \frac{\partial \mathbf{N}^T}{\partial z} \frac{\partial \mathbf{N}}{\partial z} \right) \Phi^e \right. \\ & \left. - \left[ \frac{\nu}{2} \begin{bmatrix} \frac{\partial \mathbf{N}}{\partial y} & \frac{\partial \mathbf{N}}{\partial z} \end{bmatrix} \begin{bmatrix} I_y[(\mathbf{Nz}^e)^2 - (\mathbf{Ny}^e)^2] + 2\mathbf{Ny}^e \mathbf{Nz}^e I_{yz} \\ -I_{yz}[(\mathbf{Nz}^e)^2 - (\mathbf{Ny}^e)^2] + 2\mathbf{Ny}^e \mathbf{Nz}^e I_y \end{bmatrix} \right] \right] d\xi dy = 0 \end{aligned} \quad (66)$$

$$+2(1+\nu)\mathbf{N}^T(I_y\mathbf{N}\mathbf{y}^e - I_{yz}\mathbf{N}\mathbf{z}^e)]\left[\frac{1}{2}\det|\mathbf{J}|d\eta d\xi = 0\right]$$

It gives that:

$$\begin{aligned} & \int_0^1 \int_0^{1-\xi} \left[ \left( \frac{\partial \mathbf{N}^T}{\partial y} \frac{\partial \mathbf{N}}{\partial y} + \frac{\partial \mathbf{N}^T}{\partial z} \frac{\partial \mathbf{N}}{\partial z} \right) \Phi^e \right. \\ & \quad \left. - \left[ \frac{\nu}{2} \begin{bmatrix} \frac{\partial \mathbf{N}}{\partial y} & \frac{\partial \mathbf{N}}{\partial z} \end{bmatrix} \begin{bmatrix} I_y[(\mathbf{N}\mathbf{z}^e)^2 - (\mathbf{N}\mathbf{y}^e)^2] + 2\mathbf{N}\mathbf{y}^e\mathbf{N}\mathbf{z}^e I_{yz} \\ -I_{yz}[(\mathbf{N}\mathbf{z}^e)^2 - (\mathbf{N}\mathbf{y}^e)^2] + 2\mathbf{N}\mathbf{y}^e\mathbf{N}\mathbf{z}^e I_y \end{bmatrix} \right] \right. \\ & \quad \left. + 2(1+\nu)\mathbf{N}^T(I_y\mathbf{N}\mathbf{y}^e - I_{yz}\mathbf{N}\mathbf{z}^e) \right] \frac{1}{2} \det|\mathbf{J}| d\eta d\xi = 0 \end{aligned} \quad (67)$$

From above, the element stiffness matrix  $\mathbf{K}^e$  and load vector  $\mathbf{P}_y^e$  are formulated as:

$$\begin{aligned} \mathbf{K}^e &= \int_0^1 \int_0^{1-\xi} \left( \frac{\partial \mathbf{N}^T}{\partial y} \frac{\partial \mathbf{N}}{\partial y} + \frac{\partial \mathbf{N}^T}{\partial z} \frac{\partial \mathbf{N}}{\partial z} \right) \frac{1}{2} \det|\mathbf{J}| d\eta d\xi \\ &= \frac{1}{2} \sum_{i=1}^n \left[ \frac{\partial \mathbf{N}(\eta_i, \xi_i)^T}{\partial y} \frac{\partial \mathbf{N}(\eta_i, \xi_i)}{\partial y} + \frac{\partial \mathbf{N}(\eta_i, \xi_i)^T}{\partial z} \frac{\partial \mathbf{N}(\eta_i, \xi_i)}{\partial z} \right] \det|\mathbf{J}| \end{aligned} \quad (68)$$

$$\begin{aligned} \mathbf{P}_y^e &= \int_0^1 \int_0^{1-\xi} \left[ \frac{\nu}{2} \begin{bmatrix} \frac{\partial \mathbf{N}}{\partial y} & \frac{\partial \mathbf{N}}{\partial z} \end{bmatrix} \begin{bmatrix} I_y[(\mathbf{N}\mathbf{z}^e)^2 - (\mathbf{N}\mathbf{y}^e)^2] + 2\mathbf{N}\mathbf{y}^e\mathbf{N}\mathbf{z}^e I_{yz} \\ -I_{yz}[(\mathbf{N}\mathbf{z}^e)^2 - (\mathbf{N}\mathbf{y}^e)^2] + 2\mathbf{N}\mathbf{y}^e\mathbf{N}\mathbf{z}^e I_y \end{bmatrix} \right. \\ & \quad \left. + 2(1+\nu)\mathbf{N}^T(I_y\mathbf{N}\mathbf{y}^e - I_{yz}\mathbf{N}\mathbf{z}^e) \right] \frac{1}{2} \det|\mathbf{J}| d\eta d\xi \\ &= \frac{1}{2} \sum_{i=1}^n \left[ \frac{\nu}{2} \begin{bmatrix} \frac{\partial \mathbf{N}(\eta_i, \xi_i)}{\partial y} & \frac{\partial \mathbf{N}(\eta_i, \xi_i)}{\partial z} \end{bmatrix} \right. \\ & \quad \left. \begin{bmatrix} I_y[[\mathbf{N}(\eta_i, \xi_i)\mathbf{z}^e]^2 - [\mathbf{N}(\eta_i, \xi_i)\mathbf{y}^e]^2] + 2\mathbf{N}(\eta_i, \xi_i)\mathbf{y}^e\mathbf{N}(\eta_i, \xi_i)\mathbf{z}^e I_{yz} \\ -I_{yz}[[\mathbf{N}(\eta_i, \xi_i)\mathbf{z}^e]^2 - [\mathbf{N}(\eta_i, \xi_i)\mathbf{y}^e]^2] + 2\mathbf{N}(\eta_i, \xi_i)\mathbf{y}^e\mathbf{N}(\eta_i, \xi_i)\mathbf{z}^e I_y \end{bmatrix} \right. \\ & \quad \left. + 2(1+\nu)\mathbf{N}^T[I_y\mathbf{N}(\eta_i, \xi_i)\mathbf{y}^e - I_{yz}\mathbf{N}(\eta_i, \xi_i)\mathbf{z}^e] \right] \det|\mathbf{J}| \end{aligned} \quad (69)$$

Therefore, the calculation of shear coefficients  $k_y$  can be obtained by solving the equation between the total stiffness matrix  $\mathbf{K}$  and total load vector  $\mathbf{P}_y$  and gives as,

$$k_y = \frac{\Delta^2}{A\kappa_y} \quad (70)$$

where,

$$\Delta = 2(1 + \nu)(I_{\bar{y}}I_{\bar{z}} - I_{\bar{y}\bar{z}}^2) \quad (71)$$

$$\begin{aligned} \kappa_y &= \int_A \left( \begin{bmatrix} \frac{\partial \Phi}{\partial y} \\ \frac{\partial \Phi}{\partial z} \end{bmatrix}^T - \frac{\nu}{2} \mathbf{h}^T \right) \left( \begin{bmatrix} \frac{\partial \Phi}{\partial y} \\ \frac{\partial \Phi}{\partial z} \end{bmatrix} - \frac{\nu}{2} \mathbf{h} \right) dA \\ &= \sum^{NE} \int_0^1 \int_0^{1-\xi} \left( \begin{bmatrix} \frac{\partial N}{\partial y} \Phi^e \\ \frac{\partial N}{\partial z} \Phi^e \end{bmatrix}^T - \frac{\nu}{2} \mathbf{h}^T \right) \left( \begin{bmatrix} \frac{\partial N}{\partial y} \Phi^e \\ \frac{\partial N}{\partial z} \Phi^e \end{bmatrix} - \frac{\nu}{2} \mathbf{h} \right) \frac{1}{2} \det|\mathbf{J}| d\eta d\xi \end{aligned} \quad (72)$$

$$\begin{aligned} &= \frac{1}{2} \sum^{NE} \sum_{i=1}^n W_i \left( \begin{bmatrix} \frac{\partial N(\eta_i, \xi_i)}{\partial y} \Phi^e \\ \frac{\partial N(\eta_i, \xi_i)}{\partial z} \Phi^e \end{bmatrix}^T - \frac{\nu}{2} \mathbf{h}(\eta_i, \xi_i)^T \right) \\ &\quad \left( \begin{bmatrix} \frac{\partial N(\eta_i, \xi_i)}{\partial y} \Phi^e \\ \frac{\partial N(\eta_i, \xi_i)}{\partial z} \Phi^e \end{bmatrix} - \frac{\nu}{2} \mathbf{h}(\eta_i, \xi_i) \right) \det|\mathbf{J}| \\ \mathbf{h}(\eta_i, \xi_i) &= \begin{bmatrix} -I_{\bar{y}}(\bar{z}^2 - \bar{y}^2) - 2I_{\bar{y}\bar{z}}\bar{y}\bar{z} \\ -I_{\bar{y}\bar{z}}(\bar{z}^2 - \bar{y}^2) + 2I_{\bar{y}}\bar{y}\bar{z} \end{bmatrix} \end{aligned} \quad (73)$$

$$= \begin{bmatrix} -I_{\bar{y}}[[N(\eta_i, \xi_i)\bar{z}^e]^2 - [N(\eta_i, \xi_i)\bar{y}^e]^2] - 2I_{\bar{y}\bar{z}}N(\eta_i, \xi_i)\bar{y}^eN(\eta_i, \xi_i)\bar{z}^e \\ -I_{\bar{y}\bar{z}}[[N(\eta_i, \xi_i)\bar{z}^e]^2 - [N(\eta_i, \xi_i)\bar{y}^e]^2] + 2I_{\bar{y}}N(\eta_i, \xi_i)\bar{y}^eN(\eta_i, \xi_i)\bar{z}^e \end{bmatrix}$$

Similarly, shear coefficients  $k_z$  can be generated by,

$$k_z = \frac{\Delta^2}{A\kappa_z} \quad (74)$$

$$\begin{aligned}
\kappa_z &= \int_A \left( \begin{bmatrix} \frac{\partial \Psi}{\partial y} \\ \frac{\partial \Psi}{\partial z} \end{bmatrix}^T - \frac{\nu}{2} \mathbf{d}^T \right) \left( \begin{bmatrix} \frac{\partial \Psi}{\partial y} \\ \frac{\partial \Psi}{\partial z} \end{bmatrix} - \frac{\nu}{2} \mathbf{d} \right) dA \\
&= \sum_{i=1}^{NE} \int_0^1 \int_0^{1-\xi} \left( \begin{bmatrix} \frac{\partial N}{\partial y} \Psi^e \\ \frac{\partial N}{\partial z} \Psi^e \end{bmatrix}^T - \frac{\nu}{2} \mathbf{d}^T \right) \left( \begin{bmatrix} \frac{\partial N}{\partial y} \Psi^e \\ \frac{\partial N}{\partial z} \Psi^e \end{bmatrix} - \frac{\nu}{2} \mathbf{d} \right) \frac{1}{2} \det|\mathbf{J}| d\eta d\xi \\
&\quad (75)
\end{aligned}$$

$$\begin{aligned}
&= \frac{1}{2} \sum_{i=1}^{NE} \sum_{j=1}^n W_i \left( \begin{bmatrix} \frac{\partial N(\eta_i, \xi_i)}{\partial y} \Psi^e \\ \frac{\partial N(\eta_i, \xi_i)}{\partial z} \Psi^e \end{bmatrix}^T - \frac{\nu}{2} \mathbf{d}(\eta_i, \xi_i)^T \right) \\
&\quad \left( \begin{bmatrix} \frac{\partial N(\eta_i, \xi_i)}{\partial y} \Psi^e \\ \frac{\partial N(\eta_i, \xi_i)}{\partial z} \Psi^e \end{bmatrix} - \frac{\nu}{2} \mathbf{d}(\eta_i, \xi_i) \right) \det|\mathbf{J}|
\end{aligned}$$

$$\begin{aligned}
\mathbf{d}(\eta_i, \xi_i) &= \begin{bmatrix} I_{\bar{y}\bar{z}}(\bar{z}^2 - \bar{y}^2) + 2I_{\bar{z}}\bar{y}\bar{z} \\ I_{\bar{z}}(\bar{z}^2 - \bar{y}^2) - 2I_{\bar{y}\bar{z}}\bar{y}\bar{z} \end{bmatrix} \\
&= \begin{bmatrix} I_{\bar{y}\bar{z}}[[N(\eta_i, \xi_i)\bar{z}^e]^2 - [N(\eta_i, \xi_i)\bar{y}^e]^2] + 2I_{\bar{z}}N(\eta_i, \xi_i)\bar{y}^e N(\eta_i, \xi_i)\bar{z}^e \\ I_{\bar{z}}[[N(\eta_i, \xi_i)\bar{z}^e]^2 - [N(\eta_i, \xi_i)\bar{y}^e]^2] - 2I_{\bar{y}\bar{z}}N(\eta_i, \xi_i)\bar{y}^e N(\eta_i, \xi_i)\bar{z}^e \end{bmatrix} \\
&\quad (76)
\end{aligned}$$

where  $\Psi$  is the corresponding shear function.

## 4. Verification Examples

In order to verify the accuracy and validation of this software, some examples are selected and tested, results are compared with those from the available works and design codes.

### 4.1 Section properties for thin-walled sections

Knowing that the location of the shear center ( $y_s$  and  $z_s$ ) and the Wagner coefficients ( $\beta_y$ ,  $\beta_z$ , and  $\beta_\omega$ ) are essential for an accurate analysis of a system that contains non-symmetric sections, four such sections are studied, with their dimensions given in **Figure 6**. Given that the mono-symmetric-I section is symmetric about the y-axis (**Figure 5**), the Wagner coefficients  $\beta_y$  and  $\beta_\omega$  are zero. The closed-form equation for calculating the Wagner coefficient  $\beta_z$  is derived by Ziemian (2010) and given below.

$$\beta_z = -(\chi_1 - \chi_2 + \chi_3)/I_z - 2y_s \quad (77)$$

where,

$$\begin{aligned} \chi_1 &= \frac{b_{fc}^3}{12}(d_o')t_{fc} + \frac{b_{fc}^3}{24}t_{fc}^2 + b_{fc}(d_o')^3t_{fc} + \frac{3}{2}b_{fc}(d_o')^2t_{fc}^2 \\ &\quad + b_{fc}(d_o')t_{fc}^3 + \frac{b_{fc}}{4}t_{fc}^4 \end{aligned} \quad (78)$$

$$\begin{aligned} \chi_2 &= \frac{b_{ft}^3}{12}d_o t_{ft} + \frac{b_{ft}^3}{24}t_{ft}^2 + b_{ft}t_{ft}d_o^3 + 1.5b_{ft}t_{ft}^2d_o^2 + b_{ft}t_{ft}^3d_o \\ &\quad + \frac{1}{4}b_{ft}t_{ft}^4 \end{aligned} \quad (79)$$

$$\chi_3 = \frac{(d_o')^4}{4}t_w + \frac{(d_o')^2}{24}t_w^3 - \frac{d_o^4}{4}t_w - \frac{d_o^2}{24}t_w^3 \quad (80)$$

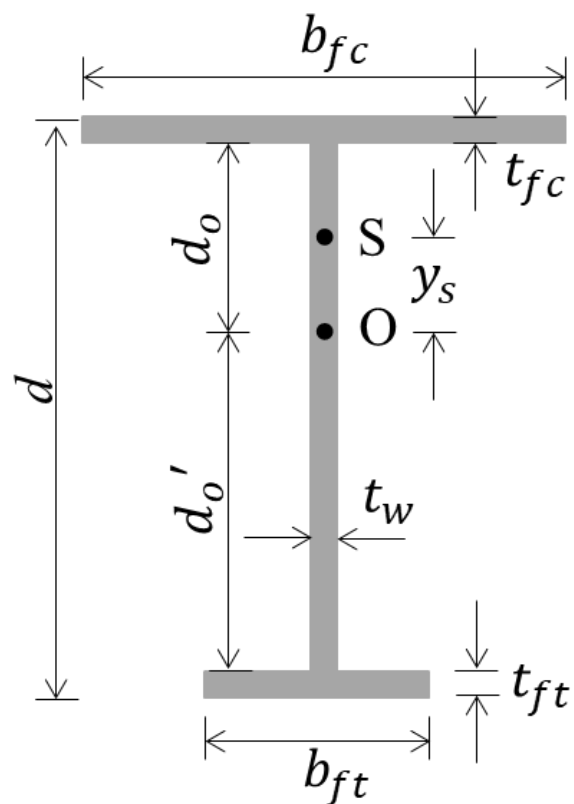
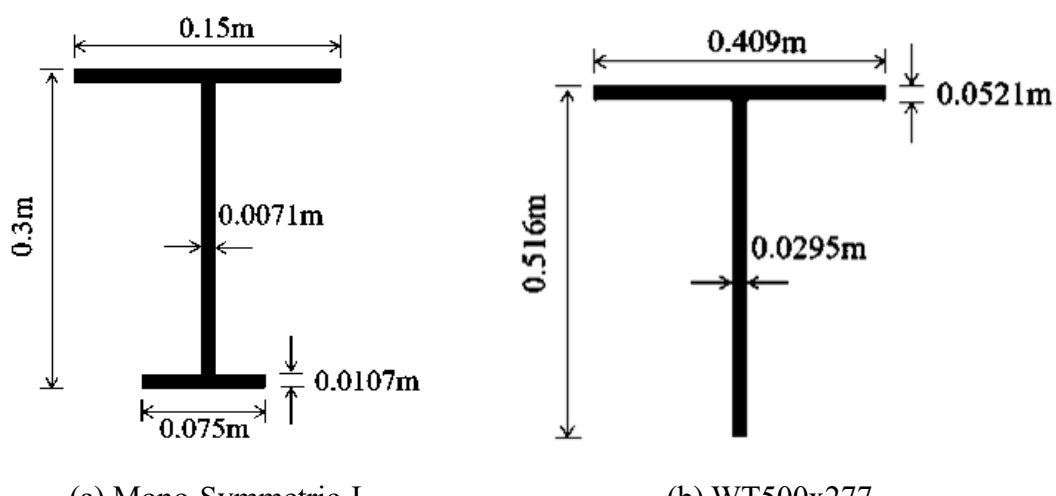


**Figure 5** Dimensions of the mono-symmetric-I section



(a) Mono-Symmetric-I

(b) WT500x277

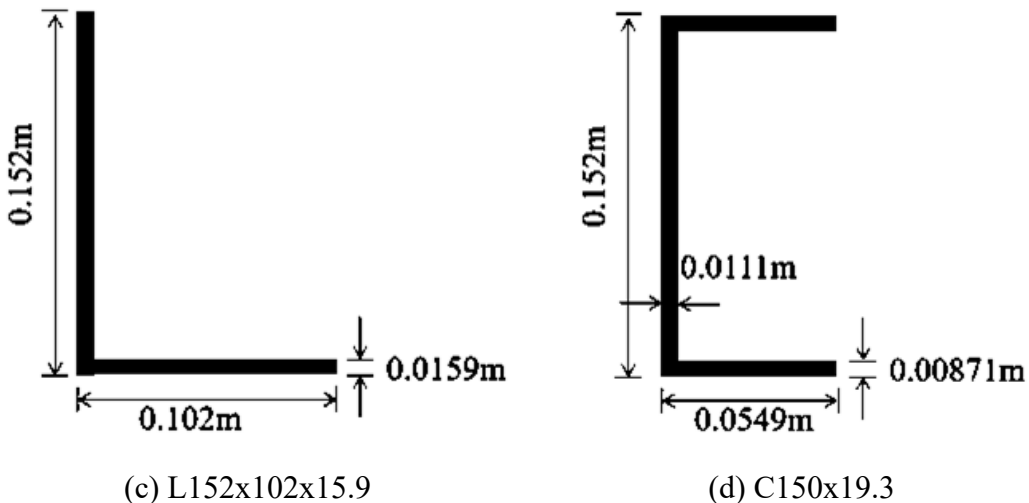


**Figure 6** Four sections for the verification of CM method

The properties for the other sections are obtained from version 15.0 of the AISC 2016 database. Using these properties as a basis, the values computed by the section definition module based on the proposed algorithm presented earlier, are then verified. Sections were constructed via a series of points and segments working from the mid-points of the through-thicknesses.

Although limited to one mono-symmetric-I section, the comparison presented in **Table 1** tends to confirm the accuracy of the proposed computational algorithm in defining properties for an open-section. In practice, the properties of common shapes such as T-, L-, and C-sections are usually obtained from the section tables in design codes, such as AISC (2016), but the Wagner coefficients are often not provided. Herein, three sections selected from the AISC shapes database, including WT500x277, L152x102x15.9, and C150x19.3, are studied, where the common section properties apart from the Wagner coefficients are compared in **Table 2** with the values calculated by the proposed computational algorithm. Any small differences are assumed to be attributed to the AISC database accounting for fillets and/or rounded edges. Of course, the generalized computational algorithm presented in this software can be used for generating the Wagner coefficients for non-symmetric sections, which may be further incorporated into current section tables with codes.

**Table 1** Section properties of the mono-symmetric-I section

Parameter	Closed-form Solution	Present Study	Differences
$A$	$4.462 \times 10^{-3} m^2$	$4.462 \times 10^{-3} m^2$	0
$I_y$	$3.394 \times 10^{-6} m^4$	$3.394 \times 10^{-6} m^4$	0
$I_z$	$6.171 \times 10^{-5} m^4$	$6.170 \times 10^{-5} m^4$	0
$J$	$1.264 \times 10^{-7} m^4$	$1.264 \times 10^{-7} m^4$	0

$I_w$	$2.799 \times 10^{-8} m^6$	$2.799 \times 10^{-8} m^6$	0
$y_c$	$8.745 \times 10^{-2} m$	$8.627 \times 10^{-2} m$	-1.3%
$z_c$	0	0	0
$\beta_y$	--	0	--
$\beta_z$	$-2.052 \times 10^{-1} m$	$-2.077 \times 10^{-1} m$	1.2%
$\beta_w$	--	0	--

**Table 2** Section properties of the WT, L, and C sections**Section B - WT500x277**

Parameter	Section Table	Present Study	Differences
$A$	$3.53 \times 10^{-2} m^2$	$3.57 \times 10^{-2} m^2$	1.0%
$I_y$	$8.03 \times 10^{-4} m^4$	$8.11 \times 10^{-4} m^4$	1.0%
$I_z$	$2.95 \times 10^{-4} m^4$	$2.98 \times 10^{-4} m^4$	1.1%
$J$	$2.40 \times 10^{-5} m^4$	$2.35 \times 10^{-5} m^4$	-2.2%
$I_w$	$1.50 \times 10^{-7} m^6$	$1.51 \times 10^{-7} m^6$	0.7%
$y_c$	$9.99 \times 10^{-2} m$	$9.87 \times 10^{-2} m$	-1.3%
$z_c$	0	0	0
$\beta_y$	--	0	--
$\beta_z$	--	$-3.47 \times 10^{-1} m$	--
$\beta_w$	--	0	--

**Section C - L152x102x15.9**

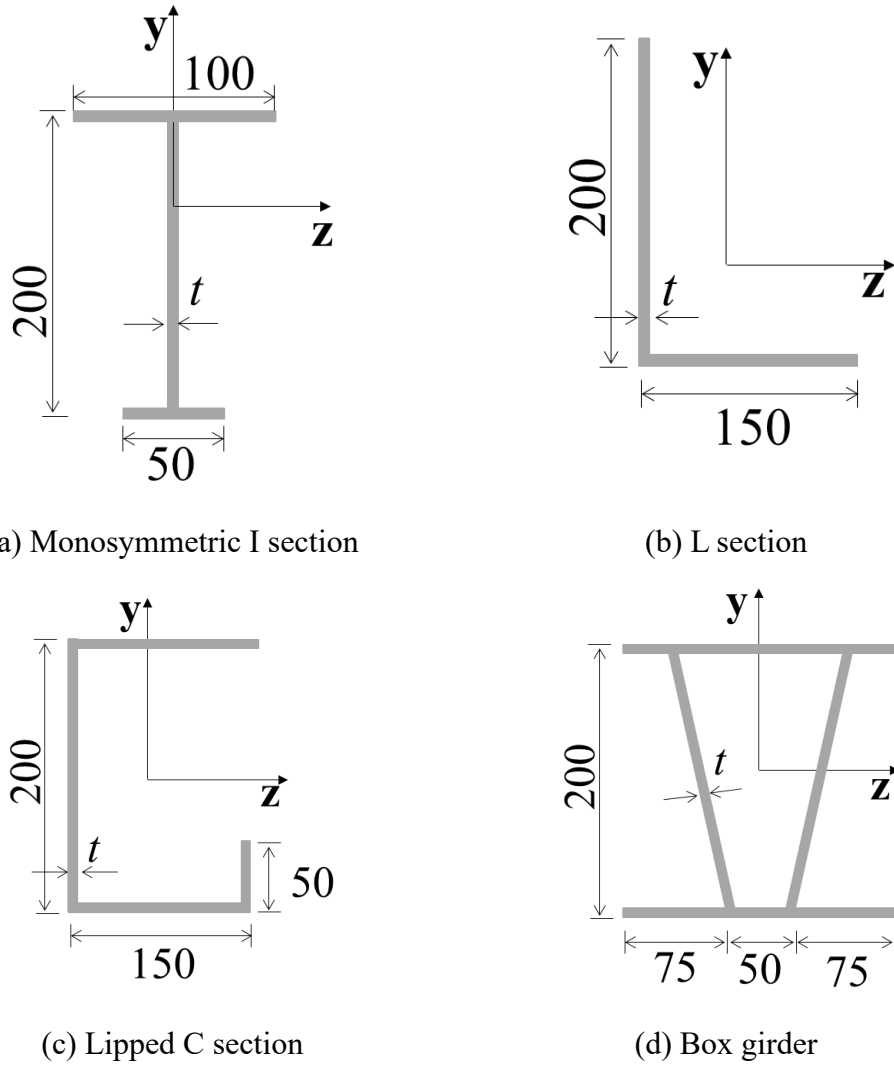
Parameter	Section Table	Present Study	Differences
$A$	$3.780 \times 10^{-3} m^2$	$3.786 \times 10^{-3} m^2$	0.2%
$I_y$	$3.11 \times 10^{-6} m^4$	$3.15 \times 10^{-6} m^4$	1.3%
$I_z$	$8.74 \times 10^{-6} m^4$	$8.69 \times 10^{-6} m^4$	-0.6%
$J$	$3.23 \times 10^{-7} m^4$	$3.19 \times 10^{-7} m^4$	-1.2%
$I_w$	$4.27 \times 10^{-10} m^6$	$4.27 \times 10^{-10} m^6$	-0.1%
$y_c$	$1.825 \times 10^{-2} m$	$1.883 \times 10^{-2} m$	3.2%
$z_c$	$4.365 \times 10^{-2} m$	$4.266 \times 10^{-2} m$	-2.3%
$\beta_y$	--	$1.071 \times 10^{-1} m$	--
$\beta_z$	--	$6.515 \times 10^{-2} m$	--

$\beta_w$	--	0	--
<b>Section D - C150x19.3</b>			
Parameter	Section Table	Present Study	Differences
$A$	$2.46 \times 10^{-3} \text{ m}^2$	$2.45 \times 10^{-3} \text{ m}^2$	-0.4%
$I_y$	$7.20 \times 10^{-6} \text{ m}^4$	$7.14 \times 10^{-6} \text{ m}^4$	-0.8%
$I_z$	$4.37 \times 10^{-7} \text{ m}^4$	$4.39 \times 10^{-7} \text{ m}^4$	0.5%
$J$	$9.86 \times 10^{-8} \text{ m}^4$	$9.75 \times 10^{-8} \text{ m}^4$	-1.1%
$I_w$	$1.93 \times 10^{-9} \text{ m}^6$	$1.92 \times 10^{-9} \text{ m}^6$	-0.5%
$y_c$	0	0	
$z_c$	$-2.275 \times 10^{-2} \text{ m}$	$-2.284 \times 10^{-2} \text{ m}$	0.4%
$\beta_y$	--	$-1.799 \times 10^{-1} \text{ m}$	--
$\beta_z$	--	0	--
$\beta_w$	--	0	--

To validate the accuracy of the proposed cross-section analysis method, two examples are presented in this section, where the section properties, including geometric properties ( $A$ ,  $I_y$ , and  $I_z$ ), the torsional properties ( $J$ ,  $I_w$ ,  $y_c$ ,  $z_c$ ,  $\beta_y$ ,  $\beta_z$ , and  $\beta_w$ ) and the shear coefficients ( $k_y$  and  $k_z$ ), from the proposed method are compared with those from other algorithms.

## 4.2 Geometric and torsional properties

The geometric and torsional properties of four nonsymmetric sections are calculated. The section width and depth of each section are given in **Figure 7**, where three different wall thicknesses, 10mm, 15mm, and 20mm, are adopted. Results generated by the proposed CST element are compared with the benchmark results obtained from SkyCiv Section Builder (2017), and the differences are plotted in **Figure 8**. Besides, the section properties from the CM method (Liu et al. 2018; Liu et al. 2019) are also given for comparison. Detailed section properties are listed in **Table 3**-**Table 6**, and the differences between the calculation results and the benchmark results are given in **Figure 8**.

**Figure 7** Verification examples of geometric and torsional properties.**Table 3** Geometric and torsional properties – Monosymmetric I Section (Unit: mm)

	Benchmark			CM Method			Present Study		
	$t = 10$	$t = 15$	$t = 20$	$t = 10$	$t = 15$	$t = 20$	$t = 10$	$t = 15$	$t = 20$
$A$	$3.30 \times 10^3$	$4.80 \times 10^3$	$6.20 \times 10^3$	$3.30 \times 10^3$	$4.80 \times 10^3$	$6.20 \times 10^3$	$3.30 \times 10^3$	$4.80 \times 10^3$	$6.20 \times 10^3$
$I_y$	$9.53 \times 10^5$	$1.45 \times 10^6$	$1.98 \times 10^6$	$9.53 \times 10^5$	$1.45 \times 10^6$	$1.98 \times 10^6$	$9.53 \times 10^5$	$1.45 \times 10^6$	$1.98 \times 10^6$
$I_z$	$1.77 \times 10^7$	$2.44 \times 10^7$	$2.99 \times 10^7$	$1.77 \times 10^7$	$2.44 \times 10^7$	$2.99 \times 10^7$	$1.77 \times 10^7$	$2.44 \times 10^7$	$2.99 \times 10^7$
$J$	$1.11 \times 10^5$	$3.65 \times 10^5$	$8.44 \times 10^5$	$1.13 \times 10^5$	$3.60 \times 10^5$	$8.27 \times 10^5$	$1.13 \times 10^5$	$3.71 \times 10^5$	$8.54 \times 10^5$
$I_\omega$	$3.43 \times 10^9$	$5.00 \times 10^9$	$6.47 \times 10^9$	$3.34 \times 10^9$	$4.76 \times 10^9$	$6.02 \times 10^9$	$3.43 \times 10^9$	$5.00 \times 10^9$	$6.48 \times 10^9$
$y_c$	$5.81 \times 10^1$	$5.45 \times 10^1$	$5.07 \times 10^1$	$5.86 \times 10^1$	$5.56 \times 10^1$	$5.25 \times 10^1$	$5.81 \times 10^1$	$5.46 \times 10^1$	$5.08 \times 10^1$
$z_c$	0	0	0	0	0	0	0	0	0
$\beta_v$	0	0	0	0	0	0	0	0	0
$\beta_w$	-	-	-	-	-	-	-	-	-
$\beta_\omega$	-	-	-	0	0	0	0	0	0

**Table 4** Geometric and torsional properties – L section (Unit: mm)

	Benchmark			CM Method			Present Study		
	$t = 10$	$t = 15$	$t = 20$	$t = 10$	$t = 15$	$t = 20$	$t = 10$	$t = 15$	$t = 20$
$A$	$3.40 \times 10^3$	$5.02 \times 10^3$	$6.60 \times 10^3$	$3.40 \times 10^3$	$5.03 \times 10^3$	$6.60 \times 10^3$	$3.40 \times 10^3$	$5.03 \times 10^3$	$6.60 \times 10^3$
$I_y$	$6.94 \times 10^6$	$9.93 \times 10^6$	$1.27 \times 10^7$	$6.93 \times 10^6$	$9.93 \times 10^6$	$1.26 \times 10^7$	$6.94 \times 10^6$	$9.93 \times 10^6$	$1.27 \times 10^7$
$I_z$	$1.41 \times 10^7$	$2.04 \times 10^7$	$2.62 \times 10^7$	$1.41 \times 10^7$	$2.04 \times 10^7$	$2.61 \times 10^7$	$1.41 \times 10^7$	$2.04 \times 10^7$	$2.65 \times 10^7$
$J$	$1.14 \times 10^5$	$3.69 \times 10^5$	$8.56 \times 10^5$	$1.13 \times 10^5$	$3.77 \times 10^5$	$8.80 \times 10^5$	$1.13 \times 10^5$	$3.72 \times 10^5$	$8.61 \times 10^5$
$I_{\omega}$	$2.89 \times 10^8$	$9.27 \times 10^8$	$2.07 \times 10^9$	$2.91 \times 10^8$	$9.40 \times 10^8$	$2.13 \times 10^9$	$2.89 \times 10^8$	$9.26 \times 10^8$	$2.07 \times 10^9$
$y_c$	$5.55 \times 10^1$	$5.43 \times 10^1$	$5.29 \times 10^1$	$5.58 \times 10^1$	$5.49 \times 10^1$	$5.40 \times 10^1$	$5.55 \times 10^1$	$5.43 \times 10^1$	$5.29 \times 10^1$
$z_c$	$3.09 \times 10^1$	$3.02 \times 10^1$	$2.95 \times 10^1$	$3.10 \times 10^1$	$3.04 \times 10^1$	$2.99 \times 10^1$	$3.09 \times 10^1$	$3.02 \times 10^1$	$2.95 \times 10^1$
$\beta_v$	$2.30 \times 10^2$	$2.23 \times 10^2$	$2.16 \times 10^2$	$2.31 \times 10^2$	$2.26 \times 10^2$	$2.22 \times 10^2$	$2.30 \times 10^2$	$2.23 \times 10^2$	$2.16 \times 10^2$
$\beta_w$	$8.20 \times 10^1$	$8.10 \times 10^1$	$7.95 \times 10^1$	$8.24 \times 10^1$	$8.17 \times 10^1$	$8.09 \times 10^1$	$8.20 \times 10^1$	$8.10 \times 10^1$	$7.95 \times 10^1$
$\beta_{\omega}$	-	-	-	$2.17 \times 10^{-1}$ 1	$2.18 \times 10^{-1}$ 1	$2.19 \times 10^{-1}$ 1	$2.73 \times 10^{-1}$ 1	$2.73 \times 10^{-1}$ 1	$2.69 \times 10^{-1}$ 1

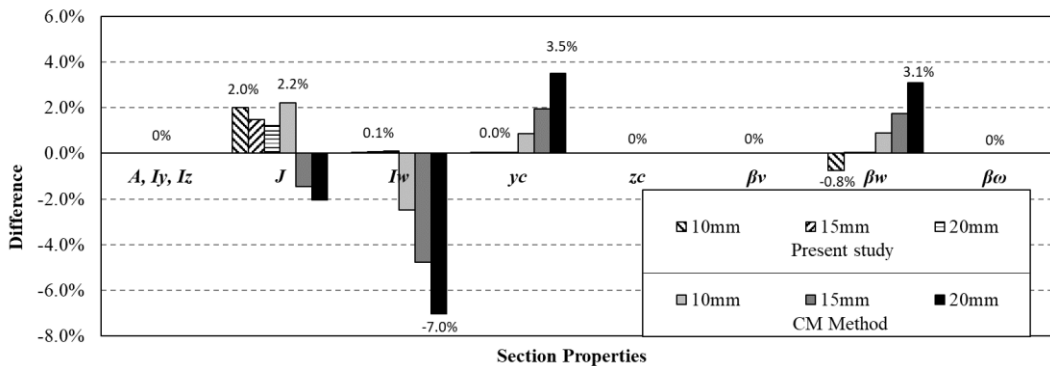
**Table 5** Geometric and torsional properties – Lipped C section (Unit: mm)

	Benchmark			CM Method			Present Study		
	$t = 10$	$t = 15$	$t = 20$	$t = 10$	$t = 15$	$t = 20$	$t = 10$	$t = 15$	$t = 20$
$A$	$5.20 \times 10^3$	$7.58 \times 10^3$	$9.80 \times 10^3$	$5.20 \times 10^3$	$7.58 \times 10^3$	$9.80 \times 10^3$	$5.20 \times 10^3$	$7.58 \times 10^3$	$9.80 \times 10^3$
$I_y$	$1.46 \times 10^7$	$2.00 \times 10^7$	$2.45 \times 10^7$	$1.45 \times 10^7$	$1.99 \times 10^7$	$2.42 \times 10^7$	$1.46 \times 10^7$	$2.00 \times 10^7$	$2.45 \times 10^7$
$I_z$	$3.38 \times 10^7$	$4.70 \times 10^7$	$5.81 \times 10^7$	$3.38 \times 10^7$	$4.68 \times 10^7$	$5.75 \times 10^7$	$3.38 \times 10^7$	$4.70 \times 10^7$	$5.81 \times 10^7$
$J$	$1.73 \times 10^5$	$5.66 \times 10^5$	$1.30 \times 10^6$	$1.73 \times 10^5$	$5.68 \times 10^5$	$1.31 \times 10^6$	$1.75 \times 10^5$	$5.72 \times 10^5$	$1.31 \times 10^6$
$I_{\omega}$	$1.17 \times 10^1$ 1	$1.52 \times 10^1$ 1	$1.76 \times 10^1$ 1	$1.16 \times 10^1$ 1	$1.50 \times 10^1$ 1	$1.72 \times 10^1$ 1	$1.17 \times 10^1$ 1	$1.52 \times 10^1$ 1	$1.76 \times 10^1$ 1
$y_c$	$2.42 \times 10^1$	$2.10 \times 10^1$	$1.77 \times 10^1$	$2.44 \times 10^1$	$2.14 \times 10^1$	$1.83 \times 10^1$	$2.42 \times 10^1$	$2.10 \times 10^1$	$1.77 \times 10^1$
$z_c$	$1.17 \times 10^2$	$1.13 \times 10^2$	$1.09 \times 10^2$	$1.18 \times 10^2$	$1.15 \times 10^2$	$1.11 \times 10^2$	$1.17 \times 10^2$	$1.14 \times 10^2$	$1.09 \times 10^2$
$\beta_v$	$2.96 \times 10^2$	$2.86 \times 10^2$	$2.75 \times 10^2$	$2.97 \times 10^2$	$2.89 \times 10^2$	$2.80 \times 10^2$	$2.96 \times 10^2$	$2.86 \times 10^2$	$2.75 \times 10^2$
$\beta_w$	$2.29 \times 10^1$	$2.09 \times 10^1$	$1.86 \times 10^1$	$2.34 \times 10^1$	$2.22 \times 10^1$	$2.10 \times 10^1$	$2.29 \times 10^1$	$2.09 \times 10^1$	$1.86 \times 10^1$
$\beta_{\omega}$	-	-	-	$7.33 \times 10^{-2}$ 2	$7.83 \times 10^{-2}$ 2	$8.37 \times 10^{-2}$ 2	$7.04 \times 10^{-2}$ 2	$7.13 \times 10^{-2}$ 2	$7.03 \times 10^{-2}$ 2

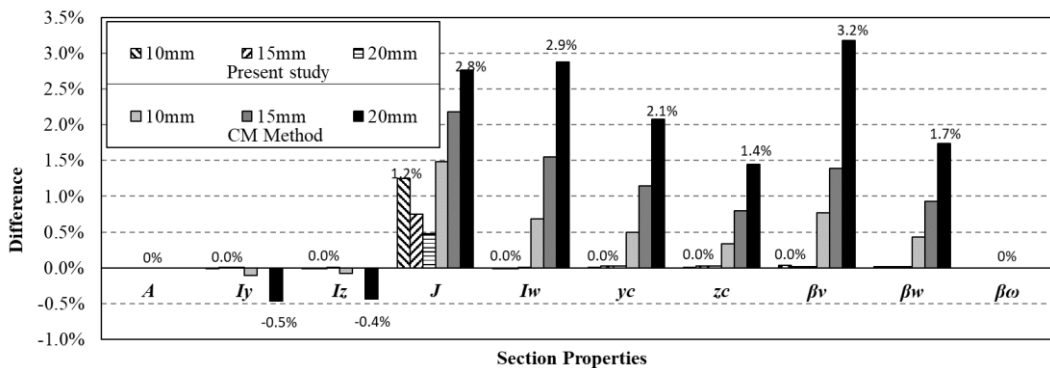
**Table 6** Geometric and torsional properties – Box girder (Unit: mm)

	Benchmark			CM Method			Present Study		
	$t = 10$	$t = 15$	$t = 20$	$t = 10$	$t = 15$	$t = 20$	$t = 10$	$t = 15$	$t = 20$
$A$	$7.74 \times 10^3$	$1.13 \times 10^4$	$1.47 \times 10^4$	$7.96 \times 10^3$	$1.18 \times 10^4$	$1.56 \times 10^4$	$7.74 \times 10^3$	$1.13 \times 10^4$	$1.47 \times 10^4$
$I_y$	$2.17 \times 10^7$	$3.07 \times 10^7$	$3.88 \times 10^7$	$2.21 \times 10^7$	$3.17 \times 10^7$	$4.05 \times 10^7$	$2.17 \times 10^7$	$3.07 \times 10^7$	$3.88 \times 10^7$
$I_z$	$4.62 \times 10^7$	$6.43 \times 10^7$	$7.94 \times 10^7$	$4.81 \times 10^7$	$6.81 \times 10^7$	$8.57 \times 10^7$	$4.62 \times 10^7$	$6.43 \times 10^7$	$7.94 \times 10^7$
$J$	$2.11 \times 10^7$	$2.85 \times 10^7$	$3.44 \times 10^7$	$2.00 \times 10^7$	$2.62 \times 10^7$	$3.04 \times 10^7$	$2.12 \times 10^7$	$2.87 \times 10^7$	$3.45 \times 10^7$
$I_{\omega}$	$9.84 \times 10^1$ 1	$6.55 \times 10^1$ 1	$5.02 \times 10^1$ 1	$6.24 \times 10^1$ 0	$9.96 \times 10^1$ 0	$1.39 \times 10^1$ 1	$5.91 \times 10^1$ 0	$8.94 \times 10^1$ 0	$1.20 \times 10^1$ 1
$y_c$	$7.54 \times 10^0$ 1	$1.13 \times 10^0$ 1	$1.54 \times 10^0$ 1	$8.31 \times 10^0$ 1	$1.21 \times 10^0$ 1	$1.54 \times 10^0$ 1	$7.56 \times 10^0$ 1	$1.15 \times 10^0$ 0	$1.57 \times 10^0$ 0
$z_c$	0	0	0	0	0	0	0	0	0
$\beta_v$	0	0	0	0	0	0	0	0	0
$\beta_w$	$6.97 \times 10^0$	$7.19 \times 10^0$	$7.54 \times 10^0$	$8.08 \times 10^0$	$8.83 \times 10^0$	$9.95 \times 10^0$	$6.95 \times 10^0$	$7.24 \times 10^0$	$7.59 \times 10^0$
$\beta_{\omega}$	-	-	-	0	0	0	0	0	0

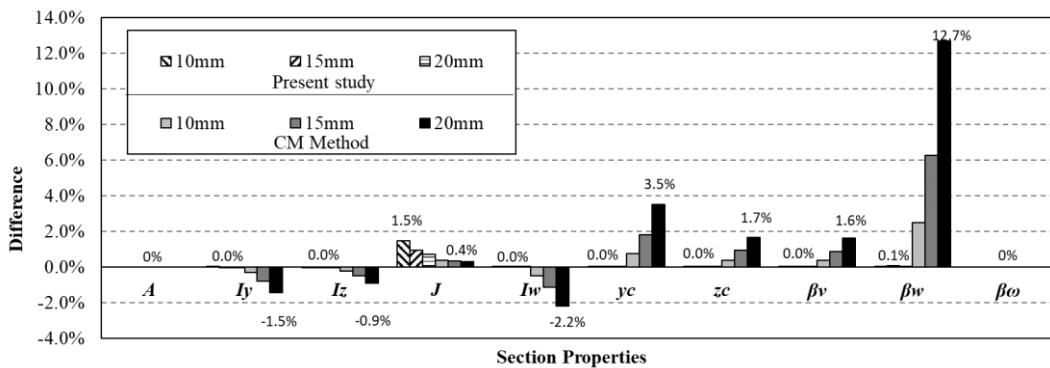
From **Figure 8**, it can be observed that with the increment of the wall thickness, the differences between the results from the CM method and the benchmark results are increasing with the differences up to 31.9%. This is because the CM method is based on the thin-walled assumption, which is not suitable for calculating the section properties of thick-walled sections. The differences between the results from the proposed CST elements and the benchmark results are relatively small (no more than 2%) for all the wall thicknesses. It can be concluded that the proposed cross-section analysis algorithm can calculate the geometric and torsional properties of nonsymmetric sections accurately regardless of the wall thickness.



(a) Monosymmetric I section



(b) L section



(c) Lipped C section

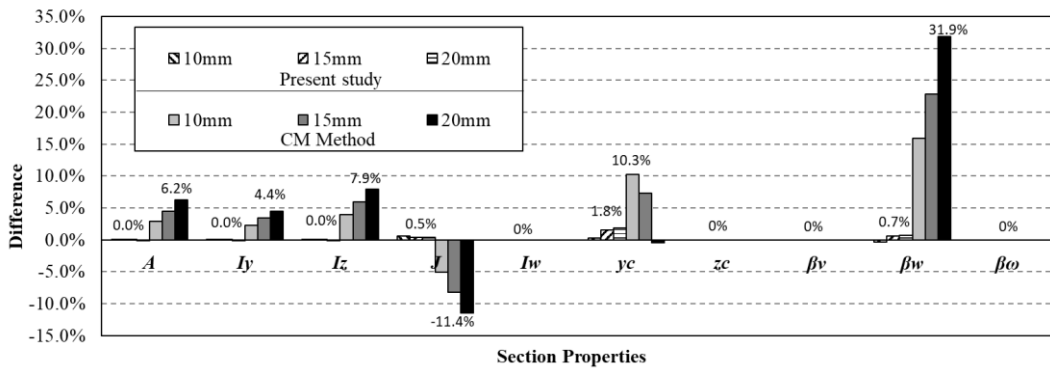
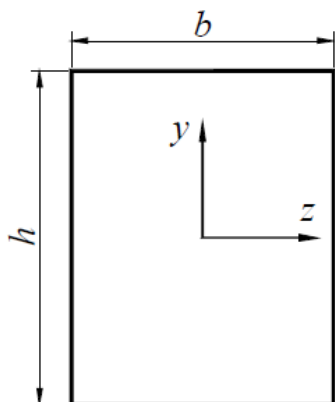


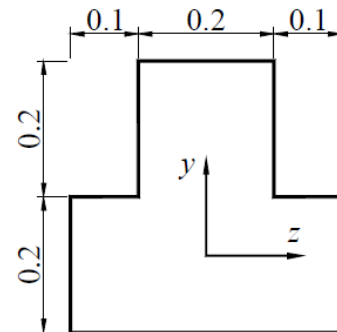
**Figure 8** Comparation results.

### 4.3 Shear coefficients

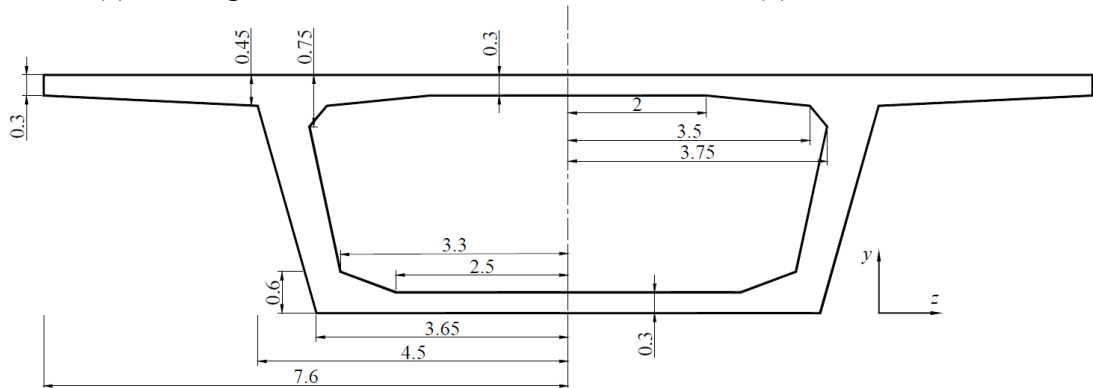
This example is given to validate the accuracy of the shear coefficients calculation. As shown in **Figure 9**, three types of cross-sections, including rectangular sections with different height-to-width ratios, a T section, and a bridge cross-section, reported by Gruttmann and Wanger (2001), are studied. Shear coefficients with different Poisson's ratios are calculated using the proposed CST element and compared with those given by Gruttmann and Wanger (2001).



### (a) Rectangular cross-section



(b) T section



### (c) Bridge cross-section

**Figure 9** Verification examples of shear deformation coefficients. (Unit: m)**Table 7** Shear coefficients of example sections

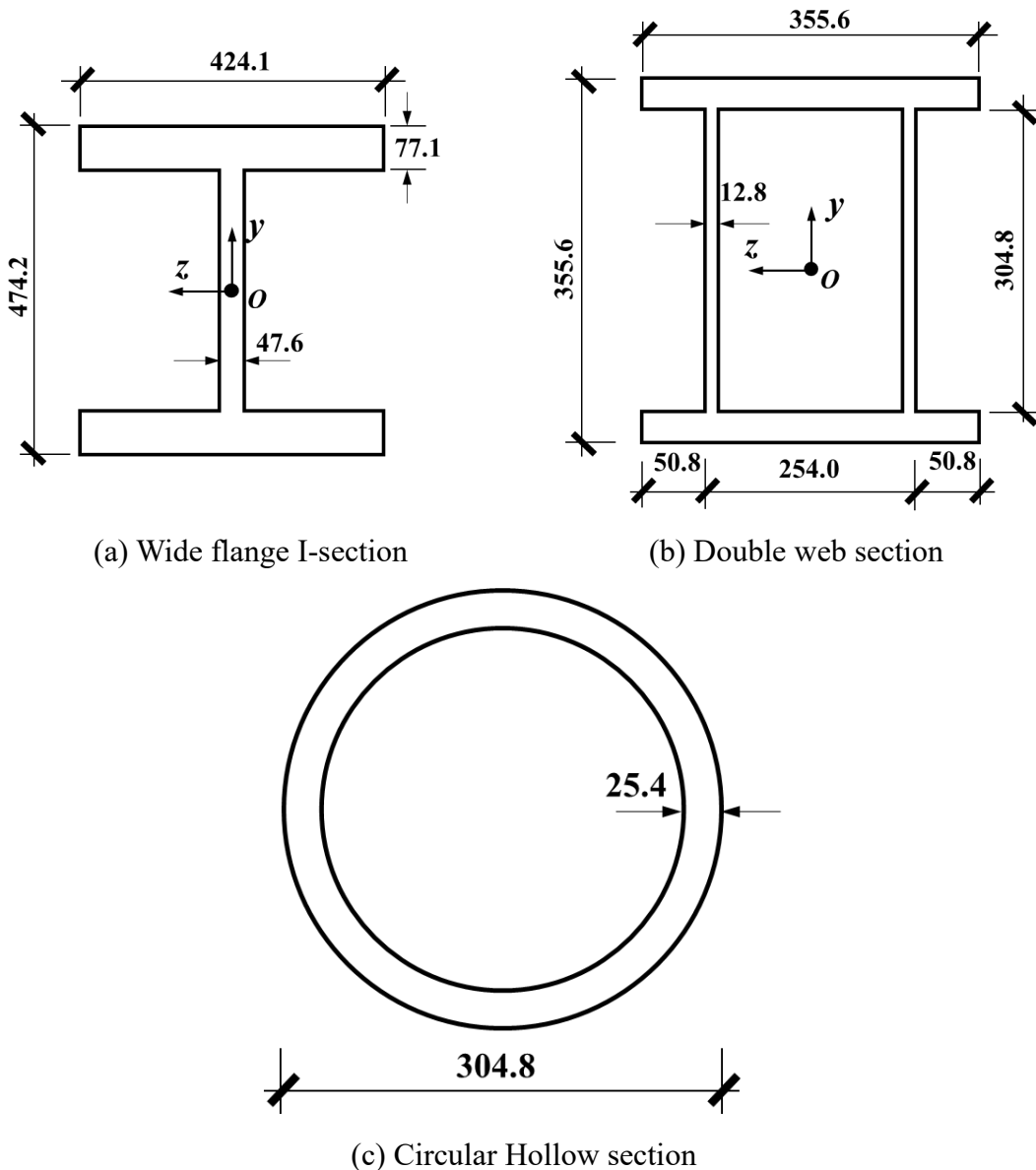
Section (1) - Rectangular Section						
Parameter		$k_y$				
		Gruttmann and Wagner (2001)	Present Study	Differences		
$v = 0$	$h/b = 2$	0.8333	0.8336	0.04%		
	$h/b = 1$	0.8333	0.8336	0.04%		
	$h/b = 0.5$	0.8333	0.8334	0.01%		
	$h/b = 0.25$	0.8333	0.8334	0.01%		
$v = 0.25$	$h/b = 2$	0.8331	0.8331	0.00%		
	$h/b = 1$	0.8295	0.8295	0.00%		
	$h/b = 0.5$	0.7961	0.7961	0.00%		
	$h/b = 0.25$	0.6308	0.6308	0.00%		
$v = 0.5$	$h/b = 2$	0.8325	0.8325	0.00%		
	$h/b = 1$	0.8228	0.8227	0.01%		
	$h/b = 0.5$	0.7375	0.7375	0.00%		
	$h/b = 0.25$	0.4404	0.4404	0.00%		
Section (2) – T section						
Parameter		$k_y$	$k_z$			
		Gruttmann and Wagner (2001)	Present Study	Differences	Gruttmann and Wagner (2001)	Present Study
						Differences
$v = 0$	0.6767	0.6773	0.09%	0.7395	0.7399	0.05%
	0.6753	0.6758	0.07%	0.7355	0.7362	0.10%
	0.6727	0.6733	0.09%	0.7294	0.7297	0.04%
Section (3) – Bridge Cross-section						
Parameter		$k_y$	$k_z$			
		Gruttmann and Wagner (2001)	Present Study	Differences	Gruttmann and Wagner (2001)	Present Study
						Differences
$v = 0$	0.2312	0.2314	0.09%	0.5993	0.5994	0.02%
	0.2311	0.2313	0.09%	0.5993	0.5994	0.02%

The shear coefficients of the cross-sections given above are listed in **Table 7**, where the results from Gruttmann and Wanger (2001) are taken as the benchmark. The results from the present study agree well with the benchmark, where differences do not exceed 0.1%, showing that the proposed cross-section analysis algorithm can get the shear coefficients accurately. It also can be seen that the Poisson's ratios have little influence on the shear coefficients of sections with large height-to-width ratios.

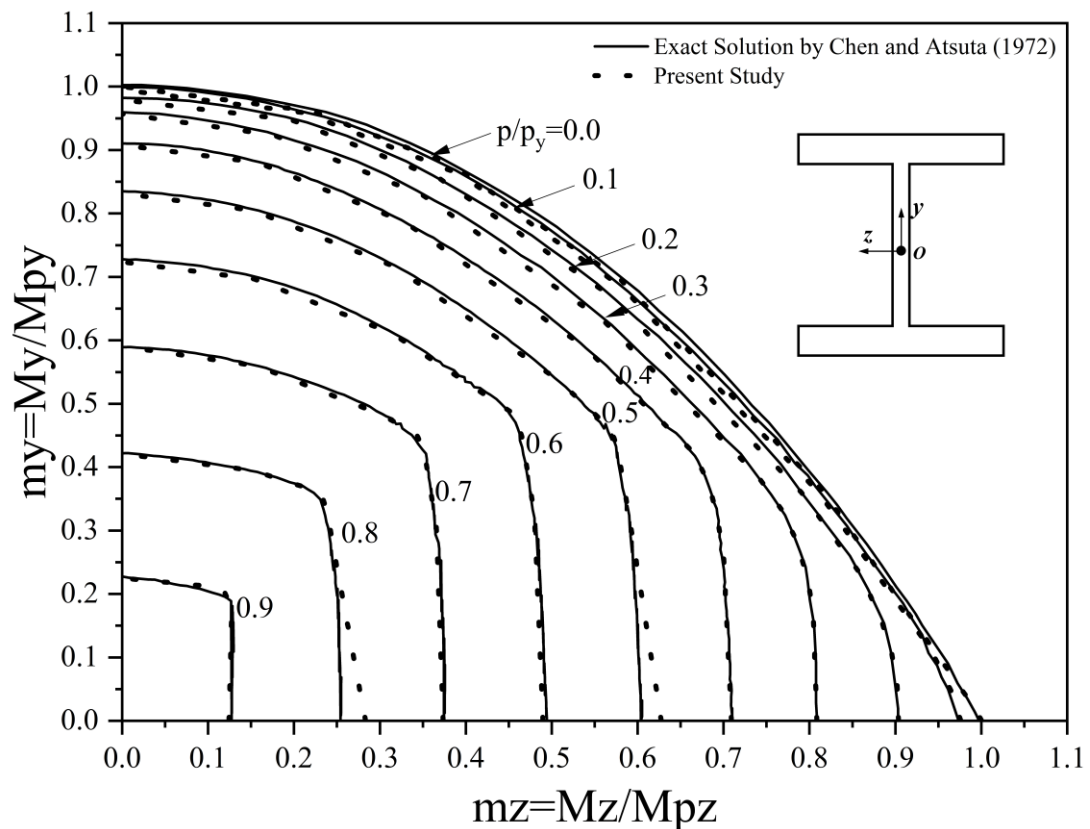
## 4.3 Yield surface

### 4.3.1 Symmetric sections

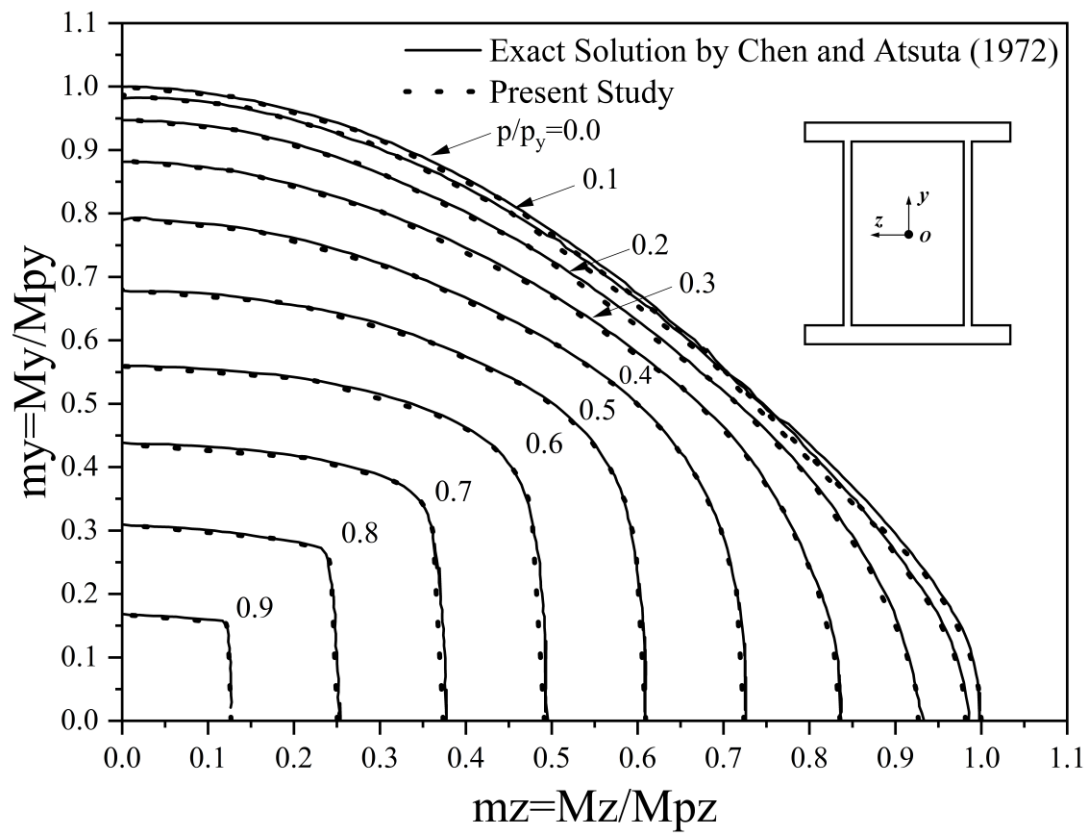
This example verifies the accuracy of the yield surface generation for symmetrical cross-sections, including a wide flange I-section, a double web section, and a circular hollow section. The dimensions of the cross-sections are given in **Figure 10**. Those cross-sections were studied by Chen and Atsuta (1972). They provided accurate results of the  $M_y$  vs  $M_z$  curve under different axial force levels. Same  $M_y$  vs  $M_z$  curves are calculated and provided in **Figure 11**. The load values were normalized to obtain a more general cross-sectional load relationship. Since the sections are doubly symmetric and the full  $M_y$  vs  $M_z$  curve will also be doubly symmetric, only one-quarter of the resulting curves are given.



**Figure 10** Doubly symmetric sections (Unit: mm)



(a) Wide flange section



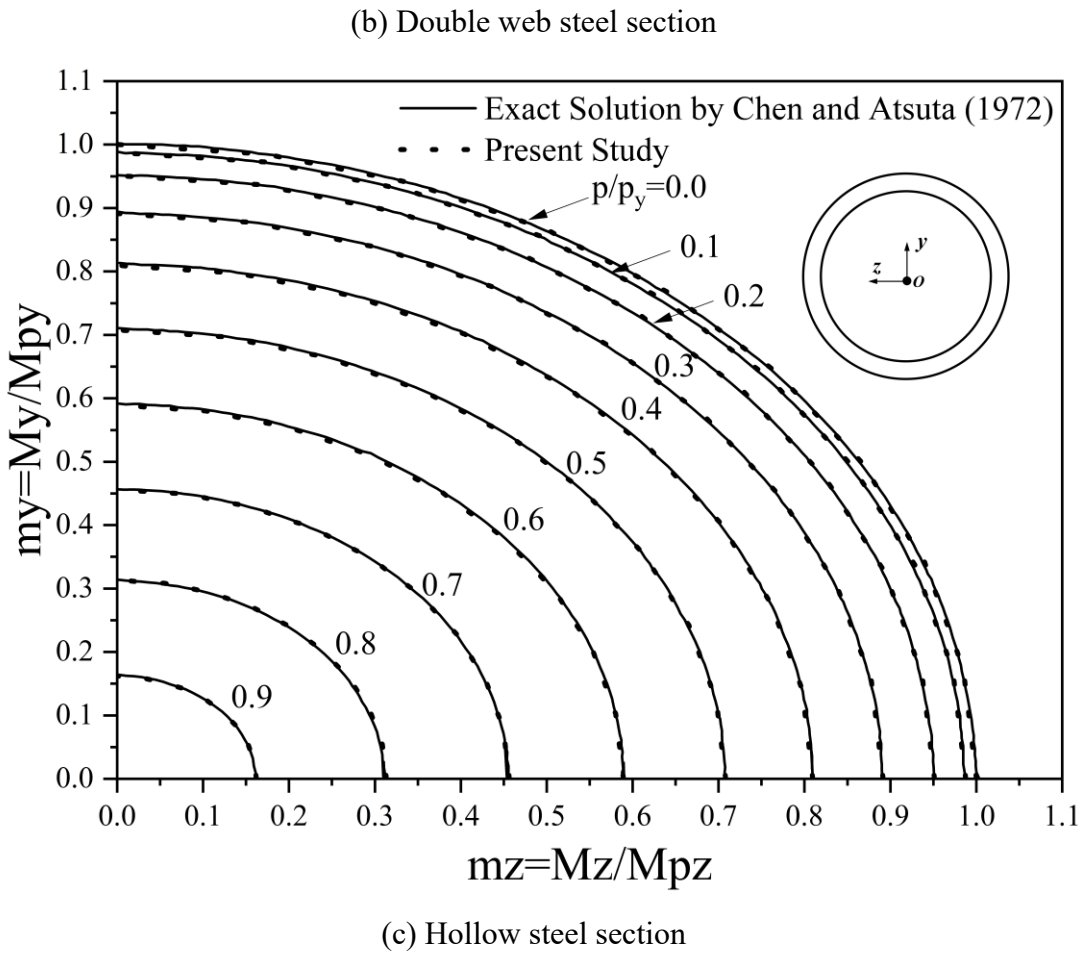
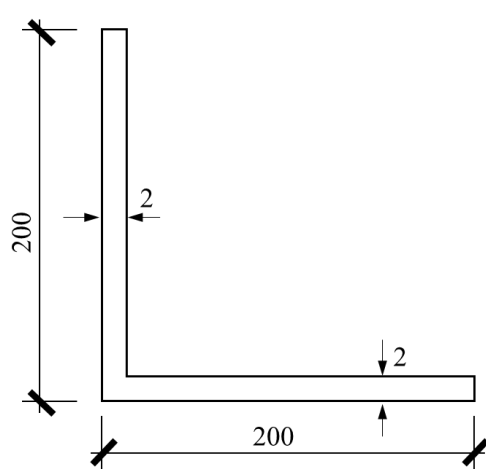


**Figure 11** Comparison results for the doubly symmetric sections

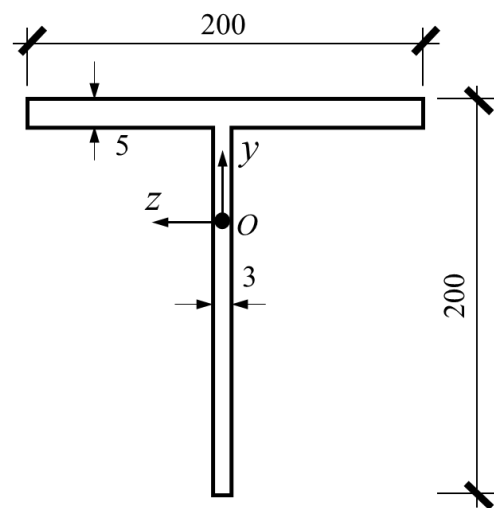
The solid lines plotted in **Figure 11** are the close-formed solutions provided by Chen and Atsuta (1972), and the dotted points depict the results from the proposed approach. The results agree with each other well, verifying the validity of the yield surface generation for symmetrical cross-section.

#### 4.3.2 Nonsymmetric sections

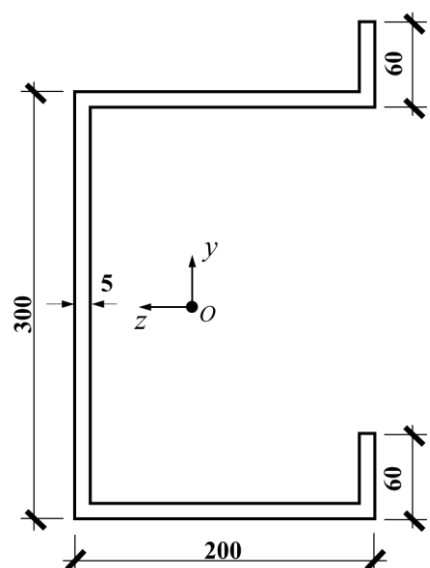
This example is given to verify the reliability of the proposed yield surface generation method for nonsymmetric sections. Four nonsymmetric sections (**Figure 12**), including an angle section, a T-section, a nonsymmetric lipped channel section, and a highly irregular section, are studied. The  $P$ - $M_y$ ,  $P$ - $M_z$ ,  $P$ - $M_v$ ,  $P$ - $M_w$ ,  $M_y$ - $M_z$ , and  $M_v$ - $M_w$  curves ( $v-w$  is the section principal axis) generated from the proposed yield surface generation algorithm are compared with those given by the advanced cross-sectional analysis method invented by Liu et al. (2012). Results from the calculation methods recommended by AISC (2016) and McGuire et al. (2000) are also plotted in **Figure 13** to **Figure 16**.



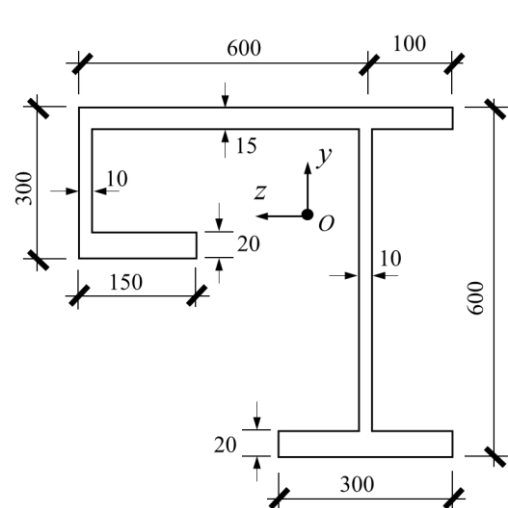
(a) Section A



(b) Section B

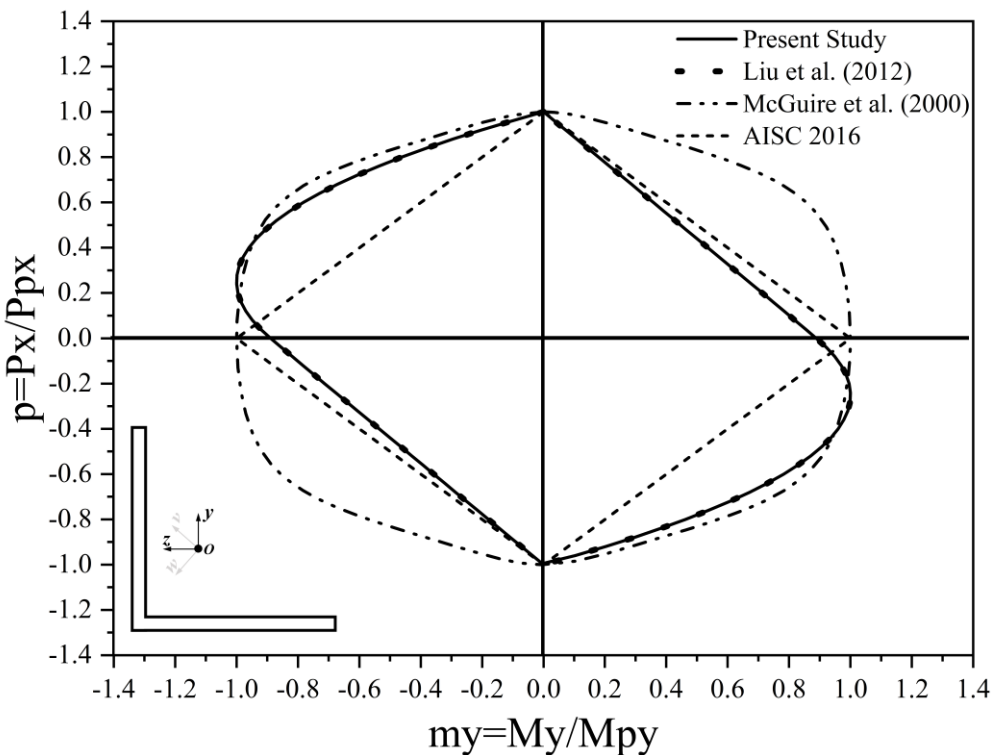
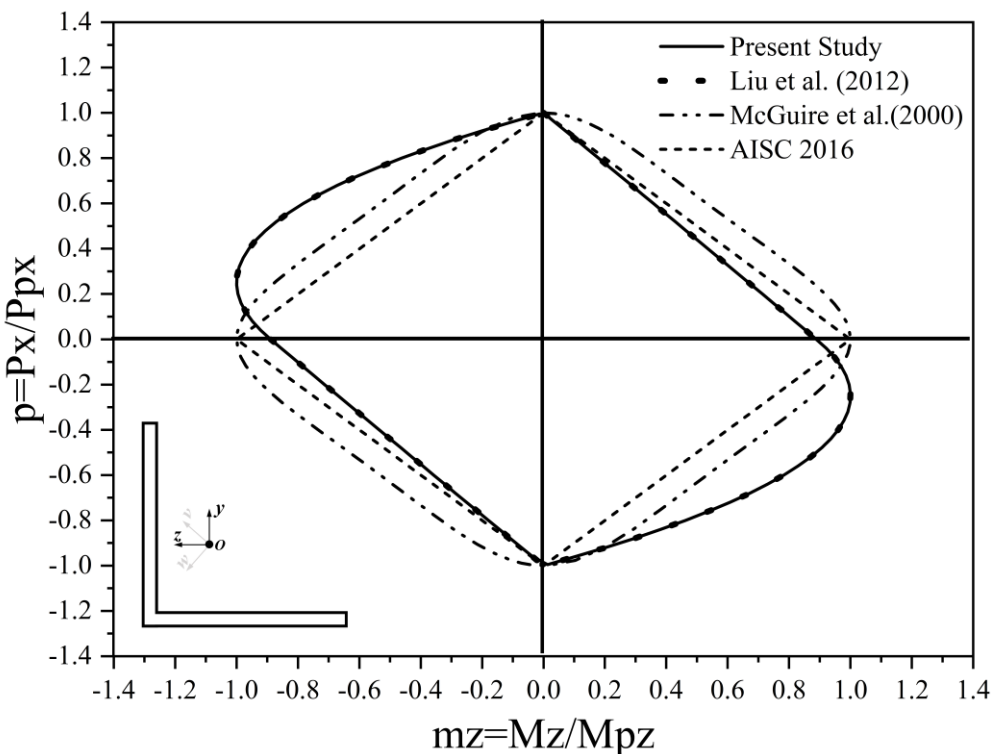


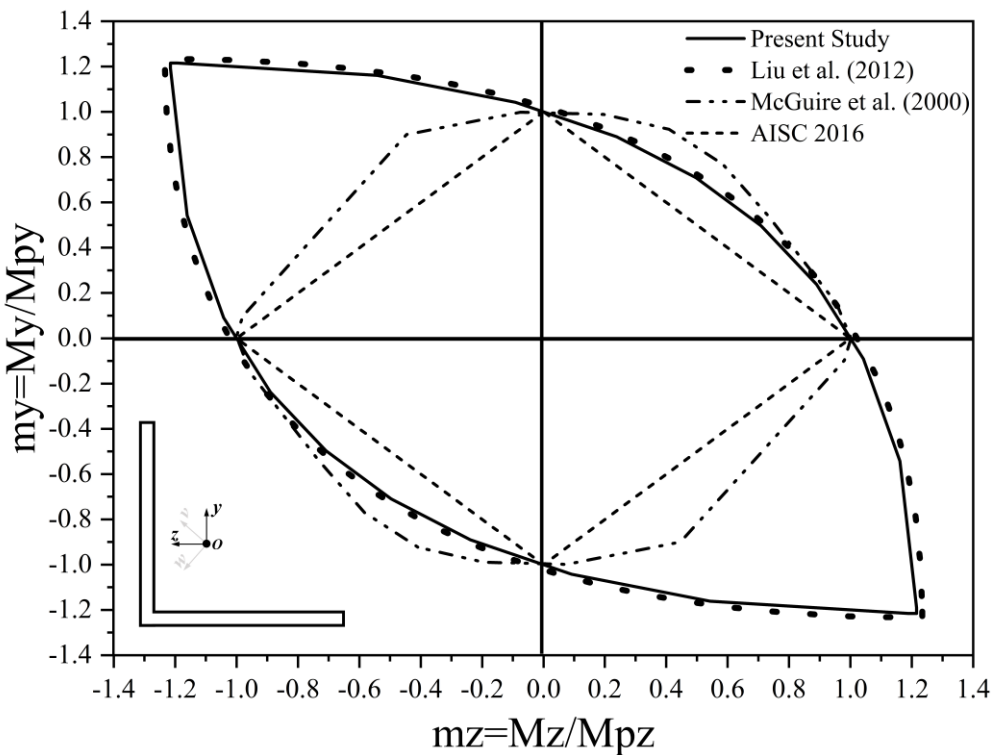
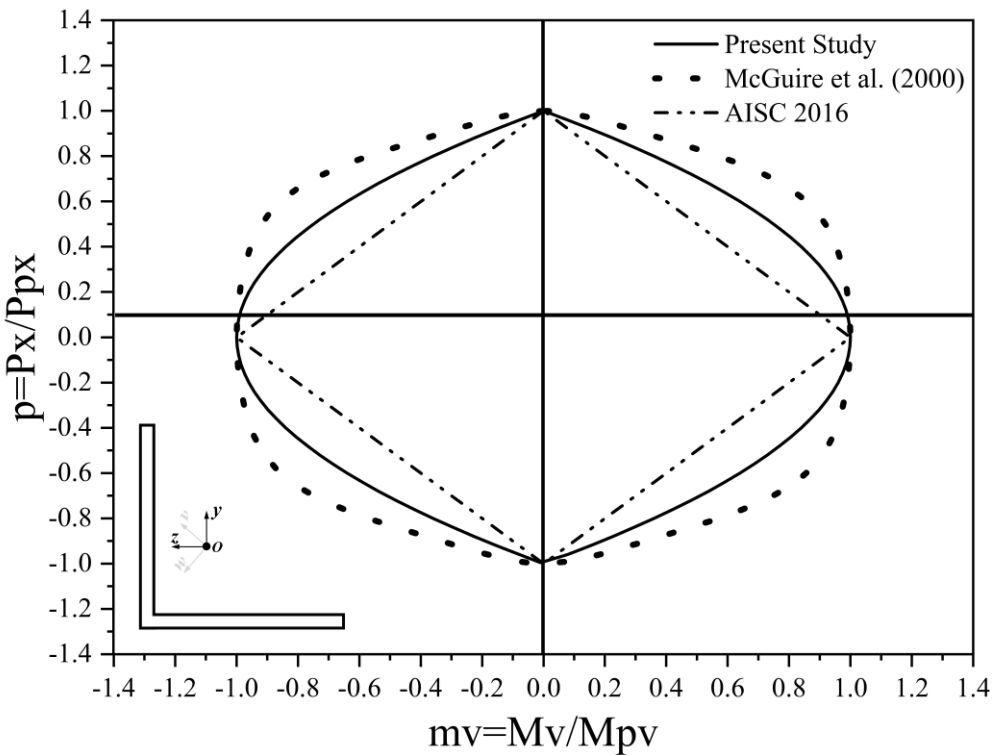
(c) Section C

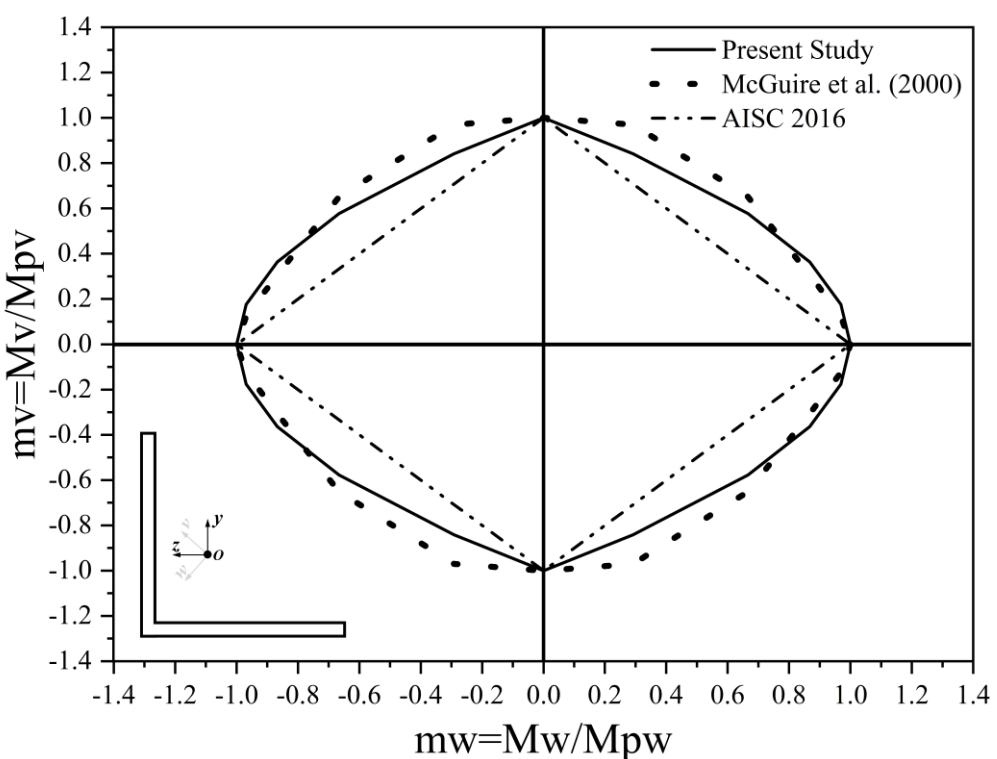
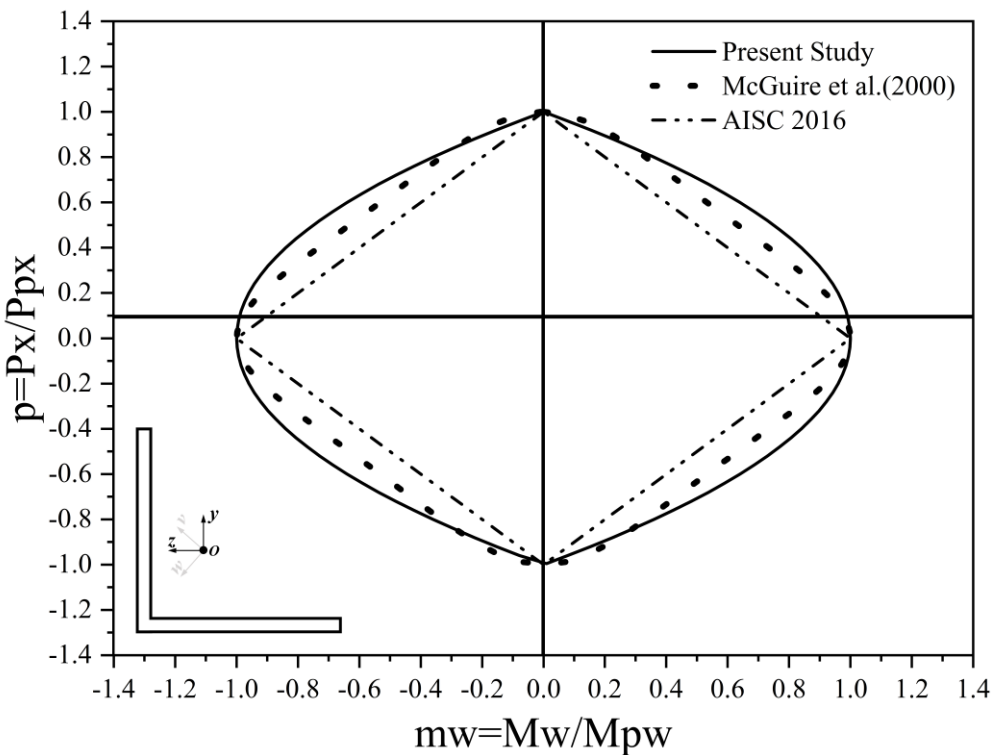


(d) Section D

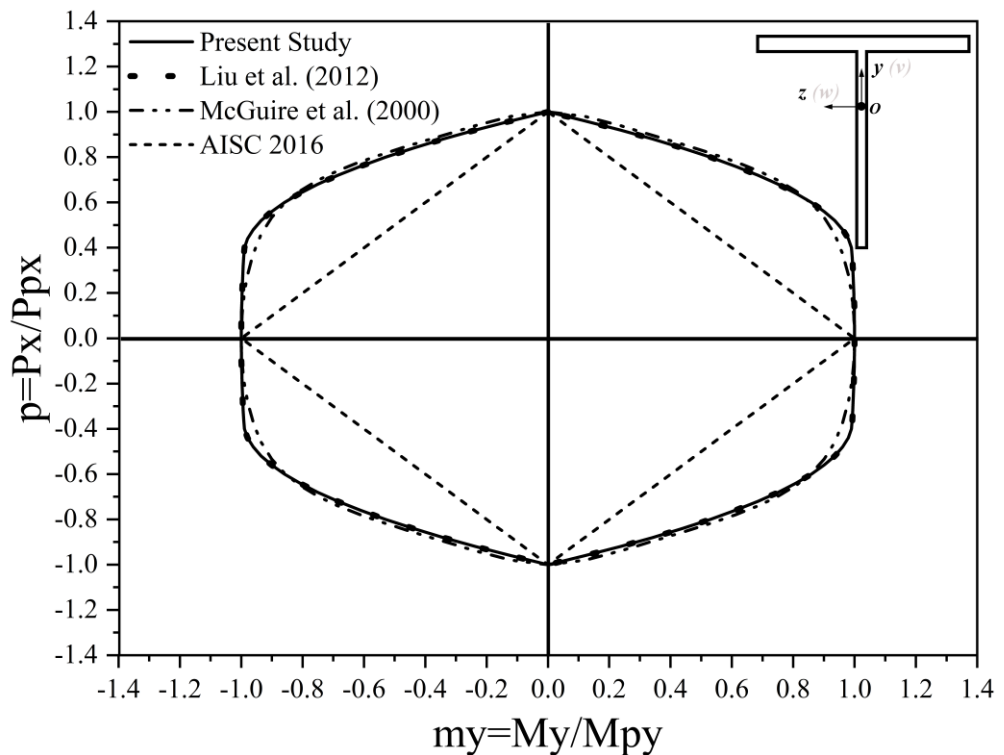
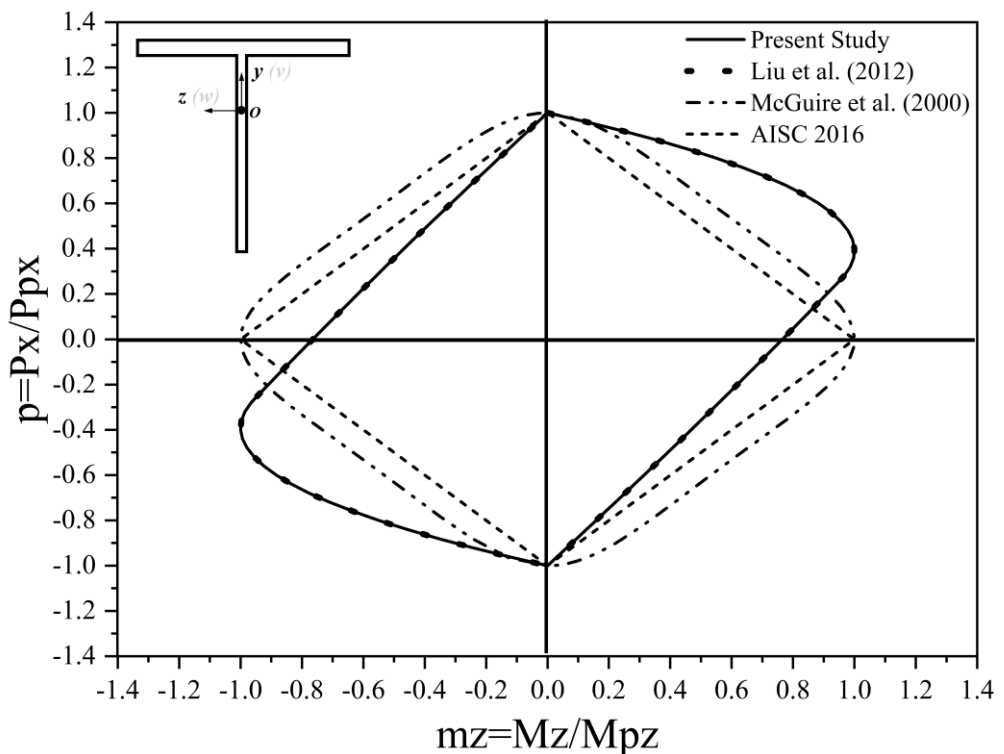
**Figure 12** Nonsymmetric sections (Unit: mm)

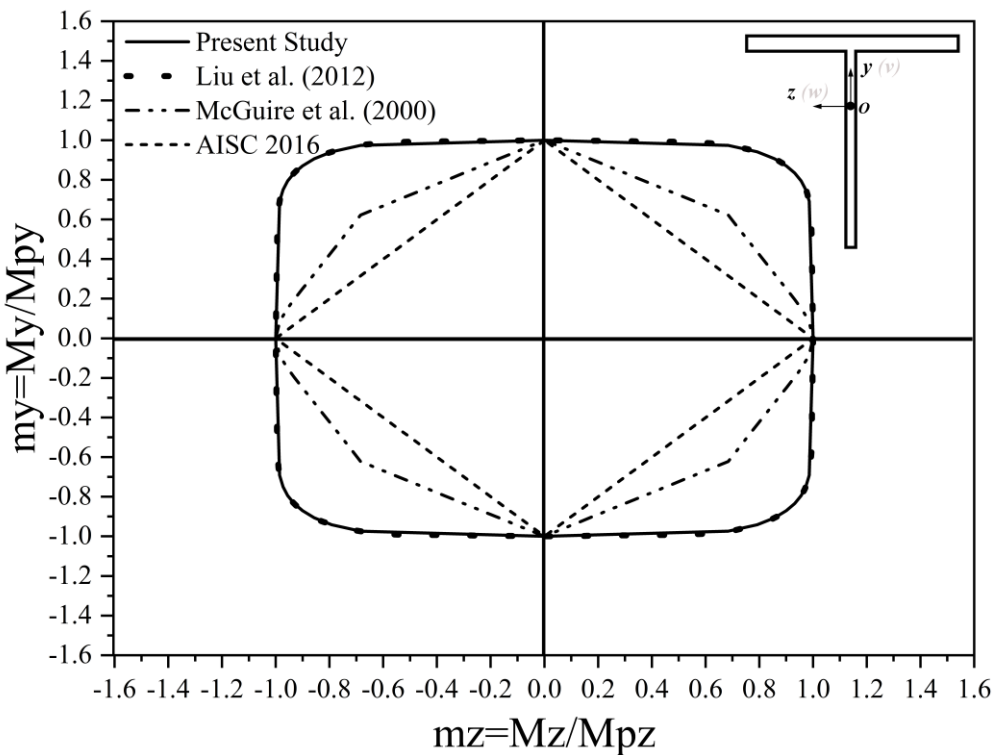
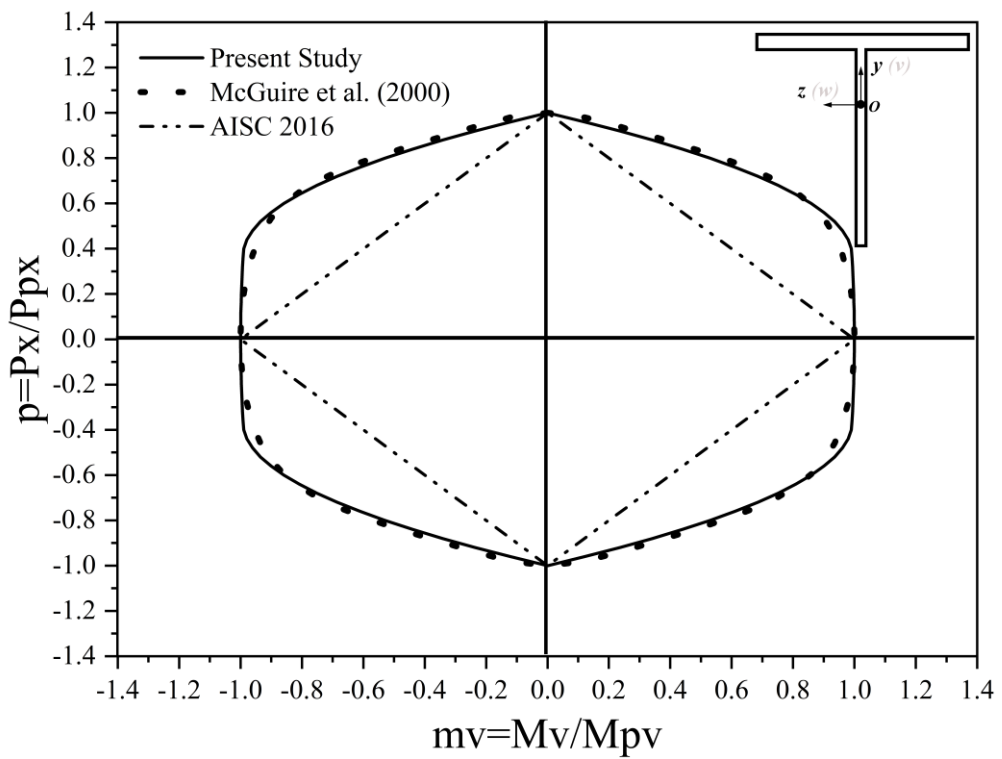
(a) Interaction curve of  $p$  vs  $m_y$  of section A(b) Interaction curve of  $p$  vs  $m_z$  of section A

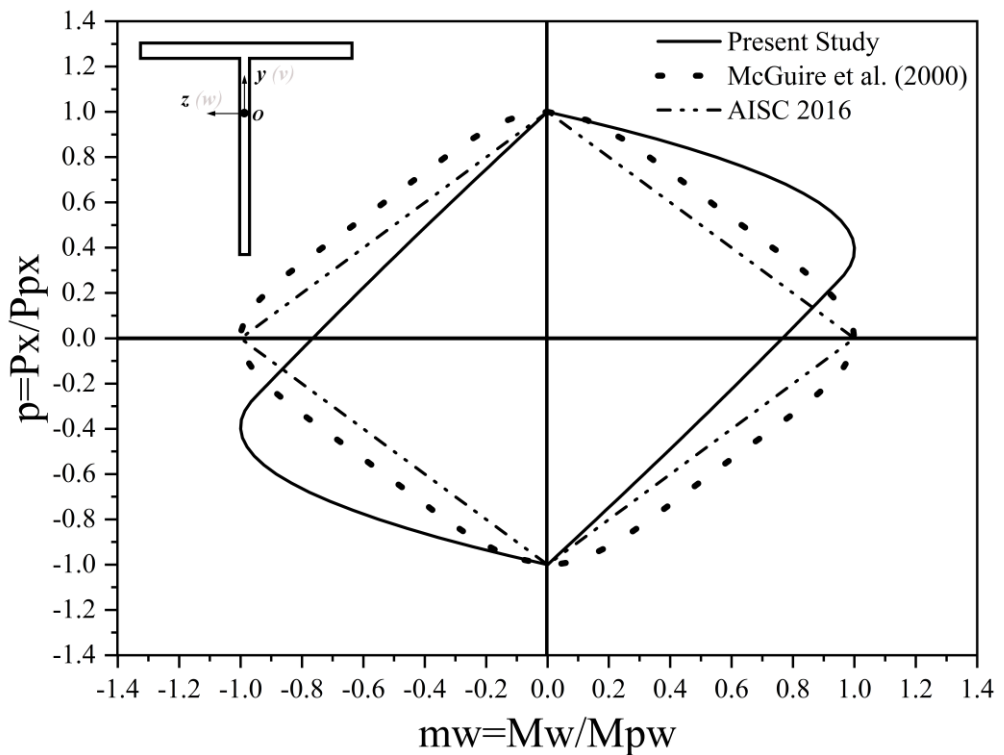
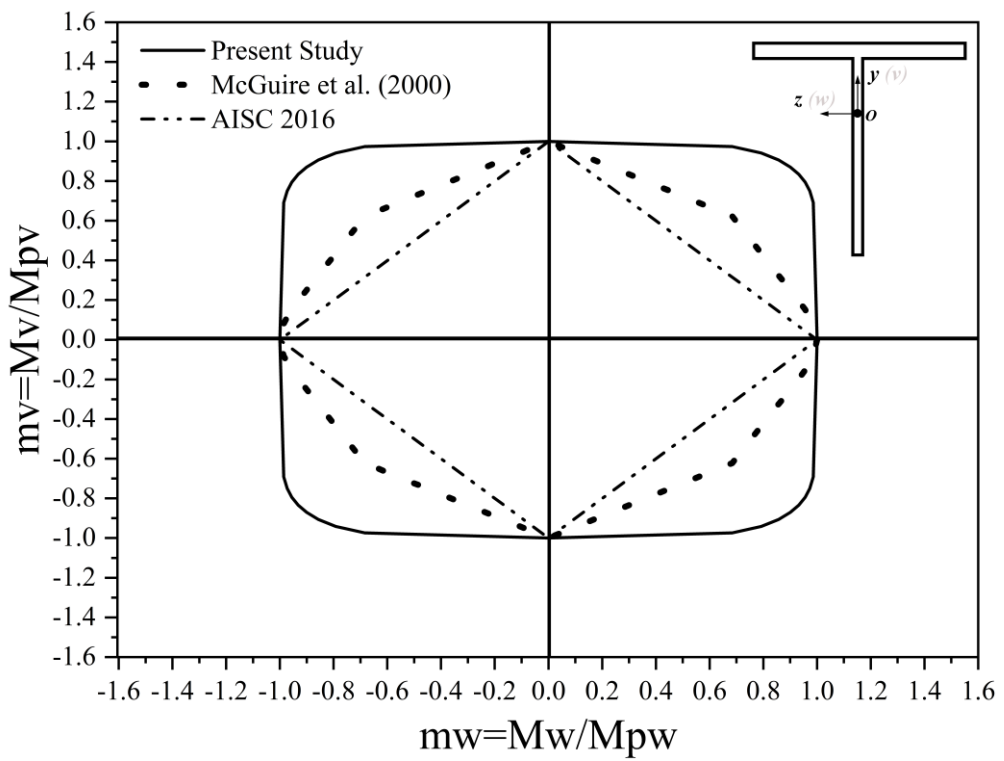
(c) Interaction curve of  $m_y$  vs  $m_z$  of section A(d) Interaction curve of  $p$  vs  $m_v$  of section A

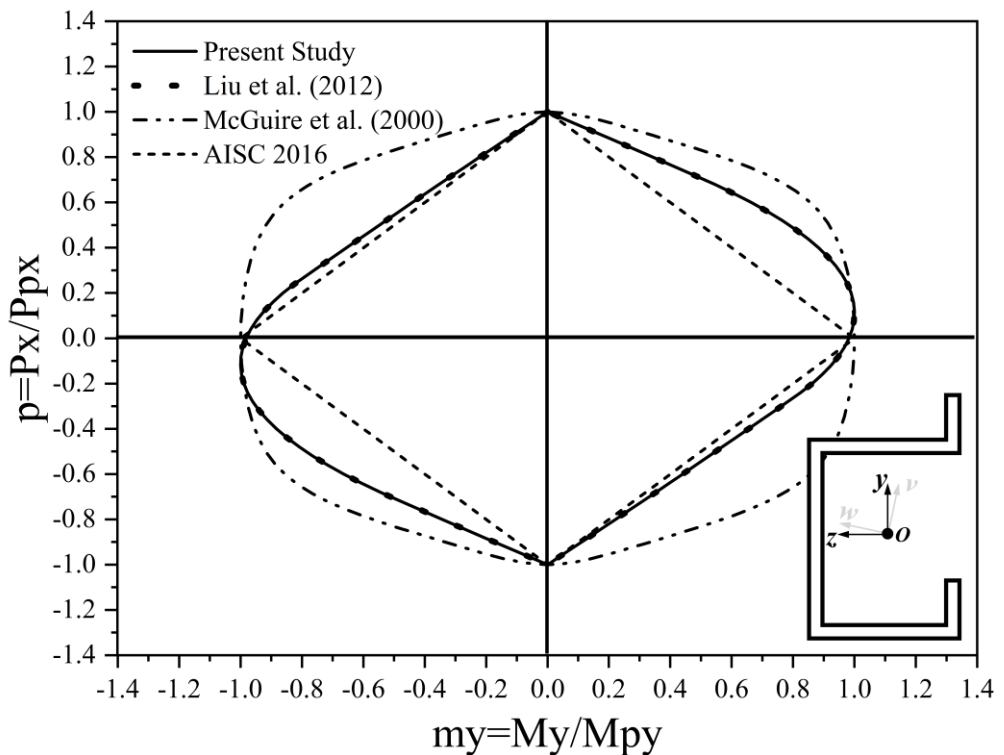
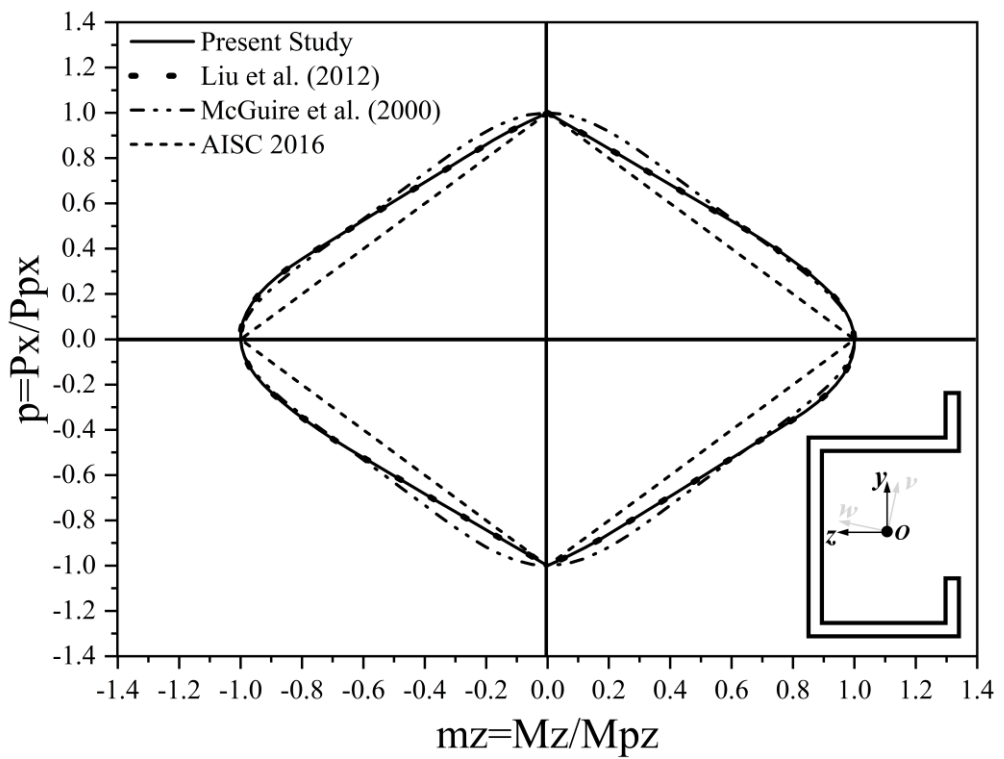


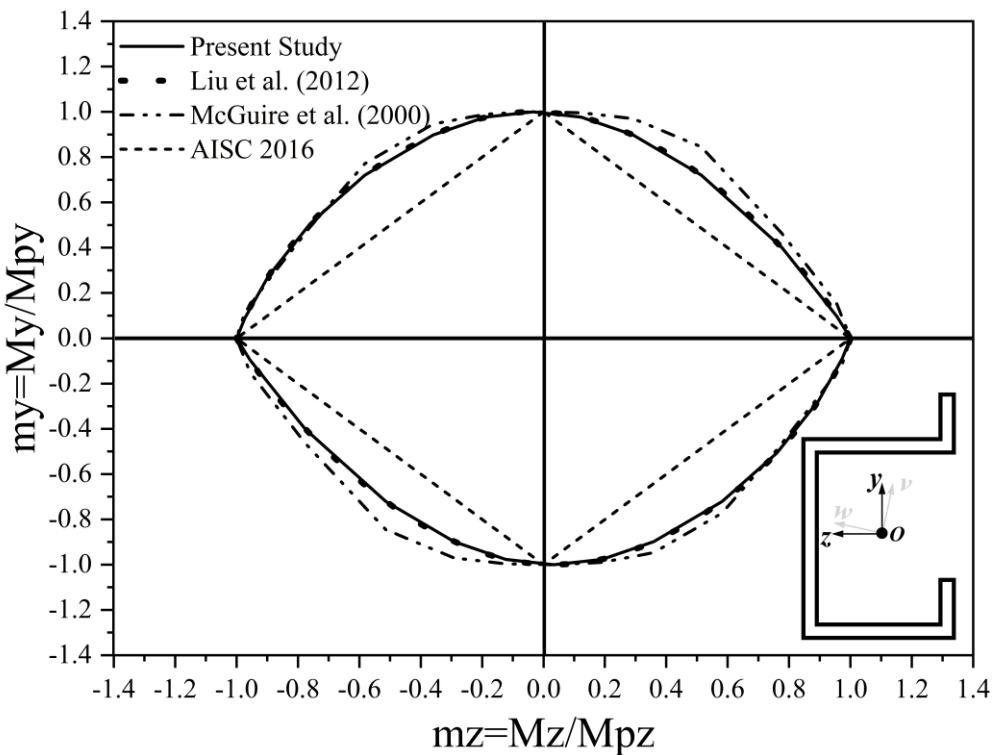
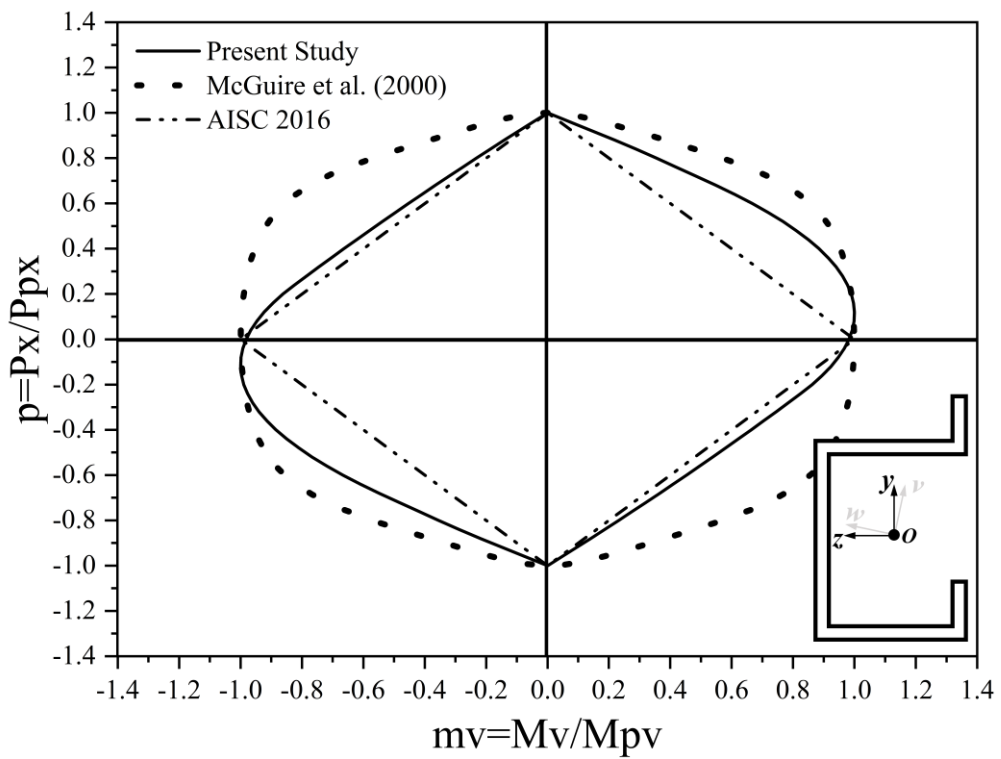
**Figure 13** Comparison results for section A

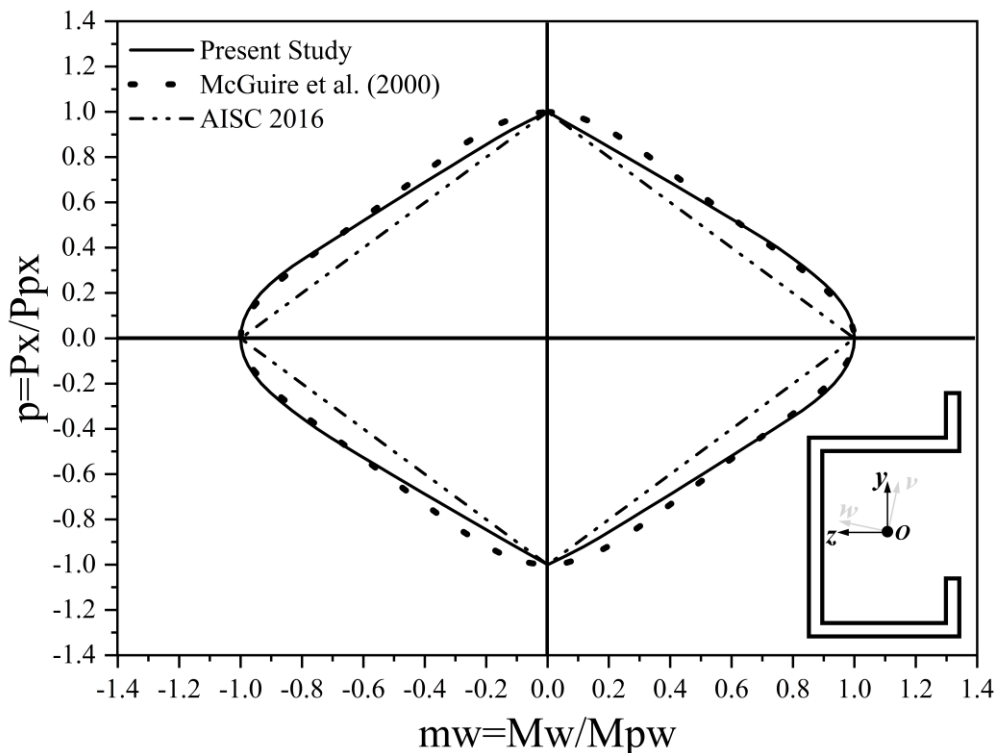
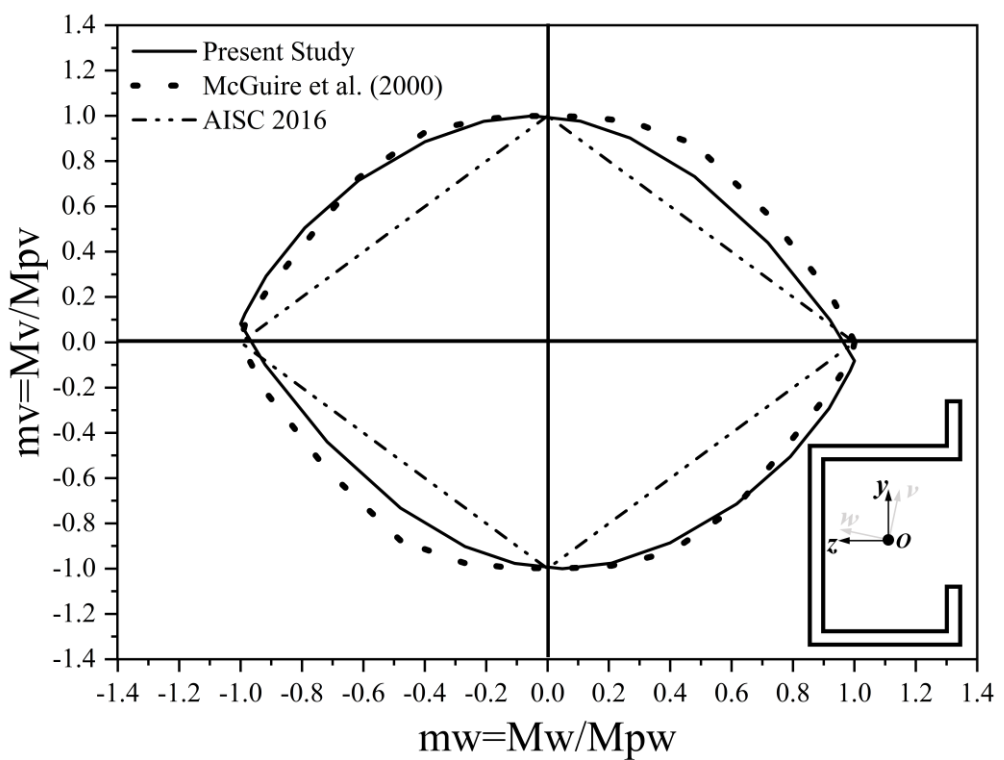
(a) Interaction curve of  $p$  vs  $m_y$  of section B(b) Interaction curve of  $p$  vs  $m_z$  of section B

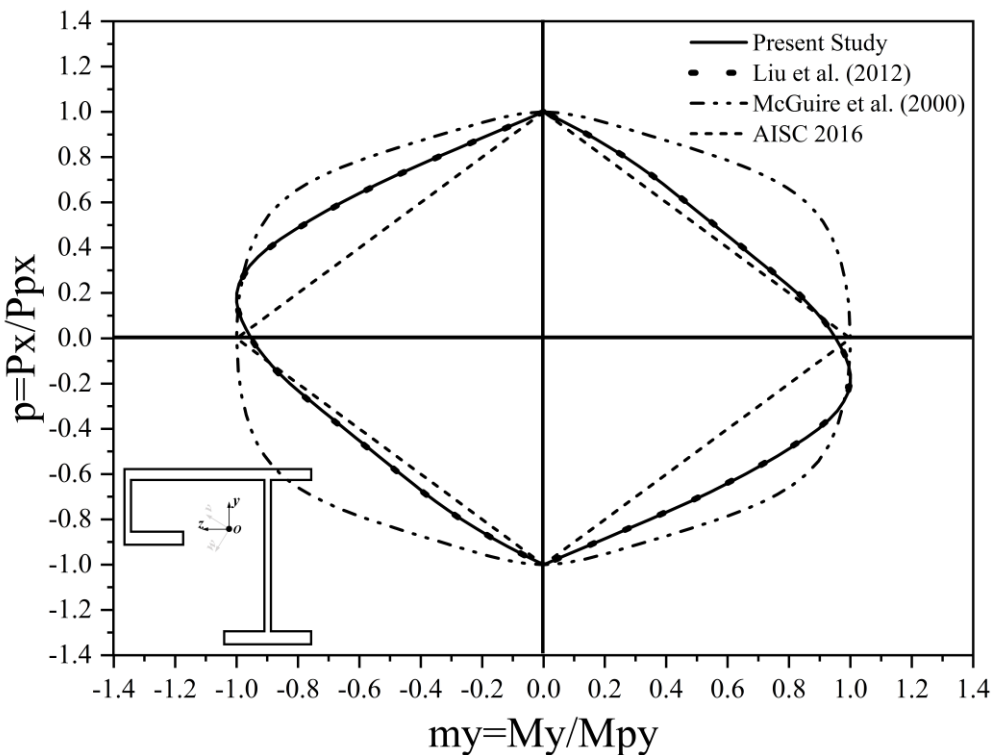
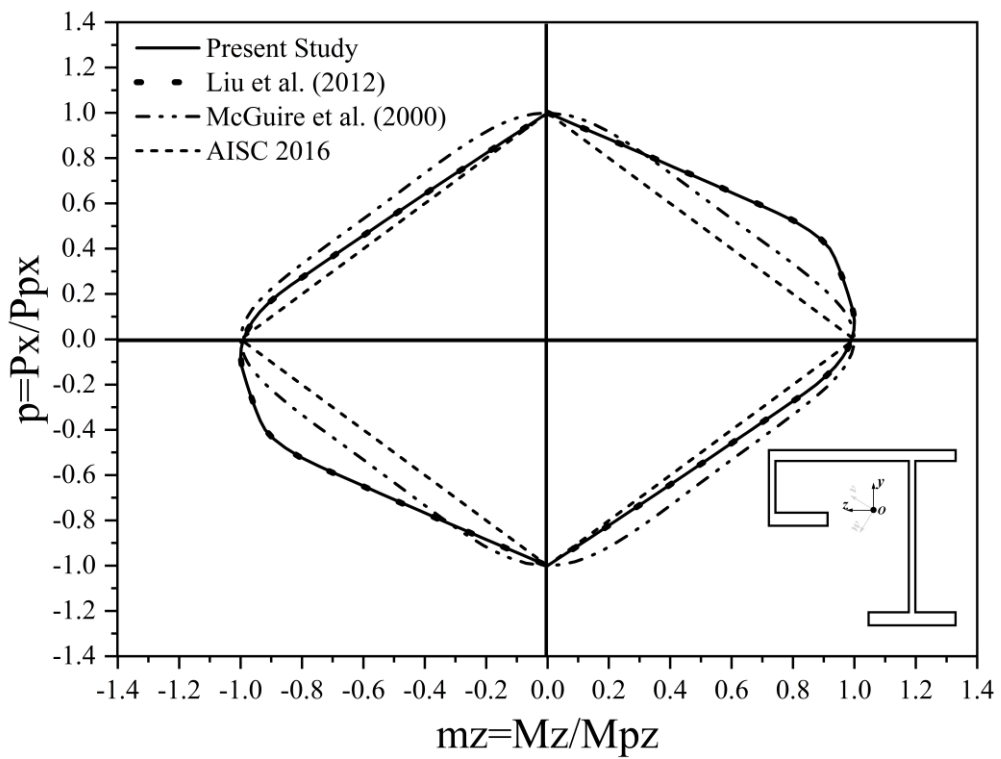
(c) Interaction curve of  $m_y$  vs  $m_z$  of section B(d) Interaction curve of  $p$  vs  $m_v$  of section B

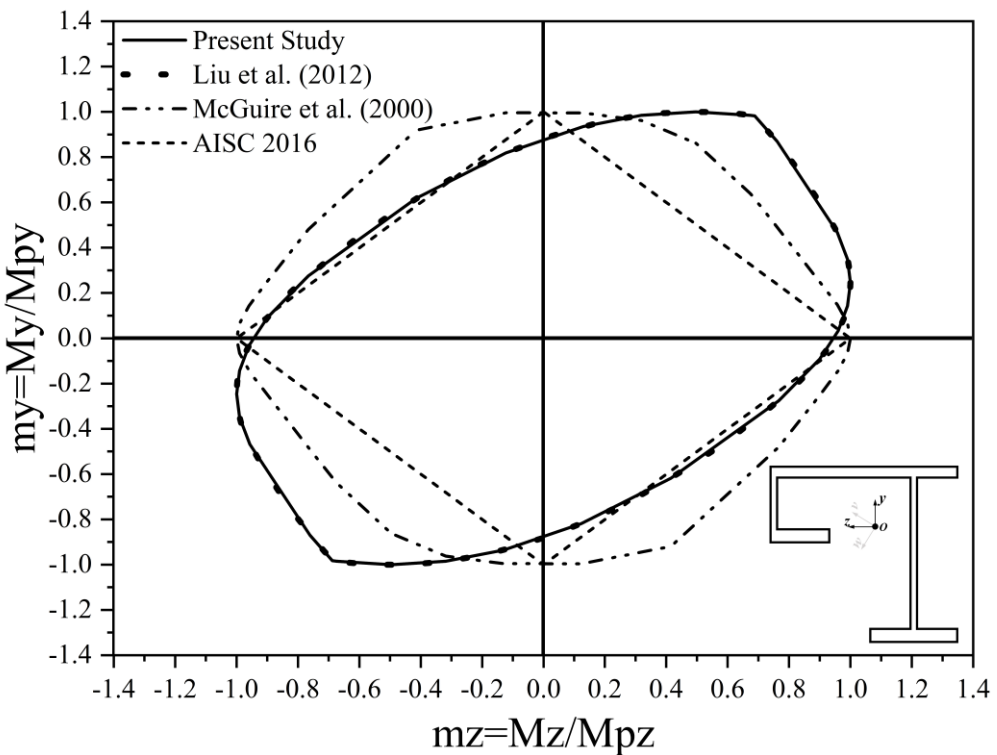
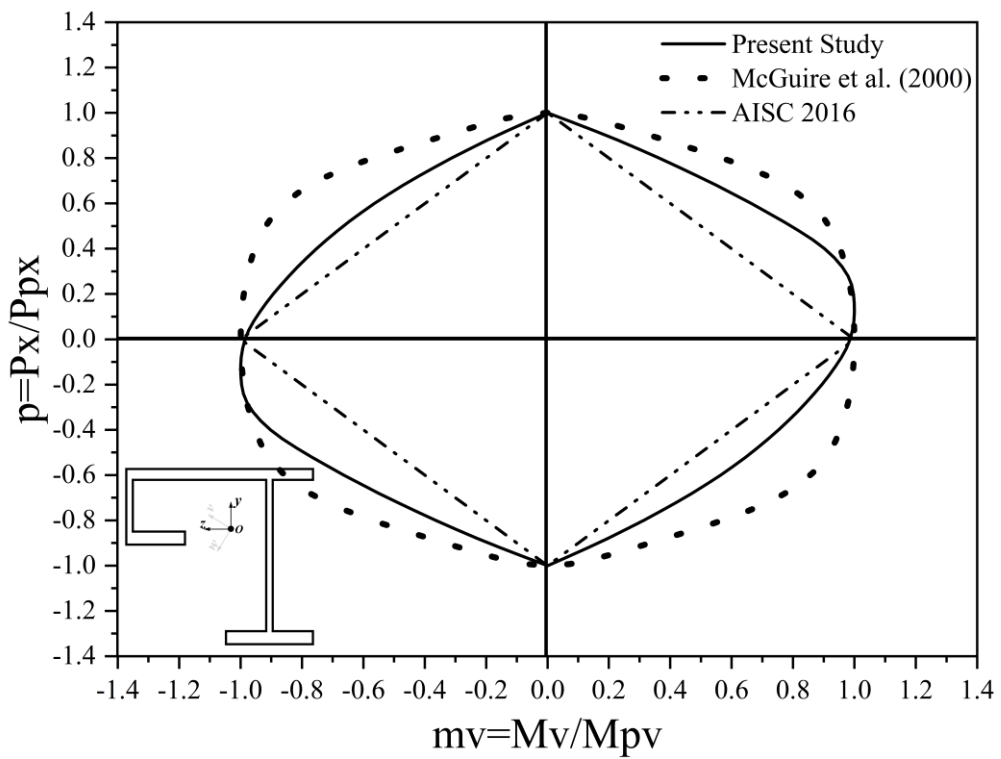
(e) Interaction curve of  $p$  vs  $m_w$  of section B**Figure 14** Comparison results for section B

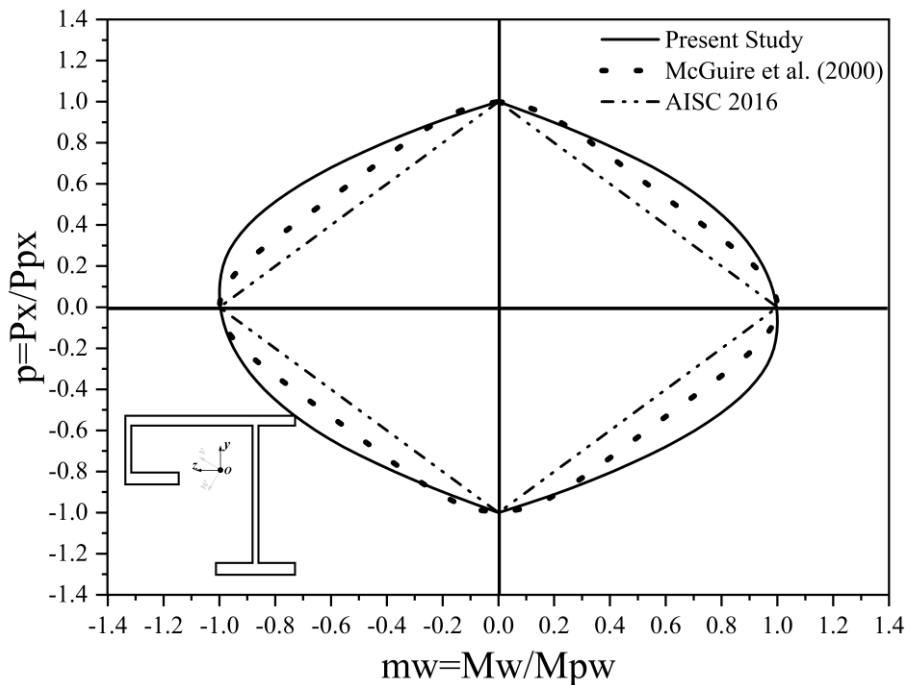
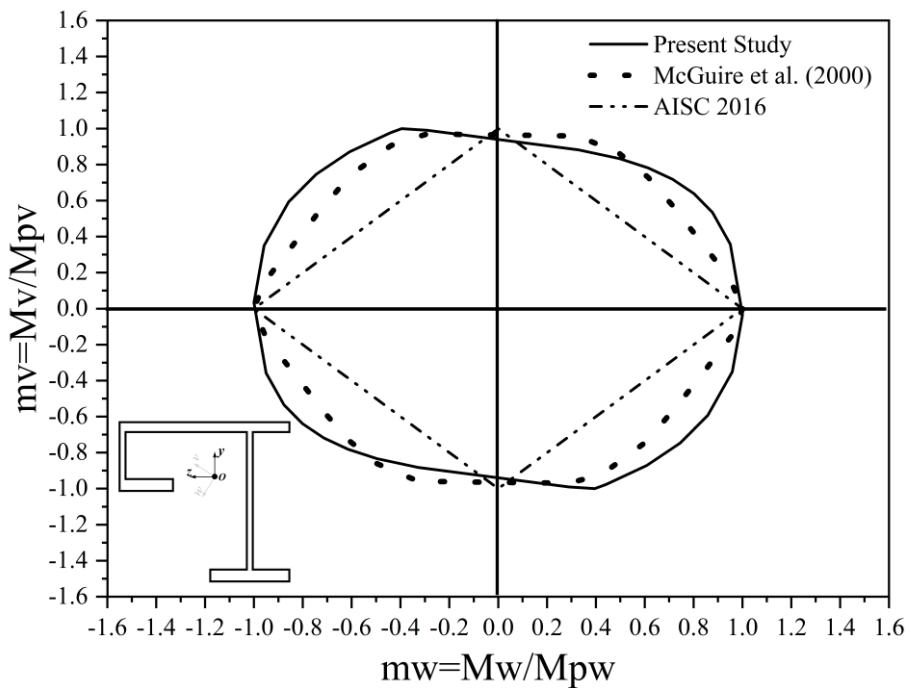
(a) Interaction curve of  $p$  vs  $m_y$  of section C

(c) Interaction curve of  $m_y$  vs  $m_z$  of section C(d) Interaction curve of  $p$  vs  $m_v$  of section C

(e) Interaction curve of  $p$  vs  $m_w$  of section C(f) Interaction curve of  $m_v$  vs  $m_w$  of section C**Figure 15** Comparison results for section C

(a) Interaction curve of  $p_x$  vs  $m_y$  of section D(b) Interaction curve of  $p_x$  vs  $m_z$  of section D

(c) Interaction curve of  $m_y$  vs  $m_z$  of section D(d) Interaction curve of  $p_x$  vs  $m_v$  of section D

(e) Interaction curve of  $p_x$  vs  $m_w$  of section D(f) Interaction curve of  $m_v$  vs  $m_w$  of section D**Figure 16** Comparison results for section D

From **Figure 13**, the results from the proposed algorithm are in line with those from the advanced cross-sectional analysis method given by Liu et al. (2012). While the calculation methods recommended by AISC (2016) and McGuire et al. (2000) are no longer suitable for the yield surface generation of nonsymmetric sections. The yield surfaces predicted by the calculation method recommended by AISC (2016) are linear,

and most of the yield surfaces are inside the yield surfaces obtained by Liu et al. (2012), which means they are safe and conservative. Some figures show that the section capacities predicted by the equation given by McGuire et al. (2000) are overestimated. This example shows the accuracy of the proposed yield surface generation algorithm for nonsymmetric sections and proves that the traditional yield surface calculation methods, such as those equations given by AISC (2016) and McGuire et al. (2000), are not suitable for nonsymmetric sections.

## References

- AISC. 2016. 'ANSI/AISC 360 - 16: Specification for structural steel buildings'. American Institute of Steel Construction.
- Bathe, Klaus-Jürgen. 2006. Finite element procedures (Klaus-Jurgen Bathe).
- Chen, Wai F, and Toshio Atsuta. 1972. 'Interaction equations for biaxially loaded sections', Journal of the Structural Division, 98: 1035-52.
- Gruttmann, F, and W Wagner. 2001. 'Shear correction factors in Timoshenko's beam theory for arbitrary shaped cross-sections', Computational mechanics, 27: 199-207.
- Liu, S. W., W. L. Gao, and R. D. Ziemian. 2019. 'Improved line-element formulations for the stability analysis of arbitrarily- shaped open-section beam-columns', Thin-Walled Structures, 144: 106290.
- Liu, S. W., R. D. Ziemian, C. Liang, and Siu-Lai Chan. 2018. 'Bifurcation and large-deflection analyses of thin-walled beam-columns with non-symmetric open-sections', Thin-Walled Structures, 132: 287-301.
- Liu, Si-Wei, Yao-Peng Liu, and Siu-Lai Chan. 2012. 'Advanced analysis of hybrid steel and concrete frames: Part 1: Cross-section analysis technique and second-order analysis', Journal of Constructional Steel Research, 70: 326-36.
- McGuire, William, Richard H Gallagher, and Ronald D Ziemian. 2000. Matrix structural analysis.
- Ziemian, Ronald D. 2010. Guide to stability design criteria for metal structures (John Wiley & Sons).